STUDY OF LIPID METABOLISM IN CORYNEBACTERINEAE USING LIPIDOMICS AND PROTEOMICS APPROACH

SUDARKODI SUKUMAR

(*B.Tech, Anna University, India)*

A THESIS SUBMITTED

FOR THE DEGREE OF DOCTOR OF PHILOSOPHY

IN COMPUTATION AND SYSTEMS BIOLOGY (CSB)

SINGAPORE-MIT ALLIANCE

NATIONAL UNIVERSITY OF SINGAPORE

2013

Declaration

I hereby declare that this thesis is my original work and it has been written by me in its entirety. I have duly acknowledged all the sources of information which have been used in the thesis.

This thesis has also not been submitted for any degree in any university previously.

12.04.2013

Sudarkodi Sukumar

Acknowledgements

I am grateful to my supervisor A/P Markus R Wenk for always inspiring me to follow new ways in Lipidomics research. His critical comments and suggestions have motivated me in my project. I am glad to have started my research career under his guidance. I would like to thank my supervisor at MIT, Anthony J Sinskey for his never failing support. His scientific enthusiasm and positive attitude helped me to pursue my project with confidence.

I am indebted to Dr. Shui Guanghou for being a great mentor. His expertise in analytical biochemistry has been very crucial for my project. His moral support pushed me forward in my PhD journey.

I am extremely grateful to Prof. Shao Q Yao (Department of Chemistry, NUS) for providing the chemical probes for *R.opacus* proteomics project. His scientific inputs have been a significant driving force for my project. I am thankful to Dr. Sebastien Gagneux (Swiss TPH, Basel) for the interesting and fruitful collaboration on Mtb lineage project. I am grateful to Dr. Damien Portevin for performing the Mtb culture and macrophage infection experiment. I have learnt a lot from his vast knowledge and experience in TB research.

I especially thank Dr. Jens K. Plassmeier (Sinskey's Lab, MIT) for performing the genetic experiments to generate *R.opacus* mutants. His timely help will enable to complete my project. I would also like to thank Dr. Kazuhiko Kurosawa and Tony DeBono for their technical help and support during my stay at Sinskey's lab, MIT.

I owe my heartfelt gratitude to Madhu Sudhanan for his help with my proteomics project during a critical stage of my PhD. His patience in teaching me many important experiments was incredible! I am grateful to Dr. Anne K Bendt for her immense help in *Mycobacterium tuberculosis* sample organization and shipment. I

am always thankful for her kindness in critically reviewing my scientific proposals and helping me to correct my English for the best. I am thankful to Li Bowen for his help and expertise with the statistic analysis. I very much respect and appreciate the scientific help provided by Federico, Shareef, Lukas and Weifun. I am very thankful to J-club members for their time and helpful suggestions for my project presentations. Special thanks to my wonder girls, Husna, Jing Yan, Jacklyn, Charmaine and Lissya for their fun and support and for making my stay in NUS memorable. I appreciate the administrative help provided by Huimin. I would like to thank other past and present members of MRW lab for their help with my project.

I would like to express my sincere gratitude to SMA for the fellowship and the administrative staff for always helping me with a smile.

I am greatly thankful to my thesis defence examination panel members for their helpful suggestions and comments.

I am blessed to have an awesome bunch of friends in Singapore who have kept me happy and positive during these five years. Padhu, Nandhu, Jagadish, Sangit, Muthu, Ghayathri, Akila, Divya, Porkodi, and Karthik: Thanks a lot! I owe special thanks to Eva for her words of encouragement.

Finally, I would like to thank my parents, my brother and my dear Pradeepkumar for supporting me throughout my life. I would like to dedicate this thesis to my appa and amma.

Table of Contents

Summary

The cell envelope is multilayered, complex and uniquely lipid rich in Corynebacterineae suborder comprising major genera *Mycobacterium* and *Rhodococcus*. The major components of the cell envelope are mycolic acids (MA) along with a wide array of free lipids. It is not surprising that the Corynebacterineae genome is devoted significantly to the metabolism of these complex lipids. Lipid metabolism is essential for the survival of Corynebacterineae members with varied lifestyle. *R.opacus* PD630 is a non-pathogenic member of the suborder, capable of accumulating large amounts of triacylglycerols (TAG) and holds a great potential for biofuel production. Despite the industrial significance, the precise lipid composition and inventory of lipid metabolizing enzymes of *R.opacus* PD630 is not well characterized. *Mycobacterium tuberculosis* (Mtb), the etiological agent of Tuberculosis, manipulates the lipid metabolism as one of the strategies to evade the immune attack of the host. Lipid diversity has been studied in detail in Mtb, but the lipid metabolic adaptations of Mtb in the host microenvironment are poorly studied. MA are common molecular features in both of the above-mentioned cases. Thus, the aim of this thesis is to investigate the different aspects of lipid metabolism in Corynebacterineae members, Mtb and *R.opacus* PD630 using a combination of omics methodology platform.

A targeted MS approach was used to explore the diversity of MA, free fatty acids, acyl glycerols in *R.opacus* PD630 and seven other *Rhodococcus* species. This descriptive analysis can be used for complementing taxonomic classification (chapter 2). Apart from lipids, the proteins (enzymes) involved in lipid metabolism of Corynebacterineae species are of great interest for biotechnological applications and for designing drug targets against disease causing species. An activity-based protein profiling approach has been applied here to identify lipid-metabolizing enzymes

using analogues of a lipase inhibitor (Tetrahydrolipstatin, THL) in *R.opacus* PD630. In this thesis, I identified 25 proteins belonging to the hydrolases, oxidoreductases and ligases classes of enzymes (chapter 3).

MA in Mtb and other Mycobacterium species has been studied in detail for their role in virulence, drug development and environmental adaptation. Our research group has earlier classified Mtb complex and other Mycobacterium species based on their MA profile using MS approaches. In this study, I have extended the targeted MS approach to study the MA variations from four different geographical lineages namely East-Asian, Indo-Oceanic, Euro-American and West African-2 (chapter 4). MA extracted from the culture of these lineages did not exhibit major lineage specific patterns. In a macrophage host environment, MA variations were of similar pattern among all the lineages. However, substantial differences were found when mycolate patterns from cultured bacteria were compared to those harvested from infected macrophages. Inside the macrophages, the alpha and C26 alkyl chain MA increased in abundance and the relative proportion of keto-MA to methoxy-MA decreased among all lineages. This signifies the highly conserved Mtb strategy to encounter the host environment despite the variable strain characteristics.

In general, Corynebacterineae have evolved a complex network of lipid metabolism. Clarifying its metabolism will not only provide a better understanding of the pathogenesis and biotechnological potential of its members, but also an understanding on the evolution of lipid metabolism in Corynebacterineae.

List of Tables

List of Figures

List of Abbreviations

ABPP	Activity based protein profiling
BCG	Bacillus Calmette-Guerin
BSL-3	Biosafety level-3
CD1	Cluster of differentiation 1
CuSO4	Copper (II) sulphate
Da	Dalton
DAG	Diacylglycerol
DIM/PDIM	Pthiocerol dimycocerosates
DMSO	Dimethyl sulfoxide
EDTA	Ethylenediaminetetraacetic acid
ESI-MS	Electrospray ionization mass spectrometry
FFA	Free fatty acid
GM-CSF	Granulocyte macrophage -colony stimulating factor
HIV	Human immunodeficiency virus
HPLC	High performance liquid chromatography
IL-12p40	Interleukin 12
INH	Isoniazid
kDa	Kilo Dalton
LB	Lysogeny broth
LC-MS	Liquid chromatography mass spectrometry
LM/LAM	Lipoarabinomannans
LSPs	Long sequence polymorphisms
LTQ-FTMS	Linear ion trap-Fourier transform-mass spectrometer

m/z	Mass by charge ratio
MA	Mycolic acid
mAGP	Mycolyl arabinogalactan peptidoglycan complex
MAME	Mycolic acid methyl ester
Mb	Mega bytes
MDAG	Mycolyl diacylglycerol
MRM	Multiple reaction monitoring
MS	Mass spectrometry
MS/MS	Tandem mass spectrometry
Mtb	*Mycobacterium tuberculosis*
MTBC	*Mycobacterium tuberculosis* complex
NTM	Non-tuberculous mycobacteria
OD_{600nm}	Optical density at 600 nm
PBMC	Peripheral mononuclear cell
PBS	Phosphate buffered saline
PGL	Phenolic glycolipids
ppm	Parts per million
QTOF	Quadrupole time-of-flight
QTRAP	Triple Quadrupole/Linear Ion trap mass spectrometer
rRNA	ribosomal Ribonucleic acid
SDS	Sodium dodecyl sulphate
Ser	Serine
SL	Sulfolipids
TAG	Triacylglycerol
TB	Tuberculosis

TBAH	Tetrabutylammonium hydroxide
TBTA	Tris[(1-benzyl-1H-1,2,3-triazol-4-yl)methyl]amine
TCEP	Tris(2-carboxyethyl)phosphine
TDM	Trehalose dimycolate
THL	Tetrahydrolipstatin
TLC	Thin layer chromatography
TLRs	Toll like receptors
TMM	Trehalose monomycolate
TNF	Tumor necrosis factor
UFLC	Ultra fast liquid chromatography

1 Introduction

1.1 Corynebacterineae

Corynebacterineae form a distinct group of high G+C, Gram-positive bacteria under the Actinomycetales order (Fig.1.1). Corynebacterineae though classified as Gram-positive, harbours cell envelope features of both Gram-positives and Gram-negatives. Genome-based phylogeny studies have placed them in between Gram- positives and negatives [1]. The cell envelope of Corynebacterineae is unusually complex with high content of lipids, which constitute 40% of the cell dry weight [2]. Corynebacterineae comprise *Corynebacterium*, *Mycobacterium*, *Nocardia*, *Rhodococcus* and other genera. *Mycobacterium* includes the important pathogens *Mycobacterium tuberculosis* (Mtb) and *Mycobacterium leprae,* which are known to cause tuberculosis (TB) and leprosy, the oldest known diseases of mankind. *Rhodococcus* includes some of the industrially important microbes involved in bioactive steroid production, biodesulfurization and production of acrylamide [3].

- Domain: Bacteria
  - Kingdom: Bacteria
    - Phylum: Actinobacteria
      - Class: Actinobacteria
        - Subclass: Actinobacteridae
          - Order: Actinomycetales
            - Suborder: **Corynebacterineae**
              - Family: *Corynebacteriaceae- Corynebacterium*
                Mycobactericeae- ***Mycobacterium***
                Nocardiaceae- ***Rhodococcus,*** *Nocardia*

Figure 1.1: Complete parentage of Corynebacterineae suborder.
Corynebacterineae includes seven families but only the families relevant to the study are listed in the parentage (www.cict.fr/classifphyla.html#Corynebacterineae).

1.1.1 *Mycobacterium*

Mycobacteria are aerobic, non-motile rods, selectively distinguished from other bacteria by their acid fastness to Ziehl Neelsen stain [4]. Mtb and *Mycobacterium leprae* were the species that originally represented *Mycobacterium*. For many years, bacterial species identified with similar staining characteristics as Mtb were addressed as 'atypical mycobacteria'. Runyon's (Runyon, 1959) classification based on phenotypic features (growth rate and pigmentation) still remains as a popular classification method even with clinicians [5]. These 'atypical mycobacteria' are widely appreciated now as potential human pathogens due to their ability to cause pulmonary infections other than TB, and hence called as non-tuberculosis mycobacteria (NTM) (American Thoracic Society, 1990). Research initiatives spanning the entire *Mycobacterium* genus are directly or indirectly providing cues to treat the worldwide spreading deadly disease, TB.

1.1.2 *Rhodococcus*

Rhodococci are aerobic, non-motile, Gram-positive, mycolate containing species resembling other Corynebacterineae genera. *Rhodococcus* live in varied environmental niches from soil to aquatic plants and with unique catabolic versatility [6, 7]. While *Mycobacterium* genus is famous for its medical significance, *Rhodococcus* gained attention owing to its medical, veterinary, ecological and industrial (Table.1.1) significances [8]. They are able to degrade various substrates such as halogenated compounds, numerous aromatic compounds and several polycyclic aromatic hydrocarbons [9]. In 1992, there were 12 established species in *Rhodococcus* genus [10]. The number increased to 48 in 2010 with 16 other new species finding arbitrary placement in the *Rhodococcus* genus [11]. Though there is a constant addition of new species in *Rhodococcus*, their strength is still behind *Mycobacterium* genus with 120 species [12]. One of the major research challenges posed by Corynebacterineae members irrespective of their lifestyle, is the elucidation

of cell wall assembly mechanism and the regulation in changing environmental conditions.

Table 1.1: Selected *Rhodococcus* species information

Species	Original habitat of isolation	Genome status	Significance
R.jostii RHA1	Lindane contaminated soil [13]	Completed [14]	Polychlorinated biphenyl degradation [13]
R.opacus PD630	Soil of gas-works plant [15]	Completed [16]	Hydrocarbon degradation; biofuel model organism [15]
R.equi 103S	Horse [17]	Completed [18]	Equine pneumonia; Opportunistic infection in immunosuppressed humans [17]
R.fascians	Plants [19]	-	Phytopathogen-leafy gall disease [20]
R.aetherovorans I24	Toluene contaminated aquifer [21]	-	Indene bioconversion [21]
R.globerulus	Soil [22]	-	Polychloro biphenyl degradation [23]
R.rhodochrous	Soil/activated sludge foam [24]	-	Immunocompromised infection [25]; Acrylamide production [26]
R.coprophilus	Herbivorous dung/activated sludge foam [27]	-	River pollution from animal faeces [28]
R.zopfii	Toluene-phenol bioreactor [29]	-	Toluene degradation [29]

1.2 Cell Envelope of Corynebacterineae

The cell envelope of Corynebacterineae is multilayered with a typical inner phospholipid bilayer, a characteristic wall of unusual structure, and a complex outer layer (Fig.1.2). Since Minnikin's landmark contribution, the cell envelope model has undergone constant revision by extensive studies [30-33]. Although cell envelope organizational studies are more detailed with mycobacteria than with other related genera, it is evident that Corynebacterineae members share similar ultra-structure and cell-wall composition [34, 35].

Meso-diaminopimelic acid-containing peptidoglycan layers are covalently linked to arabinogalactan to form the cell walls of Corynebacterineae. The arabinogalactan is in turn esterified to α-alkyl, β-hydroxy long chain fatty acids, called mycolic acids (MA). The hydrophobic chains of MA are tightly packed in a perpendicular manner to the plane of the cytoplasmic membrane [36]. This hydrophobic MA layer provides a scaffold of attachment for (glyco) lipids, polysaccharides, lipoglycans and porins [37]. The noncovalently bound lipids are arranged in an outer leaflet to form a complex asymmetric bilayer [38]. Sulfolipids (SLs), pthiocerol dimycocerosates (DIM/PDIM), methyl branched fatty acids and lipoarabinomannans (LM/LAM) are some of the outer layer lipids unique to Corynebacterineae. Some of these outer layer lipids are widely distributed in Corynebacterineae, while others are restricted to particular species [7, 39]. Thus, the cell wall permeability barriers in Corynebacterinae engage both covalently bound MA and the noncovalently bound free lipids. These chemical molecules together with various envelope proteins with pore forming properties encompass the bulk of the cell envelope [40]. This cell envelope substantially contributes to the protection of Corynebacterineae against detergents, hydrophobic drugs and other noxious substances.

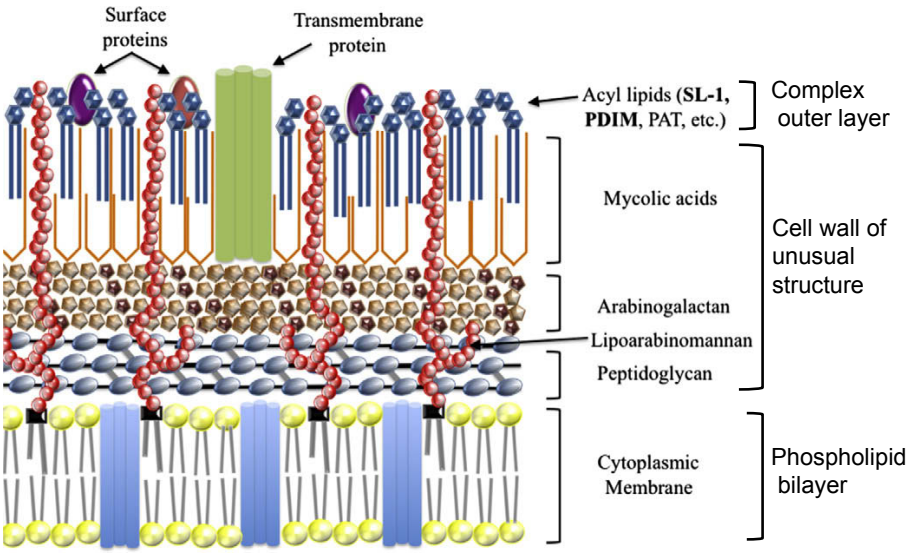

Figure 1.2: Representation of the major cell envelope features of Corynebacterineae. Figure adapted from Ouellet *et al*., 2010 [41].

1.2.1 Cell envelope and Chemotaxonomy of Corynebacterineae

Many new Corynebacterineae species are identified with increasing awareness of the significance of these species in clinical and nonclinical environment. Hence, there is a need for appropriate classification of this rapidly growing suborder [11]. Besides the consideration of numerical taxonomic features and molecular taxonomic features (16S rRNA sequence analysis), chemotaxonomic features related to cell envelope architecture were given importance in resolving classification ambiguities in Corynebacterineae members (Table.1.1) [42]. The chemotaxonomic features included were peptidoglycan structure, MA chain length, cell wall sugar chemistry, fatty acids and polar lipids composition and menaquinone chemistry [42]. Of the different chemotaxonomic features, MA receives special attention in the classification of Corynebacterineae. With improved bio analytical techniques, MA structural diversity has evolved into a powerful tool even for species level identification [43-45].

Table 1.2: Major chemotaxonomic differences between the genera of Corynebacterineae [5, 46, 47]

Character	*Corynebacterium*	*Mycobacterium*	*Nocardia*	*Rhodococcus*
Cell wall sugars	Arabinose galactose	Arabinose galactose	Arabinose galactose	Arabinose galactose
Peptidoglycan type	A1-γ	A1-γ	A1-γ	A1-γ
Muramic acid substitution	Acetylated	Glycolated	Glycolated	Glycolated
Degree of acid-fastness	Sometimes weakly acid-fast	Usually strongly acid-fast	Often partially acid-fast	Often partially acid-fast
Mycolic acid chain length	22-38	60-90	40-64	30-54
Mena-Quinone type	MK-8(H_2); MK-9 (H_2)	MK-9 (H_2)	MK-9 (H_4)	MK-8(H_2); MK-9 (H_2)
Phosphatidyl-ethanolamine	-	+	+	+
Tuberculostearic acid	(+) some	±	+	+

1.3 Mycolic acid

The long chain lipid MA exists in two different forms in the cell wall. The majority of MA are esterified to terminal arabinofuranosyl residues of arabinogalactan, which is covalently attached to the peptidoglycan moiety forming the mycolyl-arabinogalactan-peptidoglycan complex (mAGP) [48]. MA in smaller amounts exist as readily extractable esters of carbohydrate moieties or as free MA.

1.3.1 MA as free lipids

MA exists as conjugates of trehalose, glucose or glycerol moieties in the outermost layer. Trehalose can contain one or two MA moiety forming trehalose dimycolates (TDM) and trehalose monomycolates (TMM). Extensive studies in Mtb have identified the role of MA in stimulation of innate, early adaptive and both humoral and cellular adaptive immunity [49, 50]. Expecting similar functional roles for trehalose mycolates in the equine pathogen *Rhodococcus equi*, analytical methods have been recently developed for its characterization [51]. Trehalose mycolates are also essential for MA storage and act as MA carriers in Corynebacterineae [52]. Along with trehalose mycolates, MA also exists as esters of glucose and glycerol moieties. Functional roles and structural characterization studies of such molecules are limited in Corynebacterineae, even in the case of Mtb. Mono mero mycolyl diacylglycerol is one such glycerol conjugated MA identified in few *Mycobacterium* species [53]. Given the ability of some species of Corynebacterineae to accumulate significant amounts of TAG [54-56], glycerol conjugated MA could be key to carbon storage capabilities of the bacteria. Very few studies (Table.1.3) attempted to identify such molecules in *Rhodococcus*, but the functional properties of which have not been explored in detail.

Table 1.3: Literature reports on glycerol conjugated MA

Glycerol conjugated MA	Species	Reported information
Glycerol monomycolates		
[57]	*Rhodococcus erythropolis*	Structural characterization
[58, 59]	*Mycobacterium bovis* BCG	Immunostimulatory activity and structural characterization
Mono mero mycolyl diacyl glycerol [53]	*Mycobacterium kansasii*	Growth kinetics and drug impact
Mycolyldiacylglycerols [60]	*Mycobacterium smegmatis*	Impact of *lsr2* gene mutation on synthesis

1.3.2 Structural diversity of mycolic acids

Structural variations of MA have influenced chemotaxonomic classification of Corynebacterineae [43, 61]. Primarily, variations arise from the carbon chain length and functional group decorations on the meromycolate chain of MA (Fig.1.3). Total carbon chain lengths of MA are in the range of C60-90 in *Mycobacterium* [52, 62]; C42-66 in *Nocardia* [63]; C30-54 in *Rhodococcus* [64, 65] and C28-40 in *Corynebacterium* [66, 67]. Thirteen different classes of MA have been identified in *Mycobacterium*, contributed by different functional group modifications on the meromycolate chain [68]. The three major classes are (i) alpha-MA that has two cyclopropane rings in *cis* configuration; (ii) methoxy-MA that has a methoxy group and cyclopropane ring at either *cis* or *trans* configuration; (iii) keto-MA that has a keto group and cyclopropane ring at either *cis* or *trans* configuration (Fig.1.3). Methoxy-MA and keto-MA along with few other classes with oxygenated functional group on their meromycolate chain are referred to as oxygenated mycolates. Single class of MA is found in the other three genera with one or more double bonds decorating the meromycolate chain (Fig.1.3). Heterogeneity in α-alkyl chain length is

also evident within the mycolates of Corynebacterineae members. *Mycobacterium* consistent with meromycolate chain also has highest total carbon in alkyl side chains (C20-C26) [62] compared to other genus (mostly < C20). Altogether, most complex group of MA is found in *Mycobacterium*.

Ninety years back Anderson first isolated MA from extracts of tubercle bacilli [69]. Several bioanalytical techniques have facilitated the structural characterization of mycolic acids over the decades. Beginning in the 1940s, chemists characterized MA by grinding mycobacteria cells followed with separation on thin layer chromatography. With the dawn of improved mass spectrometry (MS) and nuclear magnetic resonance techniques in 1980s, the molecular and chemical signatures of MA were determined. The first in the series of MS techniques, gas chromatography MS (GC-MS) was successfully applied to characterize the MA of Corynebacterineae members [70, 71]. GC-MS analysis of MA involved elaborate derivatization procedures prior to analysis. High performance liquid chromatographic procedures overcame the need for derivatization and were widely applied for MA based speciation of mycobacteria [43, 72]. Simultaneous advent of electrospray ionization MS and matrix-assisted laser desorption/ionization (MALDI) techniques further enhanced the characterization of MA species in mycobacteria [73, 74]. In a landmark work, Watanabe *et al*., 2001 [68] identified and collated the functional group localization in meromycolate fragments, revealing the complete complexity of MA mixtures in Mtb strains. Recently our group employed ESI-MS analysis in a targeted approach to analyze MA of mycobacteria in a high throughput fashion [75]. The molecular heterogeneities of MA determined using the various bioanalytical techniques strongly emphasize their impact on MA functional capabilities in Corynebacterineae [76].

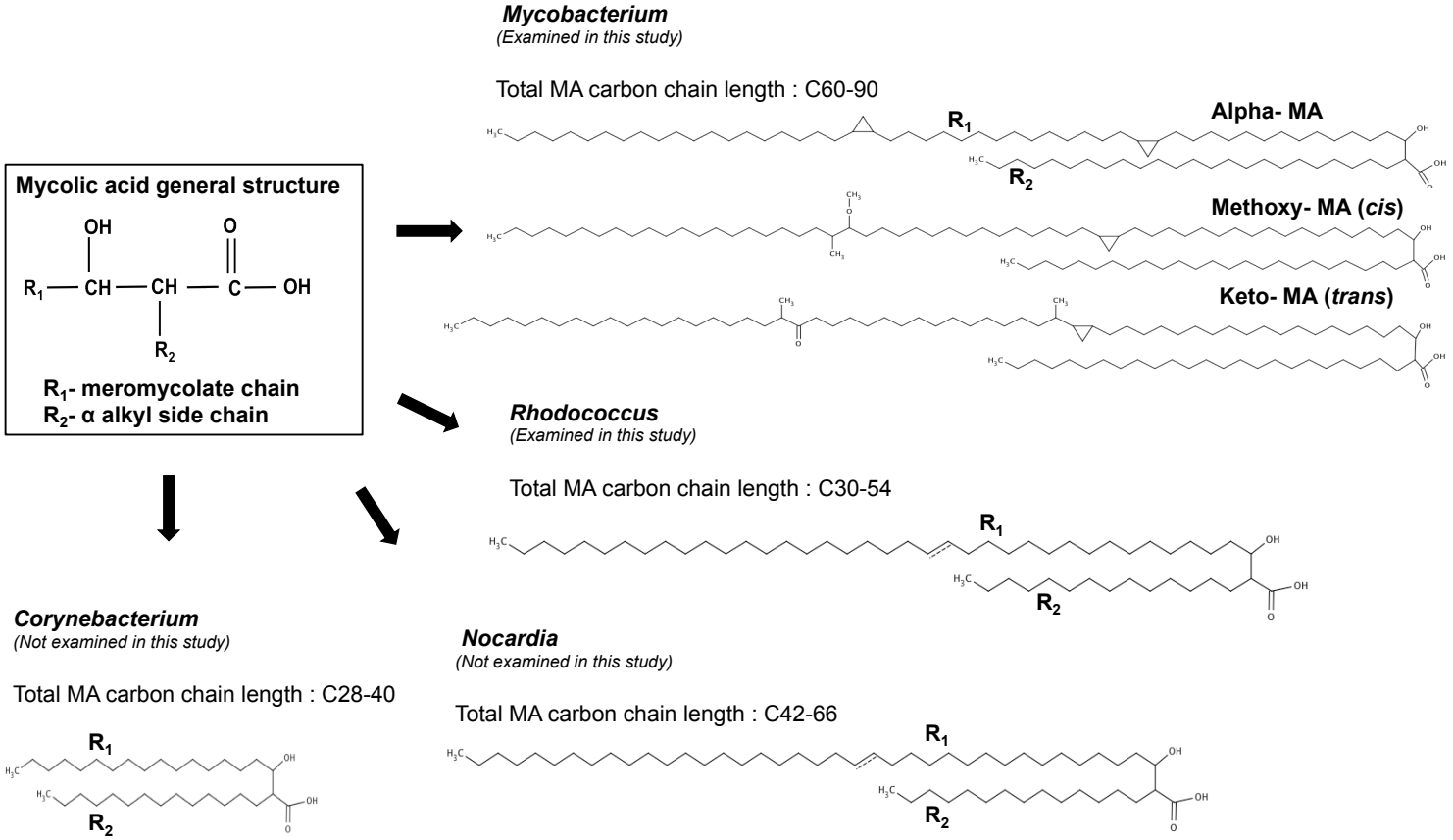

Figure 1.3: Structure of mycolic acids in Corynebacterineae.

1.3.3 Functional diversity of MA

The hydrophobic nature of MA provides protection against dehydration, chemical damage and antibiotics [62]. MA is partially responsible for the acid-fast behaviour of some Corynebacterineae [77, 78]. MA significantly attributes to the relative impermeable feature of the cell wall [78]. This makes the cell wall less permeable to hydrophobic antibiotics and extremely less permeable to hydrophilic substrates [34] [79]. Apart from the significant functional roles of attached MA and trehalose MA, recently free MA have been implicated in biofilm formation, affecting the surface adherent properties and colony formation [80]. Altogether, MA confers diverse functions in the different Corynebacterineae species.

1.3.3.1 MA of *Mycobacterium*

MA of mycobacteria have many common features, but there are typical differences both in the functional group modifications in the meromycolate chain and in the balance of different chain lengths [76]. Considerable differences in the complex mixtures of MA provides a unique biochemical fingerprint for almost each of the 100 over mycobacteria species [68]. The MA of slow growing pathogenic bacteria such as Mtb are modified with cyclopropane rings, methyl groups, methoxy and keto groups (Fig.1.3). Mtb encodes eight S-adenosyl methionine (SAM) dependent methyl transferases, out of which six are involved in mycolic acid modification [81-85]. Generally two main hypotheses have been proposed for the pathogenic function of MA modifications in Mtb. Firstly, for the importance of cyclopropanation in membrane function (cell envelope integrity and rigidity) and secondly for the role in immune activation [82, 86]. Mtb strains lacking oxygenated MA [82] or cyclopropanated MA [87] were found to be highly attenuated and hyper inflammatory in mice. Hence it is indispensable to investigate the dynamics and functional contribution of mycolic acids in the current state of TB disease pathogenicity and severity.

1.3.3.1.1 Lipids: one of the survival strategies of persistent *Mtb*

Tuberculosis is ranked second in leading cause of deaths from an infectious disease in the world after human immunodeficiency virus (HIV), with 1.4 million deaths in 2011 (WHO, TB global report 2012). HIV co-infection further compounds the problem with additional increased risk of developing active disease and occurrence of drug resistant bacteria [88]. Robert Koch discovered the tuberculous bacilli 131 years ago. Since then immense research progress have been attained in understanding the disease pathogenesis. However drug resistance and persistent behaviour of Mtb are the obstacles in the path to successful TB treatment. Inadequate and incomplete treatment strategies accompanied with inadequate treatment adherence are the major factors contributing to emergence of drug resistance in TB endemic regions of the world [89].

Isoniazid (INH), rifampicin (RIF), ethambutol (EMB), pyrazinamide (PZA) and streptomycin (STR) are the first line drugs used for TB treatment. Mtb resistant to INH and RIF, with or without any resistance towards other first line drugs are termed multi-drug resistant strains (MDR) [90, 91]. MDR necessitated the use of second line drugs such as fluoroquinones, ethionamide, cycloserine, caperomycin, kanamycin, amikacin and para-aminsalicylic acid. However these second line drugs were more toxic and less effective. Between 2000-2004 TB world witnessed the emergence of extensively drug resistant (XDR) strains [92]. Those MDR strains that are resistant to any fluoroquinone and to at least one of the three injectable second line drugs are termed XDR strains. While TB researchers are still struggling to eliminate MDR and XDR, reports started to reveal the emergence of totally drug resistant Mtb strains (TDR), which are resistant to all first and second line drugs [93, 94]. With currently no new drug candidates identified for TB treatment, the only option left is to retool the existing drugs for optimized treatments [95]. Hence aggressive efforts are required to unravel the survival strategies of Mtb, which remains key for the

discovery of better drugs and vaccine against TB. Survival of Mtb in human host despite the use of antibiotics has led to a persistent state of the bacterium [96]. Persistent Mtb not only contributes to resistance against existing TB drugs but also poses difficulty in discovering new drug targets, as there is less information on the metabolic state of the persistent Mtb. Hence, a thorough investigation of the complete infection cycle of Mtb and its interaction with the host factors are essential.

Droplets or nuclei containing tubercle bacilli are expelled by coughing and hence are the major route of transmission from infected individuals to healthy individuals. After inhalation, the bacilli are phagocytosed in the alveolar macrophages of the lungs, which is the primary site of infection (Fig.1.4A). The infected alveolar macrophages release proinflammatory cytokines there by triggering the recruitment of monocytes and neutrophils from the neighbouring blood vessel (Fig.1.4B). Through continuous cytokine and chemokine signaling, more immune cells are recruited to form the granuloma structure, [97, 98] the pathological hallmark of TB (Fig.1.4C). Macrophages differentiate into epitheliod cells or foamy macrophages that form the core of a granuloma (Fig.1.4D). The bacterium is contained in the granuloma as persistent creatures [99]. At this stage the infected individual does not show any signs or symptoms of active TB. The infected individual is a silent carrier of the bug and termed to have latent TB [100]. The progression from latent to active TB might occur when the host immune system weakens. In the case of active disease, granuloma becomes necrotic, forming lipid-rich caesums [101] at its core (Fig.1.4E). This leads to the rupture of the bacterial containment, releasing bacilli into the lung airway and finally paving way to disease transmission (Fig.1.4F) [102]. From a host centric view, the granulomatic lesions are a failure of the immune system. From Mtb point of view, it is still a mystery as to how the bacterium can manipulate the host immune response and use it for its own advantage of completing the infection cycle.

The strategies used by Mtb to evade host defenses are phagosome maturation arrest, host immune suppression and secretion of cytotoxic factors [103]. Flux analysis study has demonstrated carbon flow redistribution in growth arrested Mtb [104]. This is one such evidence of lipid metabolic adaptations of Mtb under stress conditions. Hence, it is interesting to determine the role of lipids in all these survival efforts of Mtb.

- **Phagosomal maturation arrest:** Mtb residing in the phagosomal compartments of the macrophages inhibit phagosome lysosome fusion to form phagolysosomes. Mtb achieves this inhibition by restricting the acidification of phagosomes, which is a crucial criterion for fusion event [105]. Independent studies have identified the contributions of lipoarabinomannans (LAM) [106], trehalose 6,6'dimycolate (TDM) [107] and phenolic glycolipids (PGL) [108] in the maturation arrest of phagosomes.
- **Host immune suppression:** Different bacteria employ host immune suppression as a defence mechanism against the host [109, 110]. Many mycobacterial lipids have been shown to interfere with the proinflammatory immune measures of the host, which are key to the recruitment of innate effector cells to the site of infection. For instance, LAM has been found to execute differential immune modulatory activities based on its structural variations [111]. In general mycobacterial lipids have been found to interfere in T-cell responses to stimulation [112].

While we elaborate on the role of many lipids in the persistence of Mtb, it is intriguing to decipher the role of MA, given its abundance in the cell wall core.

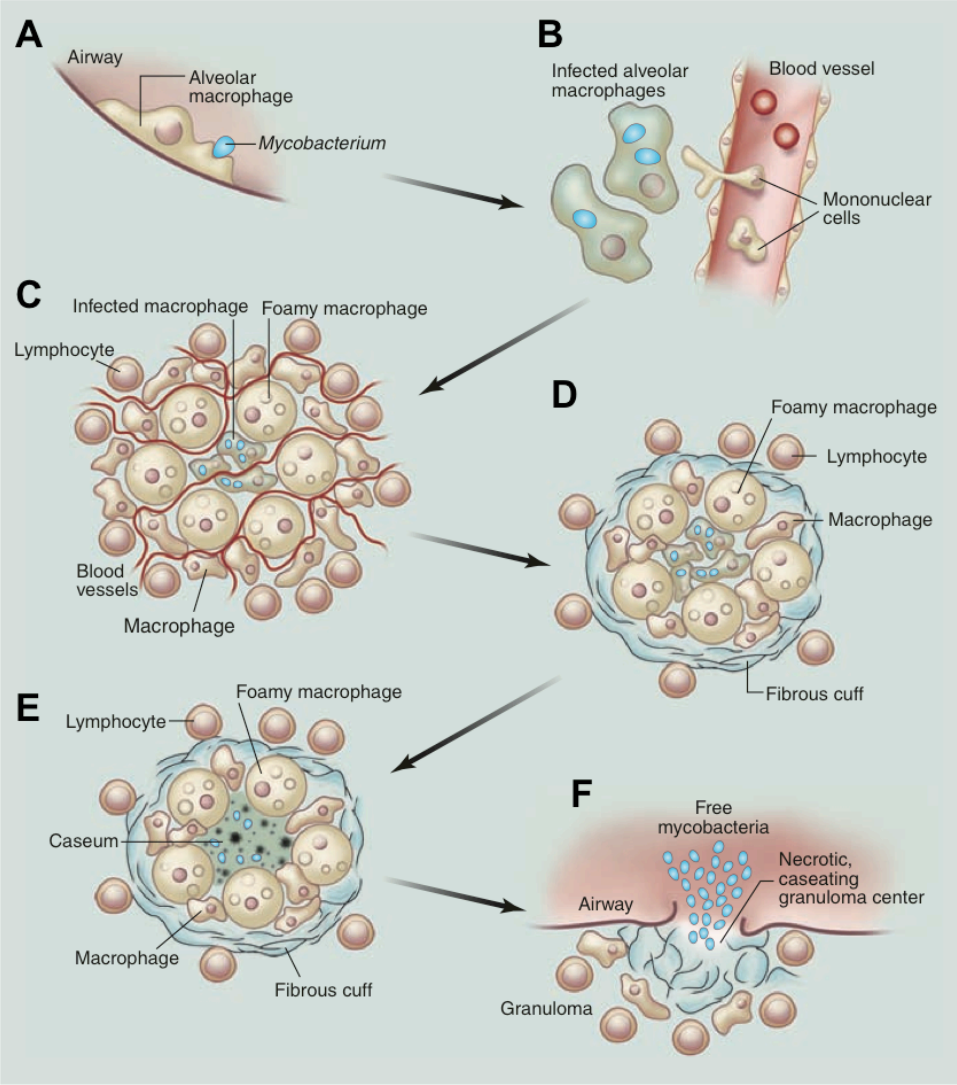

Figure 1.4: *Mycobacterium tuberculosis* infection cycle. Figure adapted from Russell *et al*., 2010 [113].

1.3.3.1.2 Mycolic acids and Mtb survival

Mtb in the human alveolar macrophage is exposed to the most toxic oxygen metabolites. However, Mtb lacks a conventional oxidative stress response system to combat the oxidative stress [114]. But as part of the constitutive defense system Mtb produces cyclopropanated MA, which offers resistance against toxic oxygen species mediated killing [62]. In addition to the defense strategies, MA also contributes to Mtb's immune evasion strategy, along with other cell envelope lipids. MA, the first known CD-1 presented lipid antigen [115] has been shown to selectively repress

macrophage IL-12p40 production. One of the methyl transferases the *mmaA4* gene, which introduces oxygenated functional groups at the distal end of MA is a key player in this immune suppression [116]. In addition, according to a model postulated by Kim *et al*., [101], upon the caseation of granulomas Mtb releases some of its cell wall mycolates in the form of vesicles that induce formation of foamy macrophages. As discussed earlier, foamy macrophages are critical for the survival of persistent Mtb. Characterization of the lipid population of the exocytosed vesicles revealed the presence of trehalose mycolates (TDM and TMM) along with PDIM and PGL [117]. Also noteworthy, some of the existing chemotherapeutic agents for TB treatment target the mycobacterial cell wall synthesis. Isoniazid (INH), the major first line drug inhibits mycolic acid synthesis in actively growing Mtb [118]. INH is still used in treating latent TB inspite of its low susceptibility towards hypoxic [119] and stationary phase *Mycobacterium* [120]. But INH treatment administered for 9 months in the case of latent TB significantly reduced the risk of the disease [121]. More effective drugs are required to completely eradicate latent TB and preferentially reduce the chemotherapy duration, which would be a more powerful weapon against TB. Given the myriad functional role of MA, its modifications during the persistent stage *in vivo* is not clearly understood. This knowledge is very much essential for justifying the choice of MA and the enzymes of mycolic acid biosynthetic pathway as potential TB drug targets.

1.3.3.2 MA of *Rhodococcus*

The genus *Rhodococcus* is a complex group of organisms, which urgently needs concentrated research initiatives on the basic biochemistry, physiology and molecular biology aspects. Such initiatives will certainly be advantageous in exploiting the complete potential of the catabolic versatility in *Rhodococcus.* This ability is based on distinctive features such as physiological robustness, ability to acquire catabolic genes, and tolerance to toxic substrates [122, 123]. Physiological robustness provided

by the lipid rich cell envelope is one another distinctive feature complementing the genome of rhodococci in its biodegradation and bioremediation potential [124]. Many rhodococci have been isolated from naturally hydrophobic environment and hence making them suitable candidates for bioremediation. The hydrophobic cell envelope and biosurfactants generation by rhodococci enable them to tolerate many hydrophobic pollutants and solvents [125, 126]. Certain alkane-degrading rhodococci can adhere to oil droplets due to the presence of the long chain, hydrophobic mycolic acids (MA) in their cell envelope [127, 128]. Furthermore, surface free lipids containing mycolic acids and other glycolipids act as biosurfactants and thereby enhance the bioremediation processes [129]. Some rhodococci even tolerate extreme growth conditions such as low temperature [130], cold climates [131] and electric current [132], owing to the rigid cell wall. Changes in temperature, pH etc., could cause structural changes in the cell envelope, predominantly in MA and thereby altering the membrane fluidity [67, 133]. The membrane properties have huge impact on the uptake of hydrophobic substrates and tolerance towards harsh chemical environments. Therefore, biochemical analysis of the MA diversity will greatly augment the efforts to understand the mechanism behind rhodococci physiological tolerance.

1.4 Lipid metabolism in Corynebacterineae

Corynebacterineae produce diverse lipids unmatched by other groups of bacteria. The members of Corynebacterineae are capable of producing simple fatty acids to complex and hydrophobic lipid molecules. Studies on Corynebacterineae provide excellent opportunities to investigate the complexity and diversity of lipid metabolic pathways in bacteria. Genome sequencing projects along with biochemical approaches aimed at deciphering the pathogenic behavior of Mtb [134] has provided enormous knowledge of lipid metabolism events in Mtb and other *Mycobacterium* species. However, it is not the case in rhodococci despite their industrial importance. With many genomes published in mycobacteria genus, comparative genomic analysis has provided immense insights into the biology of mycobacteria. The number of completely sequenced genome in *Rhodococcus* is less than ten (http://www.ncbi.nlm.nih.gov/). This disparity in the two genera reflects on the poor knowledge of *Rhodococcus* biology. Recent genome sequencing efforts [14, 16] are starting to fill the knowledge gap between *Rhodococcus* and *Mycobacterium*. Mtb has ~ 250 genes related to fatty acid metabolism whereas the common gut bacterium *Escherichia coli* has only 50 of such genes [134]. A step ahead, *Rhodococcus jostii* RHA1 (*R.jostii* RHA1) and *Rhodococcus opacus* PD630 (*R.opacus* PD630) are among the largest bacterial genomes with ~ 400 genes involved in lipid metabolism. This genomic feature of Corynebacterineae members suggests the physiological importance of lipid metabolism. Therefore, it is vital to understand the enzymatic mechanisms involved in the synthesis and degradation of lipids in Corynebacterineae.

Table 1.4: Genome comparison of selected Corynebacterineae species.

	***Mycobacterium Mycobacterium tuberculosis* H37Rv**	***Rhodococcus Rhodococcus opacus* PD630**
Genome size (Mb)	4.41	9.27
Lipid metabolism genes[a]	~ 250	~ 400
α/β hydrolases[b]	101	204
Lipases[c]	24	33
TAG synthases-Diacyl glycerol acyl transferases	15	14

[a] The number of gene products predicted to be associated with lipid metabolism in Mtb and *R.opacus* PD630 **[14, 16, 134]**.

[b] The number of gene products with α/β hydrolase superfamily domain assignments, obtained from *Superfamily 1.7* (http://supfam.cs.bris.ac.uk/SUPERFAMILY/) database.

[c] The number of predicted lipases in Mtb and *R.opacus* PD630 **[14, 16, 134]**.

1.4.1 Hydrolase

Enzymes are classified into six main classes based on the chemical reactions they catalyze (Fig.1.5). Hydrolase (EC 3) is the most populous enzyme class, catalyzing the hydrolysis of chemical bonds. Based on the type of bond (ester, ether, amide etc.,) to be hydrolyzed, hydrolases are divided into 13 subclasses. The first subclass, ester hydrolase (EC 3.1) or esterase is further sub-divided into several classes based on the nature of ester bonds they hydrolyze. Carboxylic ester hydrolase (EC 3.1.1) catalyze the hydrolysis, synthesis and transesterification of an ester bond. In the presence of water, they catalyze the hydrolysis of an ester bond, but in the presence of an organic solvent they cause the transesterification reaction [135]. Carboxylic ester hydrolases are ubiquitous and have been found in all domains of life [136]. Carboxylic ester hydrolase is clustered into 93 groups based their substrate preference. Several groups of carboxylic ester hydrolase are involved in lipid metabolism and few of them are highlighted in Fig.1.5. Two major carboxyl esterases of utmost importance are carboxyl esterase (EC 3.1.1.1) and triacylglycerol hydrolase or lipase (EC 3.1.1.3). Carboxyl esterases hydrolyze small ester (≤ 10 carbon atoms) containing molecules that are at least partially soluble in water [137]. Lipases generally catalyze the hydrolysis of ester bond of mono-, di-, tri- glycerides, resulting in the formation of long chain fatty acids and glycerol. Lipases are distinguished from carboxyl esterases by their ability to hydrolyze carboxyl esters of long chain acyl glycerols (≥ 10 carbon atoms) [138]. Lipases are also capable of exhibiting other activities such as phospholipase, lysophospholipase, cutinase or amidases activities [139]. The mechanism of ester hydrolysis is basically the same for carboxyl esterase and lipase owing to the presence of a signature α/β-hydrolase fold domain [140].

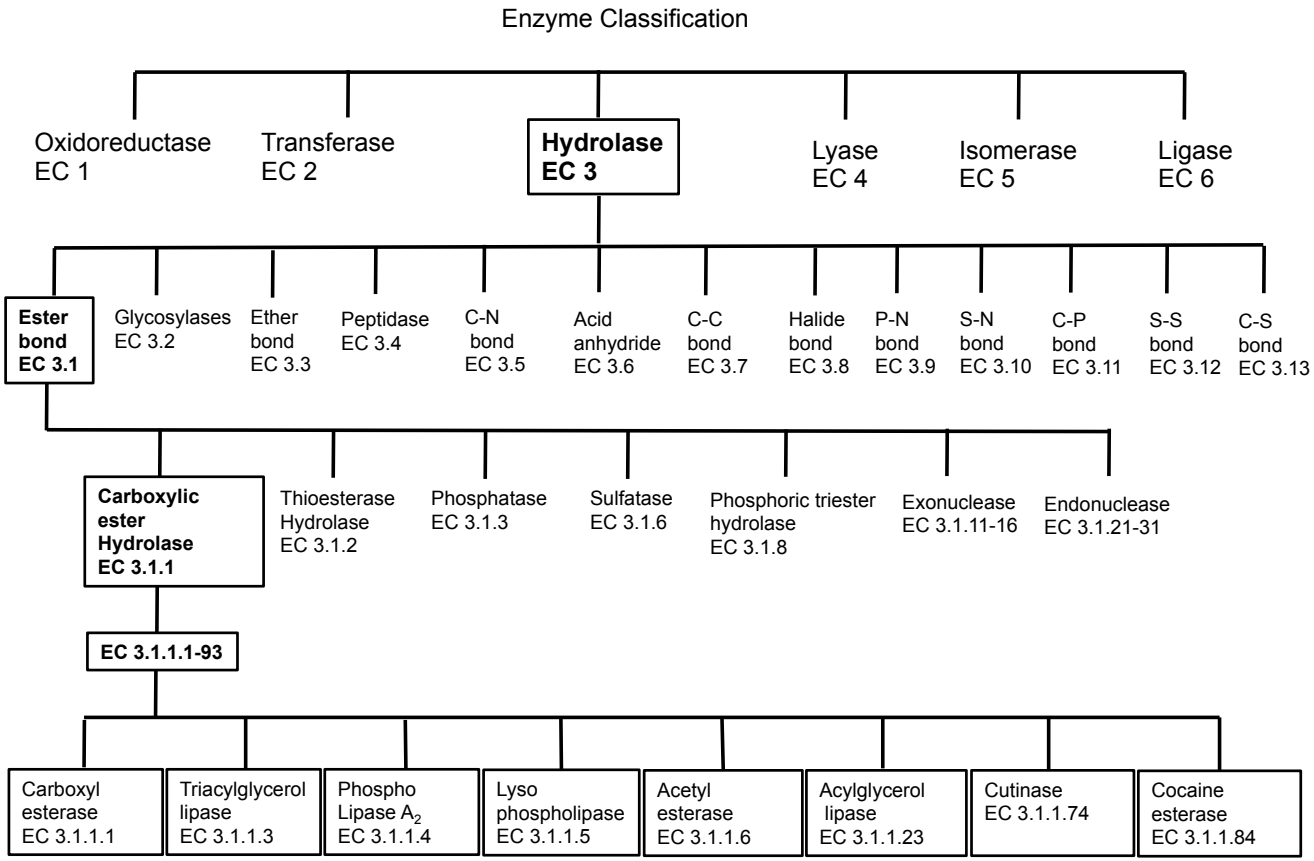

Figure 1.5: Schematic representation of enzyme classification and nomenclature. Based on reactions catalyzed, the nomenclature committee of the International Union of Biochemistry and Molecular Biology (IUBMB) has defined a system of classification for enzymes. The classification and EC (Enzyme Commission) number nomenclature for hydrolase enzymes are highlighted in rectangular boxes.

1.4.1.1 α/β hydrolase fold

Most carboxylic ester hydrolases belong to the α/β hydrolase superfamily, one of the largest known protein families [141]. The α/β hydrolase fold consists of an eight-stranded mostly parallel β sheet with the second β strand anti-parallel. The β strands are connected by the α-helices. The β sheet is highly twisted and bent to form a half-barrel structure (Fig.1.6).

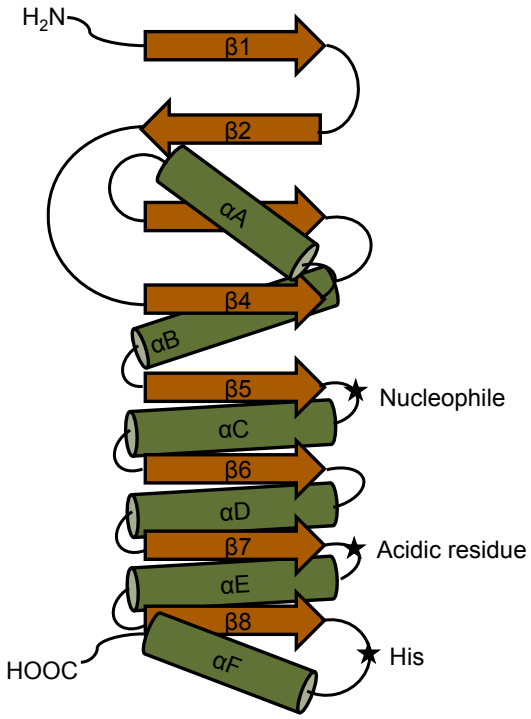

Figure 1.6: α/β hydrolase fold structure. In the topology diagram *cylinders* and *arrows* are used to represent α helices and β strands. The positions of the catalytic residues are shown as black dots.

The presence of three conserved amino acid residues characterize proteins from this superfamily [142]. The residues form a catalytic triad usually represented by serine, aspartate and histidine (His) [143]. The nucleophile is always located in a very sharp turn, referred to as the 'nucleophilic elbow'. The acidic residue of the catalytic triad is located in a reverse turn following strand β7. Histidine is an absolutely conserved residue of the catalytic triad. Thus the catalytic triad provides a stable scaffold for the active site of wide variety of enzymes like lipases, esterases, proteases and epoxide

hydrolases [142]. The broad substrate specificity and the very high region- and enantioselectivity make these enzymes suitable for biotechnological applications. The genome of Corynebacterineae members code for large number of α/β hydrolase fold proteins (Table.1.3), indicating the presence of a versatile enzyme inventory.

1.4.2 Lipid metabolism genes of *Rhodococcus*

The large genomes of *Rhodococcu*s species could bear the warehouse of genes needed to buttress the extensive catabolic pathway. The genome codes for several catabolic pathways including those for benzene, indene, phenol, naphthalene, phenyl acetate, nicotine and thiocyanate [6]. The additional number of linear plasmids provide support by further encoding genes for catabolism of alkyl benzene [144], toluene [145], biphenyl [146], and chloraromatic compounds [147]. Certain rhodococcal species upon cultivation in n-alkanes, produce fatty acids with carbon chain length related to the hydrocarbon substrates [148]. Thus, the hydrocarbon catabolic pathways seem to be coupled with the lipid metabolic pathways in *Rhodococcus* species [149]. The occurrence of *Rhodococcus* sp. in adverse environmental sites such as the arid deserts reflects their ability to metabolically cope with the prevailing nutrient limitation. It is not surprising that the highly resilient soil rhodococcal strains possess a complex metabolic pathway involved in acquisition of energy and carbon. Many *Rhodococcus* species have the ability to accumulate storage compounds such as triacylglycerol (TAG) that can be utilized as carbon sources during nutrient scarcity. Holder *et al*., [16] identified 14 putative diacylglycerol transferases in *R.opacus* PD630, which are involved in TAG synthesis. Stored bacterial TAG has to be mobilized into free acyl-residues for energy generation or to generate precursors for membrane lipid synthesis. *R.opacus* PD630 genome has 33 putative lipases that could mediate the intercellular mobilization of TAG [16], while Mtb, the intracellular pathogen has 23 putative lipases. Also, *R.opacus* PD630 has twice the number of α/β-hydrolase superfamily proteins than Mtb (Table.1.4).

Rhodococci exhibit many unique and novel lipid-metabolizing enzymes that have not been reported in any other prokaryotes [7]. But characterization and functional implication of such lipid metabolizing enzymes are still limited.

1.5 Specific aims of the thesis

Owing to their unique cell envelope architecture, Corynebacterineae suborder bacteria hold a special place in the bacterial world. The massive lipid composition of the cell envelope confers intrinsic resistance against antibiotics and chemicals. Apart from cell envelope, lipid metabolism on the whole gains significant representation in the genomes of Corynebacterineae members. It is essential to determine the influence of lipids on the physiology of a notorious pathogen like *Mycobacterium tuberculosis* as well as a non-pathogenic, industrial organism like *Rhodococcus opacus* PD630 with contrasting lifestyle habits. The first step in addressing lipid metabolism in any biological system is to capture the existing lipid diversity in the system. A sensitive and robust methodology is required to overcome the challenges posed by lipids in the form of structural complexity and magnitude. Mass spectrometry (MS) driven lipidomics approach provides the right platform to characterize and quantify lipids. A further extension of this approach enables the monitoring of lipid variations due to regulatory measures of the organism in changing environmental conditions. Our study in Corynebacterineae includes the following specific objectives:

1. To explore the MA and acyl glycerol diversity in the cell envelope of eight *Rhodococcus* species, using lipidomics platform.
2. To explore the lipid metabolizing enzyme inventory of *R.opacus* PD630, a prominent member of *Rhodococcus* genus using proteomics approach.
3. To biochemically determine the MA alterations in macrophage upon infection of different Mtb lineages.

2 Biochemical analysis of mycolyl, fatty acyl and acyl glycerol diversity in *Rhodococcus*

2.1 Introduction

Rhodococcus has a cell wall of chemotype IV like *Mycobacterium* and other Corynebacterineae members (refer Fig.1.2 for cell envelope architecture). Despite this similarity in the overall cell wall architecture, *Rhodococcus* can still be separated from other Corynebacterineae members based on the unique cell wall features. Briefly, the cell wall characteristic features of rhodococci are: presence of tuberculostearic acid; mycolic acids with total carbon chain length range of C30-54; and the major menaquinone type is dehydrogenated menaquinone [47]. In addition *Rhodococcus* comprises many free cell wall lipids that are packed outer to the mAGP complex. The various free lipids present are glycolipids including acyl and mycolyl glycolipids (refer Table.1.3), lipopeptides and glycolipopeptides. The nature of association of these free lipids with the mycolic acid bilayer is fairly unknown. Thus it is essential to explore the role of the hydrophobic cell envelope in potential applications of *Rhodococcus* such as biotransformation, bioremediation and biodegradation. This biotechnological significance of several members of *Rhodococcus* makes it unique among Corynebacterineae genera.

Apart from their excellent biodegradation and biotransformation properties, certain species of rhodococci have the ability to accumulate high levels of triacylglycerol (TAG) [15, 150]. TAGs provide fatty acids for energy utilization and membrane lipids in living organisms [151]. Previous studies identified the ability of *R.opacus* PD630 to accumulate 76% of their cell dry weight as TAG under specific growth conditions [15, 152]. A recent study claimed to have achieved 93% of *R.opacus* PD630 cell dry weight as TAG when grown in sugar cane molasses medium [153].

These results in line with Brigham *et al*., 2011 [154] work suggest the potential of *R.opacus* PD630 to generate lipid-based biofuels. Aliphatic hydrocarbons that make up the bulk molecules of gasoline are chemically similar to the fatty acyl chains of TAG [155]. The physiochemical properties of TAGs are mainly determined by the nature of fatty acids substituted in the glycerol backbone. Bacteria in the *Rhodococcus* genus have additional capability to generate odd-chain and branched chain fatty acids [55, 156].

The advent of mass spectrometry (MS) techniques has greatly benefitted the characterization of lipids. The lipid diversity in *Mycobacterium tuberculosis* has been studied extensively on account of the roles played by different lipids in disease pathogenesis. Lipidomics platform has been developed to survey the lipidic envelope in *Mtb* [157, 158]. Such studies have been instrumental in providing comparative insights into the lipid metabolism of *Rhodococcus* genus [34].

In this thesis, we used analytical techniques to screen for TAG molecules in eight *Rhodococcus* species. Additionally, we have determined the fatty acid distribution in lipids like MA and acyl glycerols. The substantial knowledge gained through the analysis of MA and TAG also allowed us to identify a new acyl glycerol related molecule.

2.2 Materials and methods

2.2.1 *Rhodococcus* strains, media and culture conditions

Rhodococcus strains used in this study are listed in Table 2.1. The strains were preserved in 20% (v/v) glycerol at -80 °C. The culture media used were lysogeny broth (LB) (Difco, Detroit, MI, USA) and a phosphate-buffered defined medium, containing 40 g glucose, 1.4 g $(NH_4)_2SO_4$, 1.0 g $MgSO_4 \cdot 7H_2O$, 0.015 g $CaCl_2 \cdot 2H_2O$, 1.0 mL trace element solution, 1.0 mL stock A solution, and 35.2 mL 1.0 M phosphate buffer per litre. The trace element solution, stock A solution, and phosphate buffer were prepared following Chartrain *et al*., [21]. Glucose, $MgSO_4 \cdot 7H_2O$ and $CaCl_2 \cdot 2H_2O$ were dissolved in deionized water and sterilized by autoclaving, and then stock A, trace elements, and $(NH4)_2SO_4$ were added to the medium as filter sterilized stock solutions. Bacteria were cultured at 30 °C. Culture optical density (OD_{600}) was used to monitor growth, and cells were harvested at mid-exponential phase. Experiments were conducted in duplicates and the mean values reported.

Table 2.1: *Rhodococcus* species examined in this thesis.

S.No.	Species	Source
1	*R.opacus* PD630	DSMZ44193
2	*R.jostii* RHA1	Gift from Lindsay Eltis, University of British Columbia
3	*R.aetherovorans* I24	*Buckland et al., 1999*
4	*R.australis*	B16935(ARS)
5	*R.coprophilus*	B16537(ARS)
6	*R.fascians*	B16939(ARS)
7	*R.globerulus*	B16938(ARS)
8	*R.zopfii*	B16942(ARS)

2.2.2 Isolation of mycolic acids from cultured *Rhodococcus* strains

MA was extracted as described by Shui.G *et al.,* [75]. Briefly, chloroform/methanol (2:1 v/v) was used to inactivate bacterial pellets (5 mg of dried cell mass). The inactivated pellets were incubating in constant shaking in chloroform/methanol (2:1 v/v) at 4 °C, overnight. Water was added to break phase and the lower organic phase containing free lipids and phospholipids was collected. A second extraction was performed using chloroform to maximally remove the free lipids and phospholipids that might cause ion suppression in MS analysis of MA. The organic phases were pooled and dried under a stream of nitrogen and stored at -80 °C. After the removal of aqueous phase, the intermediate layer was dried and subjected to alkaline hydrolysation using freshly prepared 20% tetrabutylammonium hydroxide (TBAH). After neutralization using concentrated hydrochloric acid (pH 4.5~5), two hexane extractions were performed to obtain the MA. The pooled MA extracts were dried under a stream of nitrogen and stored at -20 °C for MS analysis. All solvents and chemicals purchased were of HPLC grade (Merck, USA).

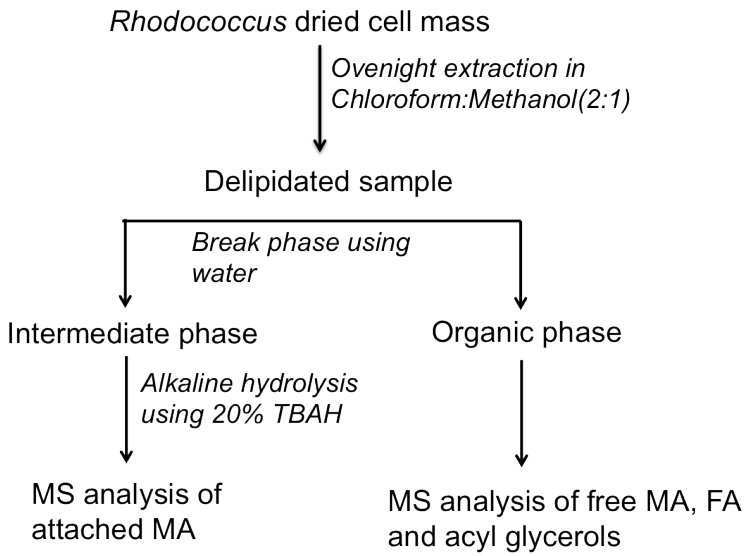

Figure 2.1: Scheme for lipid analysis in *Rhodococcus*.

2.2.3 Thin layer chromatography (TLC) of *Rhodococcus* MA

Extracted MA were subjected to methylation using freshly prepared solution of benzene: methanol: sulphuric acid (10:20:1), to obtain mycolic acid methyl esters (MAMEs). The methyl esters were extracted using hexane and dried under a stream of nitrogen and the dried lipid films were resuspended in 100μL chloroform/methanol (1:1). 10 μL of the resuspended lipid extracts were spotted onto 20 x 20 cm silica 60 coated glass plates (Merck, Darmstadt, Germany). The TLC was developed in hexane: ethyl acetate (95:5) solvent system thrice in one dimension. MAMEs prepared from commercially available MA mixture of *Mycobacterium tuberculosis* human strain (Sigma Aldrich, St. Louis, MO, USA) was used as MA standard for the chromatogram. The TLC plate was stained using 3% cupric acetate-8% phosphoric acid solution. After staining, the plate was charred at 150 °C to visualize the spots.

2.2.4 Mass spectrometric analysis

2.2.4.1 ESI/MS and tandem mass spectrometry of *Rhodococcus* MA

Electrospray Ionization Mass Spectrometry (ESI/MS) was performed on a Waters Micro mass Q-TOF mass spectrometer. The capillary voltage and sample cone voltage were maintained at 3.0 kV and 50 V, respectively. The source temperature was 80 °C, and the desolvation temperature at 250 °C. Mass spectra were acquired in the negative ion mode with an acquisition time of 3 min (mass range from 400 to 1600 m/z). Chloroform: Methanol 1:1 (v/v) with 2% piperidine (final 3 mM) at a flow rate of 15 μL/min was used as the mobile phase. Typically, 2 μL of sample was injected for analysis. Individual molecular species were identified using MS/MS. In general, the collision energy ranges from 20 – 37 eV.

2.2.4.2 Multiple Reaction Monitoring (MRM)-based MS analysis of MA in *Rhodococcus*

Based on the tandem MS of ions obtained from ESI/MS experiments, a comprehensive set of MRM transitions were generated to analyze the MA from *Rhodococcus* strains. An Applied Biosystems Triple Quadrupole/Ion Trap mass spectrometer (4000 QTRAP, Foster City, California, USA) was used for relative quantification of individual MA. The extracted MA was resuspended in 100 μL of chloroform/methanol (1:1). The MA extracts were diluted using chloroform/methanol (1:1) containing 2%, 300 mM piperidine and subjected to direct infusion at a flow rate of 15 μL/min. The individual MA intensities were normalized to the total count and further used for quantitative comparisons.

2.2.4.3 MS analysis of *Rhodococcus* fatty acids

Fatty acids were analyzed using the LTQ ORBITRAP XL mass spectrometer (Thermo Scientific) in negative ionization mode. Before MS analysis, docosahexanoic acid (DHA_C22:6) was spiked as an internal standard in all samples at a concentration of 0.05 μg/mL. The MS survey scan was performed in a window between 200 and 1200 m/z, at collision energy of 35 eV. The resolution was set at 60000 and recorded for 25 min with a mobile phase containing chloroform/methanol (1:1 v/v) with 2% of 200 mM piperidine, at a flow rate of 10 μL/min. The raw signal intensities of the 14 FFA species were normalized to the signal intensity of the internal standard (DHA) and expressed in arbitrary units for all samples.

2.2.4.4 High performance liquid chromatography-mass spectrometry (LC-MS) and tandem MS analysis of *Rhodococcus* mono mycolyl diacyl glycerol (MDAG)

A Shimadzu UFLC-XR LC system (Shimadzu, Kyoto, Japan) with a Phenomenex Kinetex 2.6μ C18 column (i.d. 4.6 x 100 mm), heated to 40 °C was used with a

binary solvent system and a flow rate of 200 μL/min. The solvent system used was chloroform/methanol (v/v, 1/1) with 2% of 100 mM ammonium acetate. The MS analysis was performed on a MS/MS mass spectrometer model 3200 Q TRAP (AB Sciex, Concord, Ontario, Canada). 20 μL of the sample was injected into the column and MS was recorded for 30 min in the mass range of 400-1700 m/z. The analyses were performed in positive ionization mode with turbo ion spray interface under the following conditions: ionspray source voltage (IS), 4500 V; curtain gas, 10 (arbitrary units); declustering potential, 70 V; entrance potential, 10 V; collision energy, 20 eV. Nitrogen served as a turbo gas and collision gas. The analyses were performed in Enhanced MS (EMS) mode, Enhanced Product Ion (EPI) mode, and Selected Ion Monitoring (SIM) mode.

2.2.4.5 High performance LC-MS analysis of *Rhodococcus* TAG and DAG

Individual species of TAG and DAG were separated by a sensitive high performance liquid chromatography method, similar to MDAG analysis. TAG were calculated as relative contents to the spiked d5-TAG 48:0 internal standard (CDN isotopes). The normalized units were expressed in arbitrary units. 10 μL of the sample was injected into the column and MS was recorded for 18 min in SIM mode. The output signal was monitored and processed using the Analyst software.

2.2.5 Clustering analysis

MA measured for different *Rhodococcus* species using MRM approach were normalized to their sum and used for clustering analysis. The different *Rhodococcus* species were grouped using hierarchical clustering, based on their MA abundance. Euclidean was chosen to be the distance metric with centroid linkage. The clustering analysis was performed using Cluster 3.0 software and the dendrogram was visualized using Treeview software.

2.3 Results

2.3.1 TLC and ESI/MS analysis of MA in *Rhodococcus* species

MA purified from cells of *R.aetherovorans* I24, *R.zopfii*, *R.fascians*, *R.jostii* RHA1 and *R.opacus* PD630 were methylated and separated on TLC as described above. As shown in Fig.2.2A, two major spots were observed for all five samples. The spot that migrated close to the origin contains mycolic acid methyl esters (MAME) with an average retention factor (*Rf*) value of 0.36. The more polar fatty acid methyl esters (FAMEs) eluted close to the solvent front, with an average *Rf* value of 0.55. Further, to identify the individual MA species in the eight species of *Rhodococcus*, these lipids were analyzed by ESI/MS in negative ion mode.

The MA peaks obtained from ESI/MS analysis from the eight species revealed a substantial amount of MA with many similar MA peaks in the mass range 440-840 m/z. The ESI-MS spectrum exhibiting the major MA peaks of *R.opacus* PD630 is shown in Fig.2.2B. A total of 39 individual MA peaks were chosen for MS/MS characterization. The tandem analysis was performed for collision energy varying from 20 to 37 volts. An example for fragmentation pattern is shown in Fig.2.2B for the MA peak 797.9 m/z with $C_{54}H_{102}O_3$ as molecular composition. The product ions obtained were predominantly 255.3 m/z and traces of 241.3 m/z and 269.3 m/z. These fragment ions correspond to alpha-alkyl side chains of length C16:0; C15:0; C17:0. Additionally, product ions corresponding to alpha-alkyl side chains of length C18:0, C16:1, C14:0 and C14:1 were also observed from different *Rhodococcus* species.

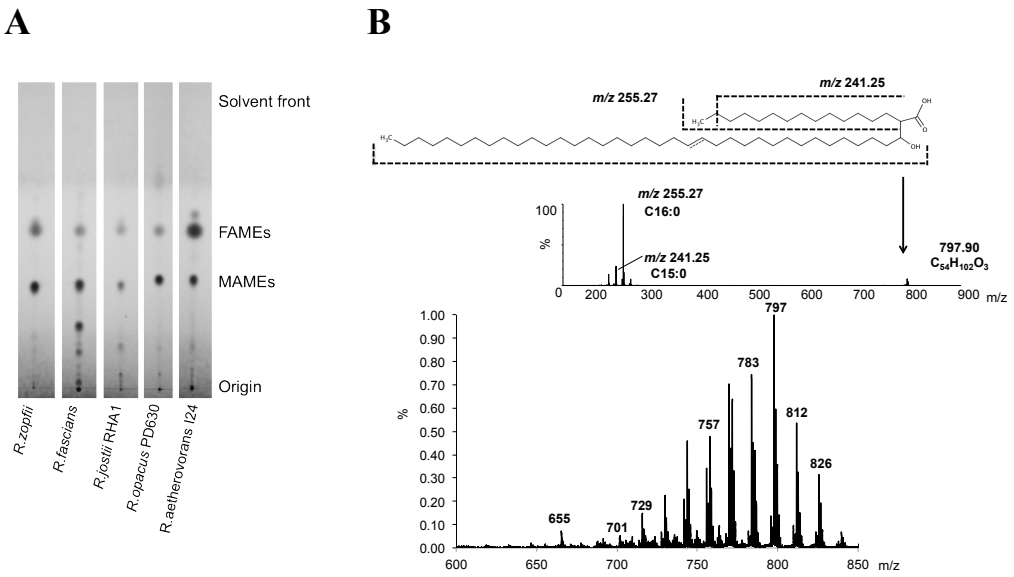

Figure 2.2: TLC and ESI/MS analysis of MA isolated from *Rhodococcus opacus* PD630. (A) TLC analysis of MA extracted from five different species of *Rhodococcus.* MA extracted from these species was methylated, separated on silica plates, stained using cupric acetate solution and the plates were finally charred to visualize the spots. The MAMEs of all *Rhodococcus* species elute as a single spot below the more polar FAMEs. **(B)** ESI/MS spectrum of MA from *R.opacus* PD630. The presence of C16:0 (255.27 m/z) and C15:0 (241.25 m/z) fatty acyls in the alpha branch of major MA 797.9 m/z are indicated in the MS/MS spectrum. Structure of the major fragment ions at m/z 255.27 and 241.25 from 797.9 m/z MA is also shown at the top of the Fig.2.2B.

2.3.2 Targeted MA analysis using MRM approach

Based on the results from the MS/MS analysis, a targeted MRM approach was developed. The MRM transition pairs were chosen such that the total mass of the MA was chosen as the parent ion and the fragment ions obtained in MS/MS analysis as the daughter ion. For example, the different MRM transitions generated for the MA peak 797.9 were 797.9/255.3 and 797.9/241.3. A total of 768 MRM transitions were generated for *Rhodococcus* species (List of MRM transitions in Appendix 1). The intensity monitored for the 768 MRM transitions were used to generate the MA fingerprint for the eight *Rhodococcus* species (Fig.2.3A). The dendrogram obtained using the normalized MA intensity measured for the eight species revealed a MA based grouping of the bacterial species (G1 and G2 in Fig.2.3A). Further similar MA fingerprints were obtained for *R.opacus* PD630 and *R.jostii* RHA1 for most of the MRM transitions (Fig.2.3B). Hence, MA with total carbon atom ranging from C28-C57 was defined in this study. Knowledge obtained from characterizing these attached MA aided our further attempts to characterize free MA possibly attached to sugars or acyl glycerols.

A

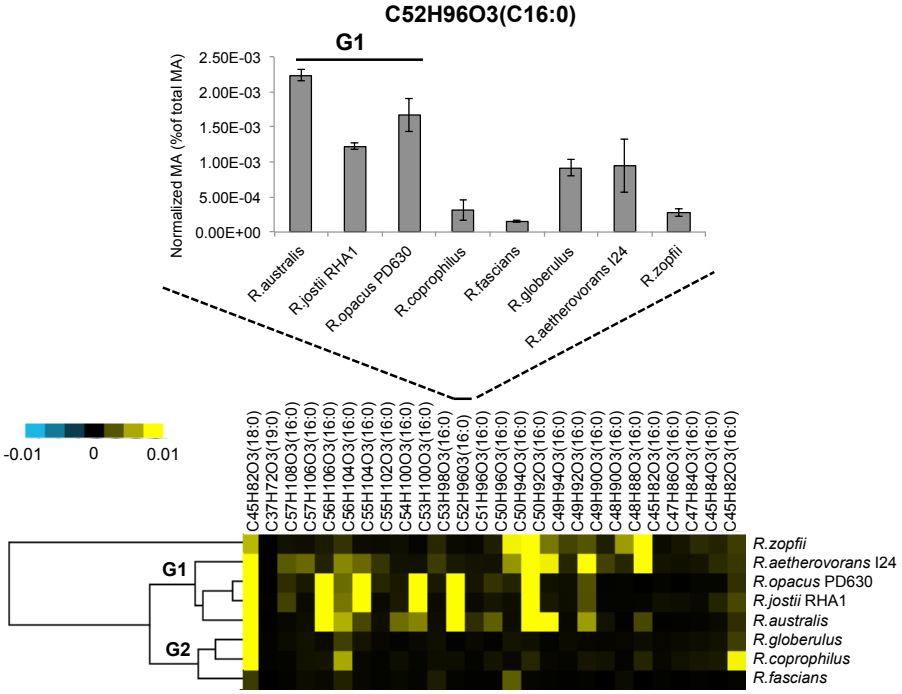

B

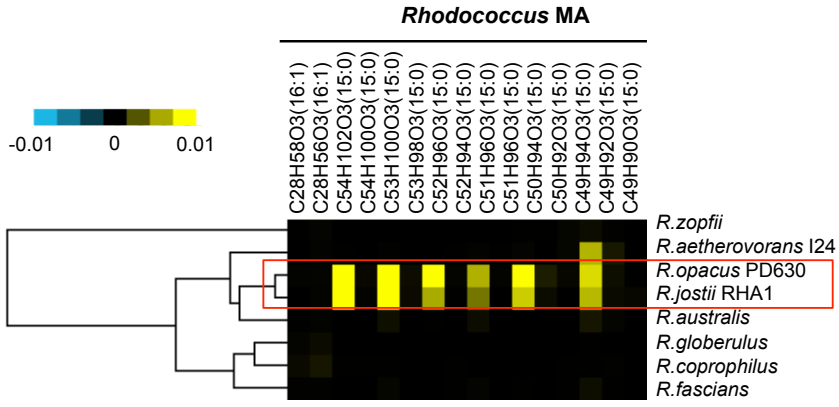

Figure 2.3: MA fingerprint of eight *Rhodococcus* species generated using targeted MRM approach. (A) The signal intensity of each MA species measured using the MRM transitions were normalized to the total MA (768 MA) and subjected to clustering analysis using Cluster 3.0 software. The resulting dendrogram was visualized using Treeview Software. The color bar indicates the range of MA variations across the eight *Rhodococcus* species. A segment of the dendrogram reveals the clustering of the eight *Rhodococcus* species into two main groups (G1 and G2) based on their MA profile. For example, the variation of C52H96O3 (C16:0) MA between the G1 and G2 is represented in the column chart. **(B)** A segment of the

dendrogram showing similar MA profile of the genetically close *Rhodococcus* species, *R.opacus* PD630 and *R.jostii* RHA1.

2.3.3 Odd-chain fatty acid distribution in *Rhodococcus*

The organic phase obtained from the lipid extraction of the *Rhodococcus* cell pellets was used to measure varied lipids, such as free fatty acids (FFA), TAG, DAG and MDAG.

The LTQ ORBITRAP allowed monitoring of 14 FFA species in the *Rhodococcus* genus. The normalized intensity of the FFA species from each *Rhodococcus* sp. was used to plot the heat map (Fig.2.4A). Hexadecanoic acid (C16:0) and Octadecanoic acid (C18:0) were the major FFA observed in all the eight *Rhodococcus* species. The odd-chain FFA, pentadecanoic acid (C15:0), heptadecanoic acid (C17:0) and heptadecenoic acid (C17:1) were abundant in *R.opacus* PD630 and *R.jostii* RHA1 than other *Rhodococcus* species used in this study (Fig2.4A- panel 'p' and panel 'q').

The FFA profile result indicates the likelihood of odd-chain fatty acid incorporation in other major lipids of *Rhodococcus* such as MA and TAG. The characterization of 768 individual MA species indicated the occurrence of odd-chain fatty acids (C17:0, C15:0, C15:1) as alpha alkyl side chains in MA (Fig.2.2B and Appendix). The organic phase was also used to measure the TAG abundance using 65 individual TAG molecular ions. Eighteen of the 65 TAG species examined were TAG with odd-chain fatty acids. In line with the FFA profile, the odd-chain TAG species were predominantly higher in *R.opacus* PD630 and *R.jostii* RHA1. TAG profiling aided our attempts to characterize a TAG related new molecule in *Rhodococcus*.

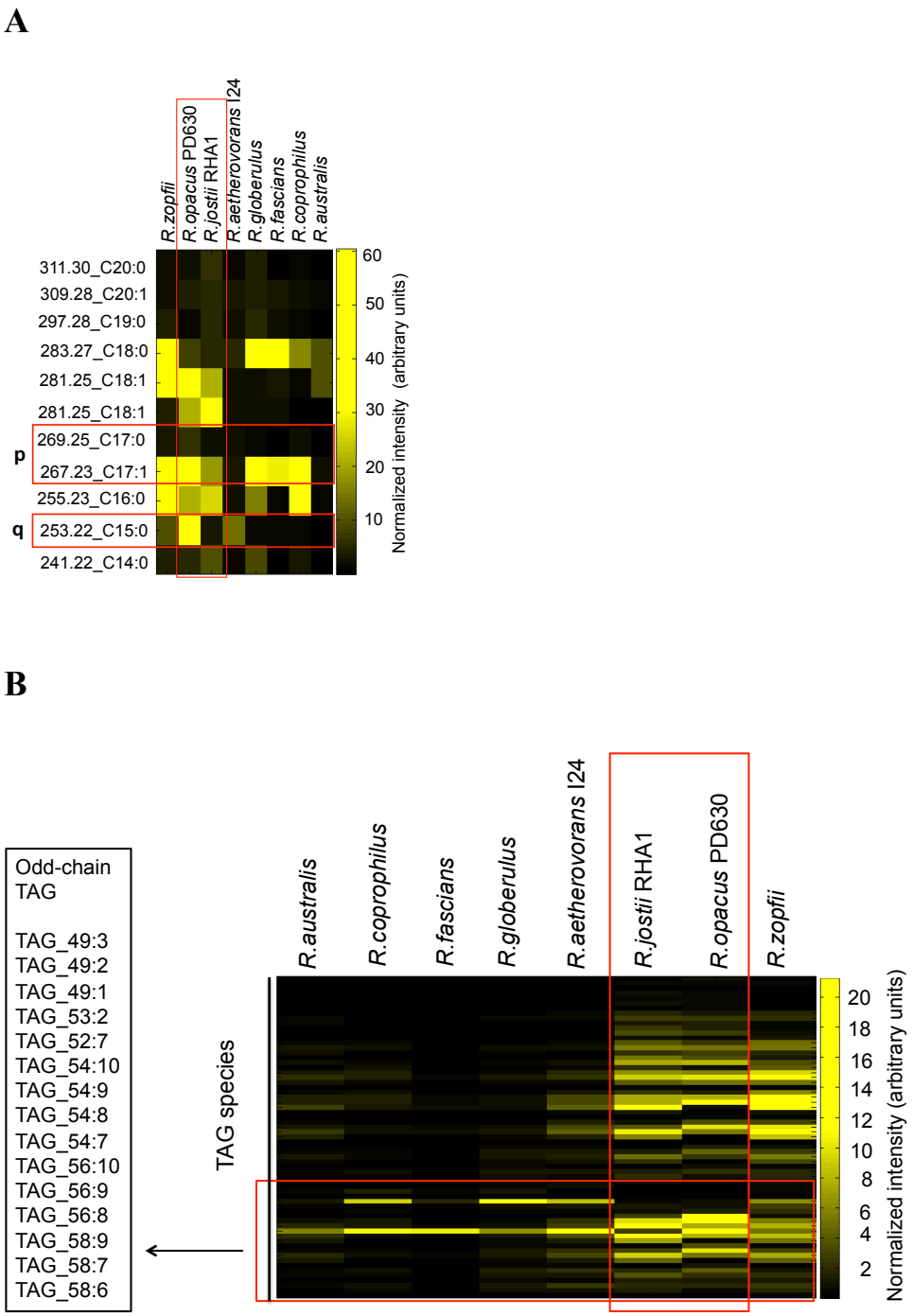

Figure 2.4: Odd-chain fatty acid distribution of *Rhodococcus* (A) The normalized intensities (raw signal intensity normalized to spiked internal standard and expressed in arbitrary units) of 14 FFA species from the eight *Rhodococcus* species were represented in a heat map. Panels 'p' and 'q' describe the higher prevalence of odd-chain FFA in *R.opacus* PD630 and *R.jostii* RHA1. **(B)** The normalized intensities (raw signal intensity normalized to spiked internal standard and expressed in arbitrary units) of 65 TAG species were also represented in a heat map. TAG species with odd-chain fatty acid substitution in their hydroxy alcohols were of higher proportion in *R.opacus* PD630 and *R.jostii* RHA1.

2.3.4 Characterization of mycolyl diacyl glycerol in *R.opacus* PD630

The structural knowledge of MA, TAG and DAG in *R.opacus* PD630 species enabled to delineate the structure of related molecular species. TAG is measured as positively charged ions in the mass spectrum. Following this, the positive ESI spectrum obtained from the organic phase extracts of different *Rhodococcus* species showed a complex pattern of peaks corresponding to molecular species with ammonium adducts (due to the presence of ammonium ions in solvent). Mass differences of 14 mass units were observed between the main peaks, suggesting the difference of a methylene unit between each molecular species. This could possibly be a result of heterogeneity in fatty acyl chain length (Fig.2.5A). We assume that these compounds contain a glycerol moiety as they eluted close to TAG in the liquid chromatogram. The composition of these molecular species can be explained by substituting one of the fatty acyl chains in the TAG molecule with a mycolic acid. For example, the MS/MS spectrum of 1104.7 m/z yielded major fragments corresponding to DAG species (563.5 m/z) (Fig.2.5B). The difference in mass between the DAG fragment and the parent ion corresponds to a MA that was lost upon fragmentation. The other minor fragment obtained by MS/MS fragmentation of the parent ion corresponded to a glycerol moiety with a fatty acyl chain and a MA esterified to two of the hydroxyl groups. The difference in mass between the minor fragment and the parent ion corresponds to a fatty acyl chain loss (255 m/z). The major MDAG species identified in this study are listed in the table in Fig.2.5A. This analysis has facilitated to relatively quantify the MDAG species in other *Rhodococcus* species as well.

A

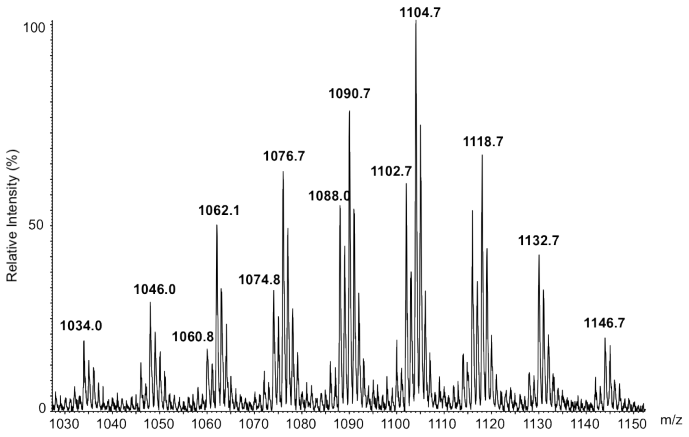

MDAG, [M]	$[M+NH_4^+]^+$
1072.7	1090.7
1142.8	1160.8
1156.7	1174.7
1084.7	1102.7
1100.7	1118.7
1128.7	1146.7
1114.7	1132.7
1042.8	1060.8
1056.8	1074.8
1070.8	1088.8
1120.7	1138.7

B

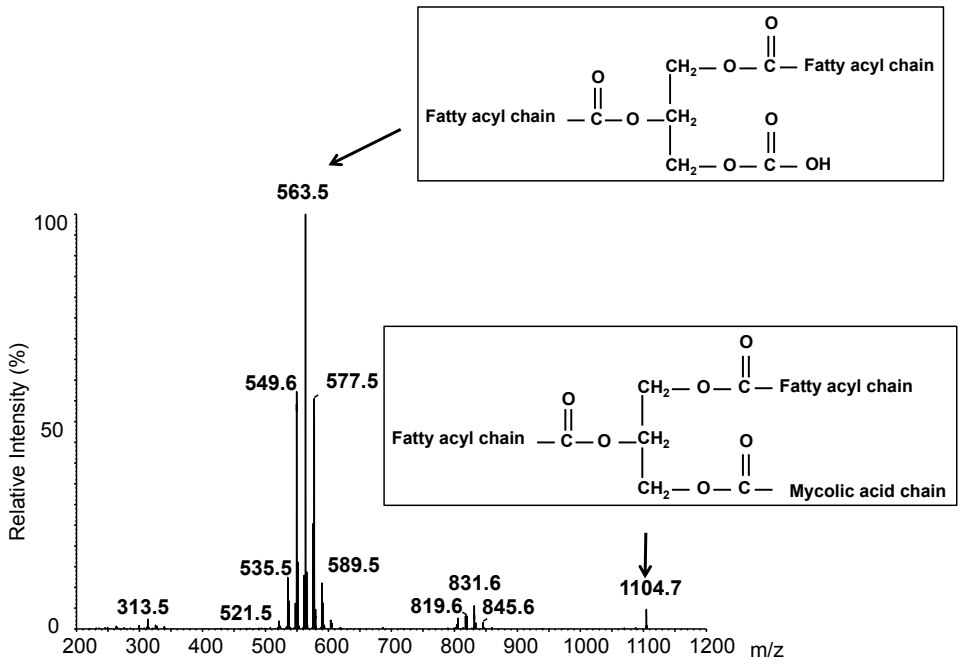

Figure 2.5: Positive mode HPLC-MS analysis of *R.opacus* PD630 MDAG. (A) MS spectrum of the possible MDAG peaks identified in *R.opacus* PD630, with the adjacent table showing the calculated masses of the ammonium adduct ions of the expected MDAG $[M+NH_4^+]^+$ as well as the exact mass, [M]. **(B)** Tandem mass analysis of 1104.7 m/z. The parent ion (1104.7 m/z) with a deduced structure fragments to give major ions of DAG (563.5 m/z). The difference in mass of the parent MDAG molecule and the fragment, DAG corresponds to the mass of a MA molecule, thereby indicating the possible substitution of MA chain for a fatty acyl chain in a TAG molecule.

2.3.5 Accumulation of MDAG in TAG accumulating *Rhodococcus* species

The identification of different MDAG species in *R.opacus* PD630 enabled the screening of TAG related molecules in other *Rhodococcus* species, using LC-MS on a SIM mode. Nineteen species of MDAG were monitored using LC-MS. The MDAG profile of different *Rhodococcus* species is depicted in a heat plot (Fig.2.6A), drawn using MATLAB. The highlighted panel 'm' in Fig.2.6A shows four *Rhodococcus* species having significant amounts of MDAG species. A comparison of total TAG and MDAG in the different *Rhodococcus* species (Fig.2.6B), indicate the considerable abundance of MDAG in those *Rhodococcus* species (panel 'm' and panel 'n') that accumulate large amounts of TAG.

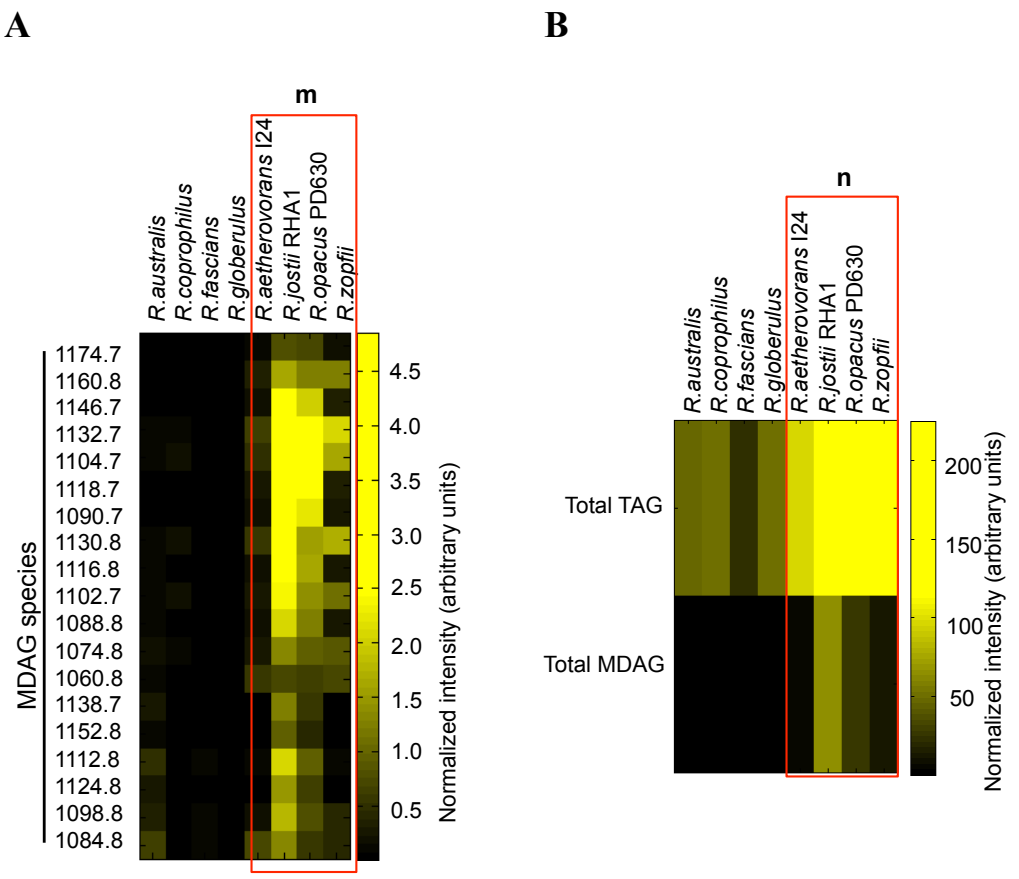

Figure 2.6: MDAG profile in *Rhodococcus* genus. The abundance of different MDAG molecular ions was measured in the eight *Rhodococcus* species. **(A)** The normalized intensity (raw signal intensity normalized to spiked internal standard and expressed in arbitrary units) values were used to plot a heat map using MATLAB 6.0. Along with *R.opacus* PD630, *R.jostii* RHA1, *R.zopfii* and *R.aetherovorans* I24 were the only *Rhodococcus* species that had substantial levels of MDAG. **(B)** A comparison of the total TAG and total MDAG in the eight *Rhodococcus* species revealed the tendency of those TAG accumulating *Rhodococcus* species to also synthesize the new TAG related molecule (panel 'm' and panel 'n').

2.4 Discussion

Using a lipidomics approach, we defined the structural diversity in MA across eight different species of *Rhodococcus*. Furthermore, we described the fatty acid distribution in free form as well as in esters of acyl glycerols. The combined knowledge of MA and acyl glycerols allowed us to characterize a new acyl glycerol related molecule named as mycolyl diacyl glycerol, MDAG.

Previously using gas chromatography mass spectrometry (GC-MS), MA profiles of *Rhodococcus* were studied [65, 159]. A number of recent studies used ESI-MS to analyze MA in single *Rhodococcus* species [64, 160]. In this study we used ESI-MS to simultaneously analyze the MA profile of eight *Rhodococcus* species. ESI-MS profile data provided a list of 39 individual MA peaks for further characterization using MS/MS. This MS/MS characterization further extended the MA species list owing to isomers differing in the lengths of meromycolate chain, alpha-alkyl group and unsaturated bonds (Fig.2.2A and Appendix 1). Following the MRM approach developed by Shui *et al*., [75] in *Mycobacterium* genus, we utilized the MS and MS/MS data to set up a MRM method for *Rhodococcus* genus. We developed a comprehensive set of 768 MRM transitions to relatively quantify MA in *Rhodococcus* species in a high-through put manner. Also, the total carbon chain length variation for MA in *Rhodococcus* was observed to be 28-57 (Refer Appendix 1), expanding the earlier findings of 28-54 [35, 65, 159]. We further detected unsaturation in alpha alkyl chain length but their localization could not be determined due to experimental limitation.

Our efforts in classifying the *Rhodococcus* species based on their MS profile using the MRM method resulted in two groups of bacteria (Fig.2.3A). 'G1' consisted of *R.globerulus*, *R.coprophilus, R.zopfii,* with major MA peaks observed in the m/z range 500-600 (Fig.1.3A). The G2 group of bacteria with major MA peaks observed in the m/z range of 600-700, included *R.opacus* PD630, *R.jostii* RHA1,

R.aetherovorans I24 and *R.fascians* (Fig.2.3A). This finding is in agreement with earlier reports on MA profile based groupings in *Rhodococcus* [65]. We also captured the similarity in MA profile for two genetically similar species namely, *R.opacus* PD630 and *R.jostii* RHA1. This emphasizes the relevance of MA in chemotaxonomy of Corynebacterineae [75, 161].

MA is important for the structural architecture of the bacterium whereas TAG is important for energy requirements. TAG accumulation was studied in *R.opacus* PD630 over the last decade [152, 162]. Structural analysis of TAG from *Rhodococcus* was mostly restricted to the analysis of the fatty acid content [16] of TAG except for very few studies [152, 156] that focused on total TAG structure determination. We extended our analysis to eight *Rhodococcus* species, and screened the TAG profile using a MS method of 65 individual TAG species. Most of the TAG species measured were abundant in *R.opacus* PD630, *R.jostii* RHA1, *R.aetherovorans* I24 and *R.zopfii* (Fig.2.4B). TAG profile of *R.opacus* PD630 coincided with earlier finding [152] and also revealed those TAG species with odd-chain fatty acid, the occurrence of which was hinted through odd-chain fatty acid isolation from TAG [16]. The odd-chain fatty acid distribution in varied lipids was also determined. More studies on the stereochemistry of TAG will reveal the localization of the fatty acids in the glycerol backbone. The structural knowledge of TAG and their fatty acid distribution will favour the efforts to engineer these bacteria for better production of energy lipids such as TAG.

Though the majority of the MA content in the cell envelope is covalently attached to the arabinogalactan-peptidoglycan complex, some MA is found in free form, either esterified to trehalose [64] or glucose [163] or glycerol moieties [57]. In this study one such free MA, the MDAG was structurally characterized and profiled in various *Rhodococcus* species (Fig.2.5 & 2.6). The structural equivalent of MDAG was earlier reported in *Mycobacterium smegmatis* and was indicated to play a possible role in

biofilm formation. Functionally MDAG could complement trehalose mycolates by serving as carriers of MA. Moreover, the DAG component signals the MDAG contribution towards carbon storage and balance [60]. This functional projection is strengthened by the fact that MDAG co-accumulated in those *Rhodococcus* species that exclusively synthesize large amounts of TAG (Fig.2.6B). Given the large genome size of *Rhodococcus* species, and enormous number of genes predicted to be associated with lipid metabolism [14, 16], more lipid species still remain to be characterized.

In conclusion, our lipidomics approach to characterize the major lipids MA and TAG is a first step towards a comprehensive analysis of complete lipidome of *Rhodococcus*. MA being a fundamental component of the cell envelope has impact on the membrane permeability, there by influencing secondary metabolites production and growth in activated sludge foams [133, 164]. The MA library defined in this study could assist in screening MA perturbations and also serve as a reference for new *Rhodococcus* species identification. TAG is a vital biomolecule for carbon storage, providing precursors for membrane lipids and for fatty acid detoxification. Structural analysis of TAG, which are specialized in *Rhodococcus* as TAG with odd-chain fatty acids will help in the better understanding of TAG metabolism. Combined knowledge of lipidomics and genomics of *Rhodococcus* will offer better opportunities to exploit the biotechnological potential of this fascinating genus.

3 Identification of lipid metabolizing enzymes in *Rhodococcus opacus* PD630 using activity based protein profiling (ABPP) approach

3.1 Introduction

The tremendous advent of genomics has created a repository of protein sequence information across all classes of organisms, but missing a functional annotation of the proteins other than sequence similarities to proteins with already known functions. There is a pressing need to functionally annotate the proteome. With *Rhodococcus opacus* PD630 (*R.opacus* PD630) genome sequenced recently, its proteome holds the key to the discovery of attractive enzyme candidates, as for synthetic biology approaches. A general technology that allows annotating proteins on a global scale will be a time saver and lead to new insights in the biochemistry of organisms. Activity based proteome profiling (ABPP) is a chemo proteomics strategy that stages on a global level, a versatile platform for enzyme annotation in the post genomic era [165].

ABPP involves the use of chemical probes targeting enzyme classes with similar enzyme activity features [166]. Chemical probes have been successfully developed for enzyme classes including varied hydrolases [167, 168], proteases [169, 170], and oxidoreductases [171]. Chemical probes are designed by two strategies:

(i) Directed approach, the probes are synthesized with affinity labels that direct them towards dedicated enzyme targets with similar catalytic mechanism or substrate specificity;

(ii) Non-directed approach a library of probes are synthesized that carry electrophilic groups to target nucleophile sites of enzyme classes [172].

Many naturally occurring small molecules are found to have fitting structural aspects to be used in ABPP experiments. β-lactones are a special group of small molecules employed in modern experiments of ABPP. β-lactone probes have a broad spectrum of targets, even labeling four different classes of enzymes in a single proteome of many prokaryotes [173]. The major enzyme families identified are hydrolases, transferases, oxidoreductases, and ligases, which require nucleophilic residues in their active site for enzyme activity [173]. These residues engage in selective attack of the electrophilic β-lactone ring of the small molecules (Fig.3.1) The stability of the covalently bound enzyme and the probe further allows a fluorescent group tagging, through a 1,3-dipolar Huisgen cycloaddition reaction ("click chemistry") [174], with the alkyne modified probe.

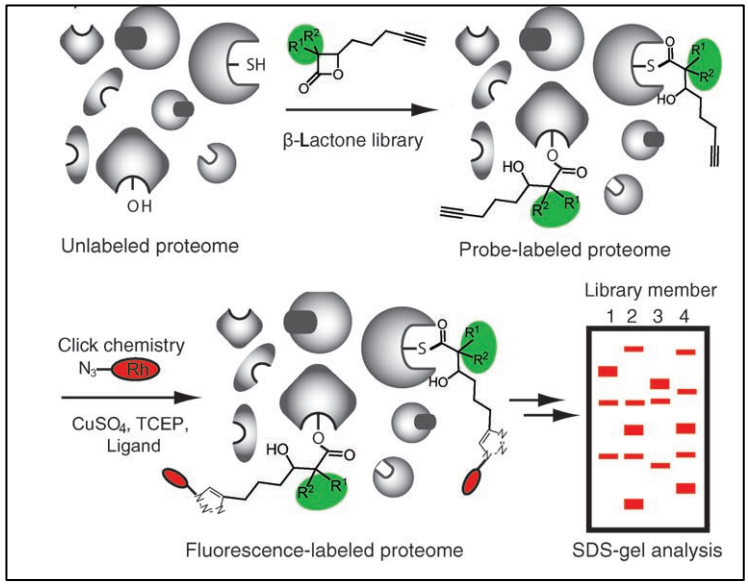

Figure 3.1: Proteomic analysis using active site directed β-lactone probes. Proteomes are incubated with the β-lactone library and then tagged with a fluorescent dye. The labeled proteome is separated by sodium dodecyl sulphate-polyacrylamide gel electrophoresis (SDS-PAGE) and visualized using fluorescent scanning. Figure adapted from Bottcher *et al*., 2008 [173].

Tetrahydrolipstatin (THL), the only FDA approved β-lactone, is an anti-obesity drug commercially sold as Orlistat. Orlistat is a semisynthetic derivative of lipstatin, which was originally isolated from *Streptomyces toxytricini* [175, 176] and found to be a

potent inhibitor of pancreatic lipase [177]. Apart from selective inhibition of fatty acid synthase in tumor cell lines, the complete target list of THL is still unknown. However, the use of chemically modified THL probes with alkyne handles in ABPP experiments has enabled identification of new targets as well as "off targets" of THL [178].

Based on β-lactone ABPP ability to target varied enzyme classes in prokaryotes, we explored the active site directed proteome of *R.opacus* PD630, using modified THL [179]. In the earlier chapters, lipidomics approach was applied to investigate lipid diversity of *R.opacus* PD630 and other *Rhodococcus* species. In this chapter, we aim to inspect the dearth of lipid metabolizing enzymes in *R.opacus* PD630, using a chemical proteomics approach.

A total of 25 significant proteins were identified using THL probes in *R.opacus* PD630 proteome. The major classes of enzyme identified were hydrolases, oxidoreductases, transferases and ligases. Selective proteins were subjected to *in silico* analysis to aid their functional study.

3.2 Materials and Methods

3.2.1 Bacterial cell lysis and protein extraction

R.opacus PD630 culture (1 litre) grown to OD_{600} 0.7 was centrifuged at 4,600 rpm for 5 min at 4 °C. The cell pellets were washed thrice in PBS-T (1x PBS with 0.05% tween 80) and once in PBS (1x). The washed pellets were resuspended in PBS and lysed using a probe sonicator at 40% amplitude for 5 min, at 4 °C. The lysate was centrifuged at 14000 rpm for 10 min at 4 °C to remove cell debris. The supernatant was snap frozen in liquid nitrogen and stored at -80 °C, until use. All cultures were grown in LB medium unless mentioned.

Lysate protein concentration was quantified using DC protein assay kit (Bio-Rad, Hercules, CA, USA), following manufacturer's instructions.

3.2.2 Azide alkyne Huisgen cycloaddition

3.2.2.1 Chemicals and reagents

Tetrahydrolipstatin (Orlistat), Tris(2-carboxyethyl) phosphine (TCEP) and Tris(1-benzyl-1H-1,2,3-triazol-4-ly)methylamine (TBTA) was purchased from Sigma-Aldrich, USA. THL-alkyne analogues, rhodamine-azide, biotin-azide were synthesized by our collaborator as described previously [179]. Table.3.1 lists all the probes and their sources. THL, its analogues and all fluorescent probes were dissolved in DMSO for all experiments. Avidin coated agarose beads slurry (NeutrAvidin) was purchased from Thermo Scientific (MA, USA).

Table 3.1: List of probes used in the click chemistry experiments.

Probes used	Source
Tetrahydrolipstatin or Orlistat (THL) 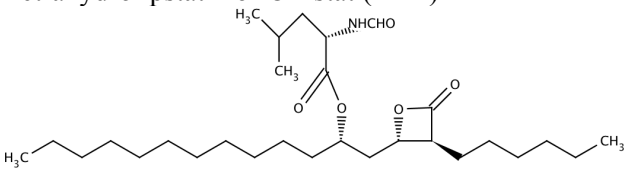	Sigma Aldrich, USA
Tetrahydrolipstatin –L (THL-L) 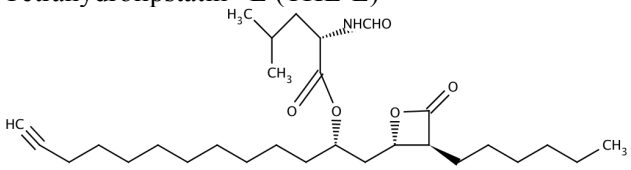	[179]
Tetrahydrolipstatin-R (THL-R) 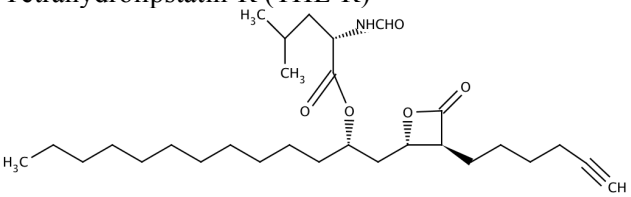	[179]
Tetrahydrolipstatin-T (THL-T) 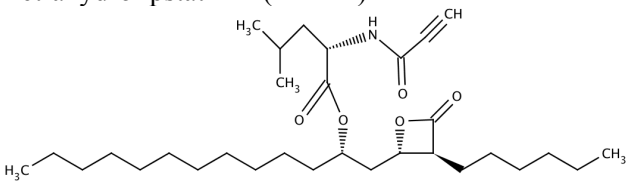	[179]
Rhodamine azide 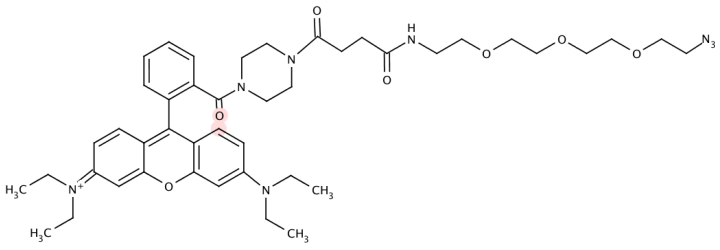	[179]
Biotin azide 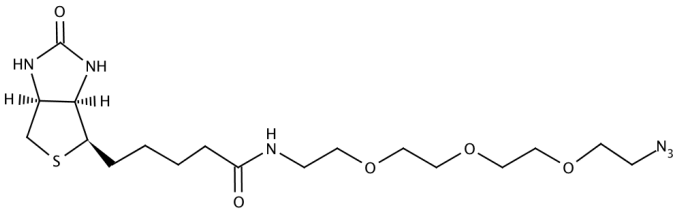	[179]

3.2.2.2 In-gel fluorescence

Protein lysate concentration was adjusted to 1 μg/μL with PBS and incubated with 5 μM of THL probes at room temperature for an hour. After incubation, freshly prepared click reaction mix in PBS [(CuSO4 (1 mM, 100 mM stock solution in deionized water), TCEP (1 mM, 100 mM stock solution in deionized water), TBTA (100 μM, 10 mM stock solution in DMSO) and rhodamine azide (100 μM, 10 mM stock solution in DMSO)] was added, vortexed and incubated in dark for 4 h at room temperature, with shaking at 300 rpm. Proteins were precipitated using five volumes of ice-cold acetone and incubated over night at -20 °C. Precipitated protein pellets were washed once with ice-cold methanol and solubilized in 50 μL 1x SDS loading dye. Approximately 10 μg of protein was separated using 12% SDS PAGE, visualized by in-gel fluorescence scanning with Typhoon 9410 Variable Mode Image scanner (GE Amersham, UK). Total protein was visualized using coomassie R-250 (Bio-Rad, CA, USA).

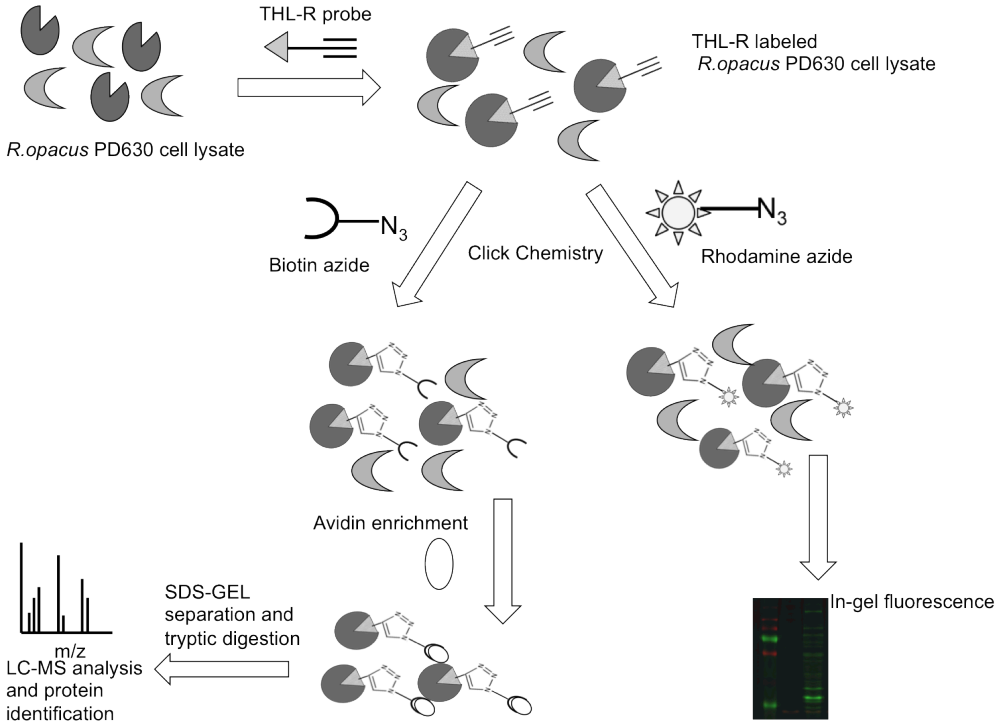

Figure 3.2: ABPP strategy for identification of lipid metabolizing enzymes in *R.opacus* PD630 proteome. THL-R, activity probe synthesized with alkyne handle, covalently binds to target proteins in the *R.opacus* PD630 cell lysate. A fluorescent tag such as rhodamine azide under click chemistry conditions tags the THL-R probe-protein complex. The tagged proteins were then separated by gel electrophoresis and visualized using fluorescent scanning. Use of biotin azide followed by avidin enrichment, selectively concentrates the target protein pool for identification by LC-MS. The structures of THL-R probe, and other click-based reporter tags are listed in Table 3.1.

3.2.2.3 Target enrichment using biotin-avidin pull down assay

To identify the targets of THL probe in *R.opacus* PD630, protein enrichment was performed using biotin-avidin pull down assay. Four milligram of cell lysate was subjected to cycloaddition reaction with biotin azide under similar conditions as mentioned in Sec. 3.2.2.2, acetone precipitated and solubilized in 0.2% SDS. The solubilized sample was then incubated with prewashed 25 μL NeutrAvidin slurry at room temperature for 1 h. The avidin coated beads were washed thrice, sequentially with 500 μL buffer A (8 M urea, 200 mM NaCl, 2% SDS, 100 mM Tris pH 8), buffer B (8 M urea, 1.2 M NaCl, 0.2% SDS, 100 mM Tris pH 8, 10% ethanol, 10%, isopropanol), buffer C (8 M urea, 100 mM Tris pH 8) and 1x PBS. For protein elution, the washed beads were boiled in 25 μL of 1x SDS loading dye at 96 °C for 20 min. The proteins were separated by a 12% acrylamide gel and visualized using silver staining. Whole gel lanes above 25 kDa from the control and THL samples were subjected to in-gel trypsin digestion.

3.2.2.4 Mass spectrometric identification of target peptides

The dried tryptic digested peptides were dissolved in 1% formic acid and peptides were separated and analyzed on a UFLC system (Shimadzu, Japan) coupled to an LTQ-FT Ultra mass spectrometer (Thermo Electron, USA). A 60 minute gradient was developed using mobile phase A (0.1% formic acid in water) and mobile phase B (0.1% formic acid in acetonitrile). The MS scan was performed in positive mode in the mass range of 350-1600 m/z. The MS parameters used were gas-flow (2 L/min), ion-transfer tube temperature (180 °C), electro potential (1.5 kV) and collision-gas pressure (0.85 mTorr).

Peptide and protein identification was performed using MASCOT (version 2.2.07; Matrix Science, US) search engine (*Rhodococcus* proteome as reference – http://rhodocyc.broadinstitute.org/) with an MS tolerance of 10 ppm and MS/MS

tolerance of 0.8 Da. Two missed cleavage sites of trypsin were allowed. Those proteins with an ion score greater than 80 [180] and with minimum two matching peptides were chosen as significant hits. MS/MS spectra were controlled manually to exclude random protein identifications from low quality spectra with high MASCOT scores.

3.2.3 *In silico* analysis

Blast similarity searches for the protein hits were performed using the NCBI protein blast feature (http://blast.ncbi.nlm.nih.gov/Blast.cgi?PAGE=Proteins). Conserved domains in the protein hits were identified using conserved domain search tool at National Center for Biotechnology Information (NCBI) (http://www.ncbi.nlm.nih.gov/Structure/cdd/cdd.shtml). Protein family classification and proteins with α/β hydrolase fold were obtained from SUPFAM (SUPER FAMILY) (http://supfam.cs.bris.ac.uk/SUPERFAMILY/). The ProtParam tool at the ExPASy proteomics server was used to analyze the physio-chemical properties of the protein hits (http://web.expasy.org/protparam/). PSIPRED was used to detect the secondary structure features of the protein hits (http://bioinf.cs.ucl.ac.uk/psipred/). Presence of signal sequences and trans membrane helice motifs were executed using SignalP 3.0 (http://www.cbs.dtu.dk/services/SignalP-3.0/) and TMHMM (http://www.cbs.dtu.dk/services/TMHMM/). Active site prediction of the protein hits were obtained using PROSITE tool at the ExPASy server (http://prosite.expasy.org/). Three-dimensional (3D) structure modeling of selected protein hits were created using Phyre^2 (Protein Homology/analogy Recognition Engine) v2.0 (http://www.sbg.bio.ic.ac.uk/phyre2/html/page.cgi). 3D protein models were visualized using Jmol, an open source Java viewer (http://jmol.sourceforge.net/).

3.3 Results

3.3.1 *In vitro* proteome profiling

We applied ABPP approach to identify lipid-metabolizing enzymes in *R.opacus* PD630. Yang *et al*., [179] synthesized a library of THL probes with alkyne handles at varied positions earlier. We chose three of the probes for our experiments. The three probes namely THL-L, THL-T and THL-R (Refer Table 3.1 for structure of probes) were incubated with whole cell *R.opacus* PD630 cell lysate at a concentration of 5 μM. After an hour of incubation, THL target proteins were tagged to a fluorophore rhodamine azide by cycloaddition reaction. The targeted proteins were separated on a 1D SDS-PAGE gel and visualized using a fluorescent scanner. The in-gel fluorescence image (Fig.3.3A) shows the comparative protein profiling efficiency of the three probes. THL-R revealed many protein bands whereas the other two probes were very weak and did not reveal any significant protein bands. Further, to confirm the specificity of modified THL such as THL-R, a competitive experiment was carried out with unmodified THL (Orlistat) (Fig.3.3B). Whole cell lysate was first incubated with unmodified THL (100 μM) followed by incubation with THL-R. The in gel fluorescence image (Fig.3.3B) showed that all the protein bands observed with THL-R were competed away by THL. Collectively, these experiments suggest the better efficiency of THL-R probe in ABPP experiments of *R.opacus* PD630.

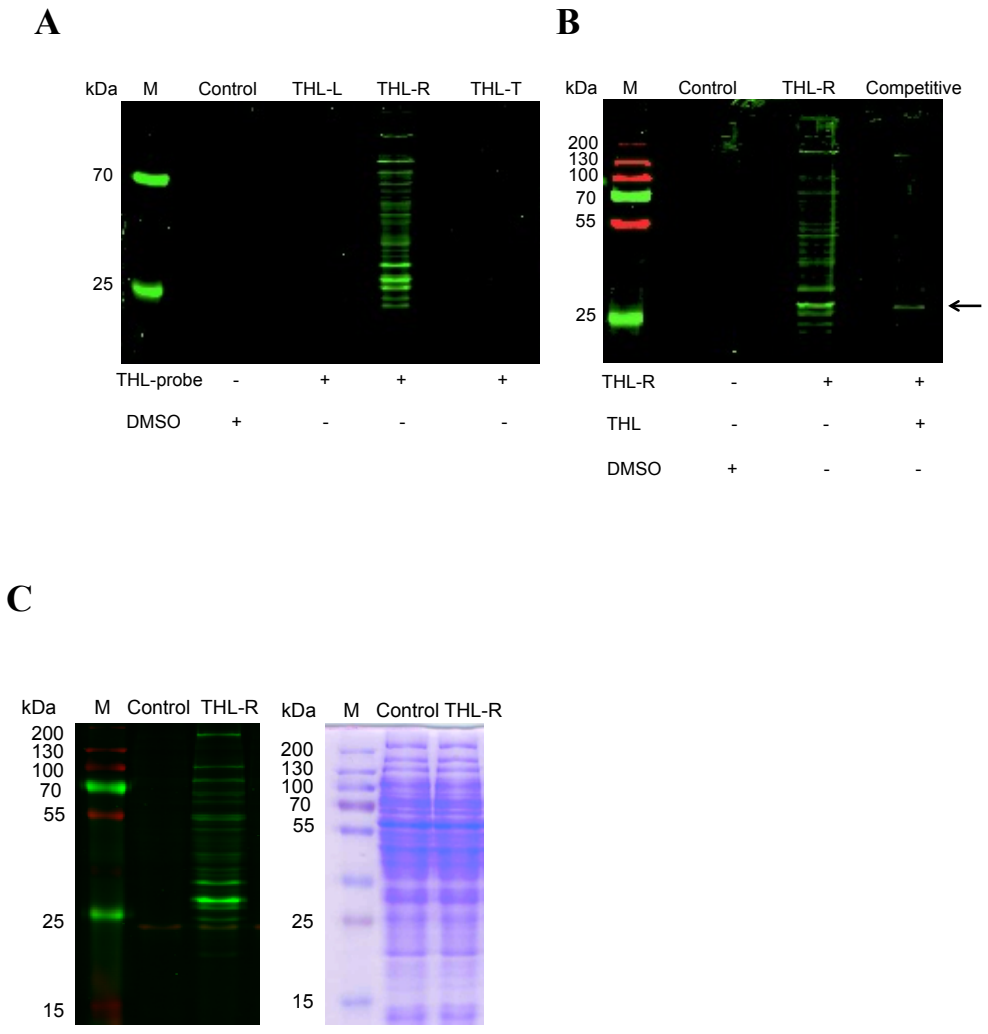

Figure 3.3: *In vitro* proteome profiling of *R.opacus* PD630 using THL probes. Protein lysate from exponentially grown *R.opacus* PD630 cultures were subjected to click chemistry with THL probes to obtain the *in vitro* proteome profile. **(A)** Three THL probes from the library were subjected to ABPP analysis in *R.opacus* PD630 proteome, followed by SDS-PAGE analysis and in-gel fluorescence scanning. The fluorescent scan image is displayed with M (Protein marker), Control (DMSO) and the three THL probe protein profile (THL-R, THL-L and THL-T). (**B***) In vitro* proteome profiling of *R.opacus* PD630 with or without THL (5μM), followed by click chemistry with rhodamine azide. The competitive lane does not show any significant fluorescence except for one band (marked by arrow) around 25 kDa that was not completely competed away by THL. (**C**) In-gel fluorescence image and corresponding coomassie staining for total protein.

3.3.2 Protein target identification

Following in-gel fluorescence experiment, we performed protein enrichment to facilitate the identification of THL targets by mass spectrometry. Whole cell protein lysate was incubated with THL-R followed by cycloaddition reaction with biotin azide. Biotin tagged proteins were subjected to pull down experiment using avidin coated agarose beads. The avidin bound proteins were then eluted and separated on a SDS-PAGE gel. Protein bands were visualized using silver staining.

In the silver stained gel (Fig.3.4A) THL-R lane exhibited many distinct bands comparable to the fluorescent gel image in Fig.3.3. THL-R and control (DMSO) lanes were excised from 25-200 kDa (marked by asterisk in Fig.3.4A) and subjected to in gel trypsin digestion. The digested peptides were identified by LC/MS/MS with a MASCOT search against the *R.opacus* PD630 proteome. All protein hits with an ion score above 80, with minimum two peptide matches and identified exclusively in THL-R lane as compared to the control lane, were considered as significant hits. Eighty proteins were identified in the first sample replicate, while 56 proteins were identified in the second sample replicate (Appendix 2 & 3). A total of 25 protein hits (Fig.3.4B) were consistently identified in the two experimental sample replicates and summarized in Table.3.2. Of the 25 protein hits, 22 were enzymes including 7 oxidoreductases, 3 transferases, 7 hydrolases, 2 lyases, 1 isomerase, 2 ligases and 3 other proteins. Hydrolase class of enzyme proteins was subjected to further bioinformatics analysis to predict their role in lipid metabolism.

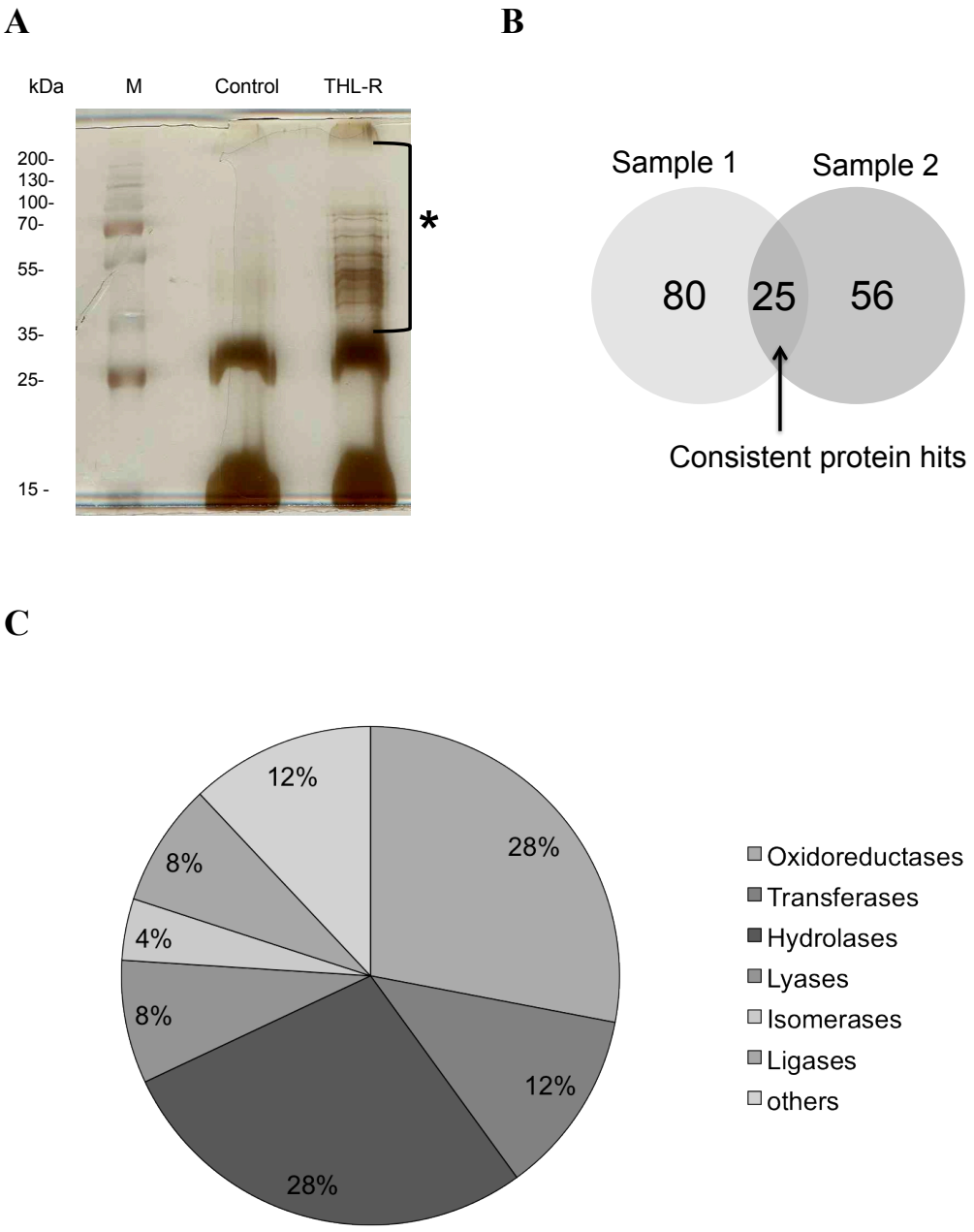

Figure 3.4: Protein enrichment and mass spectrometric identification. Protein lysate of *R.opacus* PD630 was labeled using THL-R. (**A)** Labeled proteins were enriched using biotin-avidin pull down assay and separated on 12% acrylamide SDS-PAGE followed by silver staining. Lanes from 25-200 kDa were cut correspondingly from the control and THL-R lanes (marked by asterisk). After in-gel tryptic digestion, proteins were identified by LC-MS analysis. (**B)** To improve the reliability of our analysis, two experimental trials were carried out, resulting in 25 consistent proteins. **C**. The 25 protein hits were categorized into 7 groups after searching against the *R.opacus* PD630 genome and performing other *in silico* analysis.

Table 3.2: Proteins identified by ABPP approach in whole cell lysates of *R.opacus* PD630.

R.opacus	Protein description	aa	MW	Protein score	Peptide match	EC no.	Enzyme class
OPAG_04877	**hydrolase**	**354**	**37835**	**534**	**11**	**Ec.-.-.-**	**Hydrolase**
OPAG_07191	**hypothetical protein OPAG_07191***	**575**	**59145**	**403**	**7**	**Hypothetical**	**Hypothetical**
OPAG_05885	anthranilate phosphoribosyltransferase	362	37206	292	7	EC 2.4.2.18	Transferase
OPAG_06327	**beta-lactamase**	**437**	**45821**	**207**	**2**	**EC 3.5.2.6**	**Hydrolase**
OPAG_05109	mycothiol-dependent formaldehyde dehydrogenase	341	36129	185	3	EC 1.1.1.306	Oxidoreductases
OPAG_01370	hypothetical protein OPAG_01370	473	49667	184	7	Hypothetical	Hypothetical
OPAG_09096	betaine aldehyde dehydrogenase	484	51096	160	8	EC 1.2.1.8	Oxidoreductases
OPAG_03492	tartrate dehydrogenase	336	35364	158	5	EC 1.1.1.93	Oxidoreductases
OPAG_02340	3-oxoacyl-[acyl-carrier-protein] reductase	448	46133	157	7	EC 1.1.1.100	Oxidoreductases
OPAG_05435	proteasome component	447	50888	154	8	NA	Others
OPAG_03759	UDP-glucose 4-epimerase	427	35016	153	6	EC 5.1.3.2	Isomerases
OPAG_03810	uroporphyrinogen decarboxylase	362	38215	153	3	Ec.-.-.-	Lyase
OPAG_01900	pyruvate dehydrogenase E1 component beta subunit	334	36215	144	4	NA	Oxidoreductases
OPAG_06066	acyl-CoA synthetase	992	106876	142	13	EC 6.2.1.-	Ligase
OPAG_06519	beta-ketoadipyl CoA thiolase	397	41183	130	2	EC 2.3.1.174	Transferase
OPAG_02598	luciferase	329	36152	119	3	EC 1.-.-.-	Oxidoreductases
OPAG_04938	**carboxylesterase**	**500**	**53112**	**116**	**9**	**EC 3.1.1.1**	**Hydrolase**
OPAG_05674	**dipeptidyl aminopeptidase**	**682**	**74234**	**113**	**24**	**EC 3.4.14.-**	**Hydrolase**
OPAG_02754	adenylosuccinate lyase	473	51625	109	14	EC 4.3.2.2	Lyase
OPAG_05840	**proline iminopeptidase**	**321**	**35881**	**106**	**5**	**EC 3.4.11.5**	**Hydrolase**
OPAG_00543	heptaprenyl diphosphate synthase component II	346	36563	98	3	EC 2.-.-.-	Transferase
OPAG_05427	**5~-3~ exonuclease**	**318**	**33360**	**90**	**5**	**EC 3.1.-.-**	**Hydrolase**
OPAG_02259	pyruvate dehydrogenase complex dihydrolipoamide acetyltransferase	511	54111	86	3	EC 1.-.-.-	Oxidoreductases
OPAG_07833	**carboxylesterase**	**509**	**54634**	**85**	**2**	**EC 3.1.1.1**	**Hydrolase**
OPAG_05807	propionyl-CoA carboxylase beta subunit	477	50065	83	4	EC 6.4.1.3	Ligase

3.3.3 Sequence and structure analysis of hydrolases

The seven hydrolases were chosen for bioinformatics analysis, hypothesizing possible role in lipid metabolism. Secondary structure analysis revealed the typical α/β hydrolase fold (of lipases and esterase) in four proteins OPAG_04877, OPAG_07191, OPAG_04938 and OPAG_07833. Each of the protein hits was individually subjected to various *in silico* analysis to predict their physiochemical properties, 3D structure and conserved domains.

OPAG_04877

OPAG_04877 was annotated to be a hydrolase in the published genome of *R.opacus* PD630. Physiochemical property analysis revealed a deduced *p*I of 6.01 and a high content of non-polar amino acids (53.5%). SignalP analysis did not reveal any signal peptide. Secondary structure analysis revealed the typical α/β hydrolase fold and the presence of catalytic serine residue in the nucleophilic active site (VLLVGH**S**MGG). A 3D homology model constructed using Phyre[2] permitted the confirmation of the catalytic Ser[154] residue (Fig.3.5A).

OPAG_07191

Sequence analysis of OPAG_07191, a hypothetical protein revealed a deduced *p*I of 4.41 and non-polar amino acid content of 49.2%. SignalP analysis and trans membrane motif search indicated a signal peptide (43 amino acids) at the N terminus. Due to low sequence homology results, the 3D model obtained was of poor accuracy and hence neglected for further analysis.

OPAG_04938 and OPAG_07833

OPAG_04938 and OPAG_07833 annotated as carboxyl esterases belong to the class of serine hydrolases closely resembling acetylcholine esterases. OPAG_04938 has a predicted *p*I of 6.10 and 52.4% of non-polar amino acids. OPAG_07833 has a

predicted pI of 5.24 and 53.4% of non-polar amino acids. Secondary structure analysis revealed the typical α/β hydrolase fold and the characteristic nucleophilic elbow in both the carboxylesterase proteins. The 3D homology model of OPAG_04938 and OPAG_07833 allowed confirmation of the catalytic serine residue (Ser^{190}-OPAG_04938 and Ser^{198}- OPAG_07833) at the nucleophilic elbow (Fig.3.5B & C).

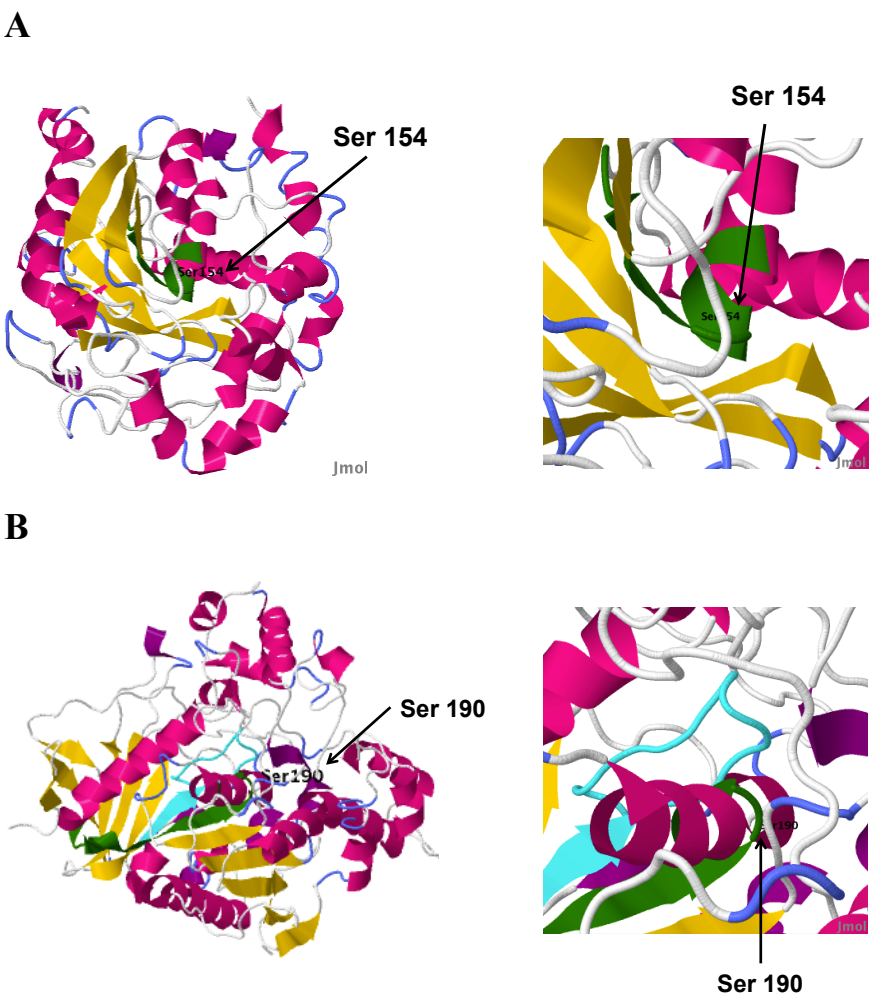

Figure 3.5: 3D homology model of OPAG_04877, OPAG_04938 and OPAG_07833. The 3D homology model of OPAG_04877 **(A)**, OPAG_04938 **(B)** and OPAG_07833 **(C)** were generated using Phyre[2]. The secondary structure features α helix and β sheets are coloured in *magenta* and *yellow*. The nucleophilic active site residue in the nucleophilic elbow of all three proteins are coloured in green. The zoomed in orientation beside the 3D models of each protein show the position of catalytic serine residue at the nucleophilic elbow.

3.4 Discussion

Up to date, very few lipid-metabolizing enzymes have been characterized in *Rhodococcus opacus* PD630. Most of them are described to be associated with triacylglycerol metabolism [150, 181, 182]. In addition, the recent publication of *R.opacus* PD630 genome creates new avenues to explore the rich enzyme repository of this potential biofuel producing bacterium. In this thesis, using activity based proteomics, 25 proteins were identified in *R.opacus* PD630, which belong to seven different enzyme classes.

In vitro proteome profiling efficiency of the three THL probes were compared using in-gel fluorescence scanning. THL-R probe revealed many bright bands from 25 kDa to 200 kDa, while THL-L and THL-T yielded weak or almost no bands (Fig.3.3A). Weak labeling in the case of THL-T could be due to inefficient click chemistry reaction, as the alkyne handle would have been rendered inaccessible in its buried orientation in the protein [179, 183]. However, inefficiency in the case of THL-L could not be explained as previous studies with THL-L did not report any such weak labeling [179]. One possible reason could be the difference in proteome lysates examined. Additionally, treatment with unmodified THL (5 μM), followed by THL-R treatment and click chemistry conjugation with rhodamine azide resulted in the absence of bright bands. The initial treatment of THL blocked all the protein targets and hence THL-R label did not reveal any fluorescence. This confirmed the target specificity of the chemically synthesized THL-R probe similar to the unmodified THL. Collectively, these experiments provided confidence in exploring the *R.opacus* PD630 proteome using THL-R probe.

The appearance of fluorescent bands from 25 to 200 kDa indicated the possibility of multiple targets of THL in *R.opacus* PD630. Labeled proteins were enriched using biotin-avidin pull down assay (Fig.3.4A) and analyzed using LC-MS/MS. Despite the multiple bands spanning the entire molecular weight range (25-200 kDa), the number

of significant protein hits from the two experiments was only 80 and 56 (Fig.3.4B). This could be explained due to the loss of proteins during the stringent buffer washes (refer to protocol in section 3.2.2.3), followed as part of the protein enrichment protocol. Also, the strict threshold set to filter hits post LC-MS/MS analysis could have attributed to this reduction in number of proteins identified. Certain steps can be taken in order to improve the reproducibility of protein hits obtained from different experiments. In the two technical replicate experiments for protein identification, whole gel bands were excised in the molecular weight range of 25-200 kDa. This could also have contributed to reduction in reproducibility. To overcome this disadvantage, dual functional probe comprising of both a fluorescent tag and biotin tag for enrichment can be used in place of the biotin tag. This could lead to prominent visible bands after silver staining. Thus single bands can be excised and subjected to protein identification. This approach could enable us to increase the reproducibility of ABPP experiment using THL-R probes. Nevertheless, the consistent list of 25 proteins obtained after the filtering procedure stood out as significant and confident list of targets (Table.3.1).

Previous studies using activity probes have reported either restricted reactivity within a specific enzyme class [174] or diverse reactivity with different enzyme class [184]. The list of 25 proteins was categorized into seven enzyme classes, which confirmed the diverse reactive nature of THL probe (Fig.3.4C). Also reports on β-lactone target spectrum inferred the divergent behaviour [173, 185]. The majority of labeled enzymes belonged to oxidoreductases (28%) and hydrolase class (28%). Oxidoreductase is one of the largest enzyme family encoded by the genome of *R.opacus* [16] and even the close relative *R.jostii* [14]. Also adding to the abundance, the possible nucleophilic attack by oxidoreductases could have added competition to hydrolase class of enzymes. Furthermore, six of the seven hydrolases carried the signature α/β hydrolase fold. SUPFAM analysis indicated the presence of ~200

proteins with α/β hydrolase fold in *R.opacus* PD630. This is twice the number of α/β hydrolase fold proteins in Mtb. Among the different subclasses of hydrolases, serine hydrolases are one of the widely distributed in all three kingdoms of life [186]. Serine hydrolases include esterases, lipases, peptidases and amidases. The seven hydrolase identified in this study included two carboxyl esterases, one hydrolase and two peptidases representing the different sub classes of serine hydrolases (Table.3.2). Extended *in silico* analysis was carried out on these seven hydrolase proteins, hypothesizing lipid metabolism associated functional role.

Four proteins OPAG_04877 (hydrolase), OPAG_07191 (hypothetical protein), OPAG_04938 (carboxylesterase) and OPAG_07833 (carboxylesterase) were further subjected to intense bioinformatics analysis. The predicted extracellular location (due to the N-terminus signal peptide prediction) and the anticipated cutinase-like function (from homology BLAST search and SUPFAM search) of OPAG_07191 signals the importance of characterizing this protein for use in industrial applications, similar to the use of bacterial cutinases in bioscouring [187]. The 3D homology models of the three other proteins demonstrated the characteristic nucleophilic elbow with the catalytic serine residue, a significant enzymatic feature of majority serine hydrolases [141]. The nucleophilic core of these hydrolase enzymes facilitated the attack on the β-lactone ring of THL, consistent with previous observation [179]. Altogether these results confirm the specificity of these protein targets towards THL.

The dedicated ABPP approach together with the LC-MS based proteomics platform enabled the identification of proteins from different enzyme classes. Further the *in silico* analysis of selected serine hydrolases from this study lent a peek into the huge enzyme inventory of *R.opacus* PD630. The predicted function and catalytic mechanism of the ABPP identified proteins emphasize the need for functional verification. In future, this approach could be further extended to analyze the lipid droplet proteome of *R.opacus* PD630. *R.opacus* PD630 has served as a model

organism to study the mechanism of lipid droplet formation [15, 188]. ABPP could help to decipher the contribution of specific enzyme classes in lipid droplet genesis.

4 *Mycobacterium tuberculosis* lineage independent variations of mycolic acids in macrophages post mycobacteria infection

4.1 Introduction

The long-standing association between *Mycobacterium tuberculosis* complex (MTBC) and the human host has led to coevolution and hence, adaptive genetic changes in the host and the bacteria [189]. Gagneux *et al*., [190] described substantial genetic diversity between strains of the MTBC phylogeny. Six phylogeographical lineages were defined to demonstrate the global population structure of *Mycobacterium tuberculosis* (Mtb) (Figure 4.1). This pioneering work has accelerated the search for genomic signatures of Mtb in different regions of the world [191-193].

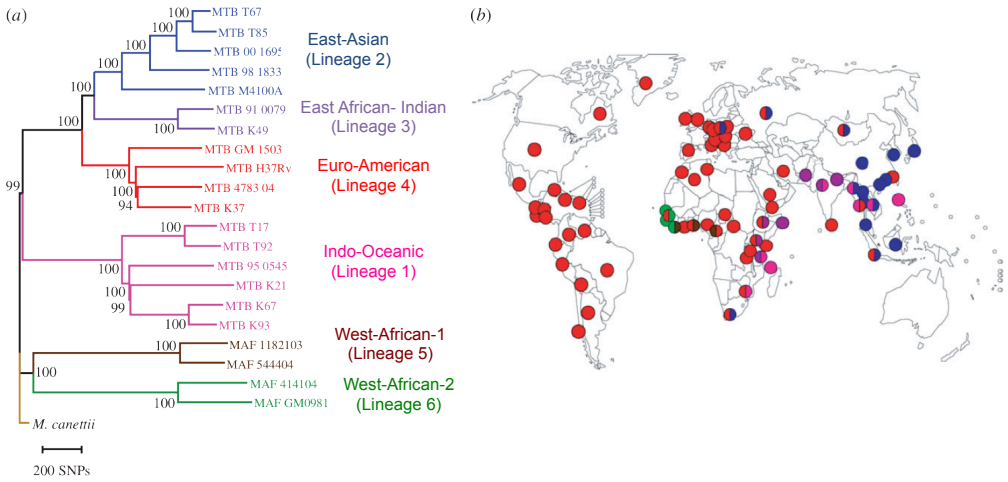

Figure 4.1: Global population structure and geographical distribution of Mtb. (a) Large sequence polymorphisms (LSPs) define a global phylogeny for Mtb. The six main lineages are Indo-Oceanic (Lineage 1), East-Asian (Lineage 2), East African-Indian (Lineage 3), Euro-American (Lineage 4), West-African-1 (Lineage 5) and West-African-2 (Lineage 6) [194]. (b) The six main lineages of Mtb are geographically structured. Each dot corresponds to one of 80 countries represented in the global strain collection. The colours of the dots relate to the six main lineages defined in Fig.2.1a and indicate the dominant lineage(s) in the respective countries [190]. The figure was adapted from Comas *et al*., 2010 [194].

Lineages 1, 5 and 6 were addressed as ”ancient” lineages owing to their early evolution whereas Lineage 2, 3 and 4 were grouped as “modern” lineages, which evolved at a later stage from the common ancestor [195, 196]. The demonstration of genomic diversity has hastened the efforts to decipher the links between Tuberculosis (TB) disease diversity and genomic diversity. Long before the characterization of distinct genotypes of Mtb, studies in animal models reported differential virulence among Mtb strains [197-199]. Several studies were focused on strain specific immune responses [200-202]. However, the contribution of these differences in the pathogenesis of tuberculosis and the virulence factors involved are not well understood.

Several studies have identified strain specific lipid profile pattern (Table.4.1) but none have been successful in delineating their role in differential immune responses. A variety of mycobacterial lipids, like mycolic acid (MA) for instance, were described as potent immune regulators by affecting the macrophage cytokine responses following phagocytosis [203, 204]. More recently, Beken *et al*., [205] demonstrated the effect of functional group modification of MA in eliciting a unique inflammatory pattern. Consequently, specific lipid profile changes are very likely to lead to the differential immune responses of Mtb lineage strains. The phylogenetic evolution of MA as well as its possible contribution to the strain specific immune responses is still unknown.

Table 4.1: Literature reports on Mtb lineage-specific lipid profiles

Lipid	Lineage	Finding
Pthiocerol dimycocerosates (DIM) and Phenolic glycolipid (PGL)	Lineage2 (Beijing)	Rv2952 mutation and the resulting changes in DIM and PGL profiles had no major impact in virulence in the mouse model [206]
Triacylglycerol	Lineage2 (Beijing)	Overproduction of triacylglycerols and DosR is constitutively up regulated [207]
Phenolphthiocerol dimycocerosates (PDIM)	Lineage 1	Production of unique unidentified lipid dependent on intact *pks15/1* [208]

The aim of this study was to characterize the variations in MA profiles between different strains from various lineages of the MTBC. It was hypothesized that the relative composition of the different classes of MA may confer different level of protection from the hostile environment of macrophages. Some MA modifications were thought to contribute to the resistance against oxidative stress during macrophage infection [209]. In this context, we also aimed to study the MA changes within the envelope of Mtb that might undergo in its natural host by performing macrophage infection experiments with various genetically distant Mtb strains.

We found substantial variations in MA patterns across MTBC and some degree of sub-clustering within strains from the same lineage. We showed that this pattern was affected in the macrophage environment with an overall increase in α-MA and keto to methoxy MA ratio. All these changes of MA in macrophages were independent of the Mtb genotype.

4.2 Materials and Methods

4.2.1 *Mycobacterium tuberculosis* culture

For each clinical isolate, mycobacterial cultures were expanded from a single colony-forming unit. Stationary phase pre-culture of mycobacteria were performed in Middlebrook 7H9 medium with ADC supplement (BD Biosciences), 0.05% Tween-80 (Sigma-Aldrich) and sodium pyruvate 40 mM. For lipidomic analysis, culture was diluted with 100 volumes of the same medium in the absence of detergent and incubated static for 10 days at 37 °C. Mycobacterial flakes were pelleted by centrifugation (10 min, 3000 rpm) and inactivated with 750 µL of chloroform/methanol (2:1). For the preparation of single cell suspension for infecting monocyte derived macrophages, mycobacterial cultures were passed in complete medium containing Tween-80 in order to be processed on the day of infection at an OD_{600} comprised between 0.38 and 0.71 units. At this stage, bacteria were pelleted by centrifugation and washed twice with PBS-Tween 0.05% to be resuspended in PBS before a final centrifugation at 500 rpm for 10 min. OD_{600} of the supernatants were measured and adjusted to 0.16 unit with PBS and 50 µL used to infect 4.10^5 macrophages.

4.2.2 Blood processing and isolation of peripheral blood mononuclear cells

Peripheral blood mononuclear cells (PBMCs) from healthy anonymous donors were isolated from cones provided by the National Blood Services, Colindale, UK. PBMCs were prepared on a Ficoll-Paque density gradient (Amersham Biosciences AB, Uppsala, Sweden) by centrifugation (800 xg, 30 min, RT). PBMCs were washed twice with RPMI (Gibco, Invitrogen) and resuspended in RPMI supplemented with FCS (4%), methyl-cellulose (2%) and DMSO (9%) for gradual overnight freezing in a NalgeneTM Cryo 1 °C container before storage in liquid nitrogen.

Table 4.2: Mtb lineage strains used in this study and the corresponding culture model used to characterize mycolic acids.

Strain identity		Culture model	
Strain name used in this study	**Lineage**	**7H9 Culture**	**Macrophage**
157L1	Lineage 1	+	
73L1	Lineage 1	+	+
121L1	Lineage 1	+	
72L1	Lineage 1	+	
14L1	Lineage 1	+	
70L1	Lineage 1	+	+
43L1	Lineage 1	+	+
132L1	Lineage 1	+	
63L1	Lineage 1	+	
62L1	Lineage 1	+	
134L1	Lineage 1	+	
64L1	Lineage 1	+	
57L1	Lineage 1	+	
65L1	Lineage 1	+	
81L1	Lineage 1	+	
32L1	Lineage 1	+	
145L2	Lineage 2	+	+
128L2	Lineage 2	+	
162L2	Lineage 2	+	
31L2	Lineage 2	+	+
44L2	Lineage 2	+	
53L2	Lineage 2	+	

52L2	Lineage 2	+	+
41L2	Lineage 2	+	
130L2	Lineage 2	+	
116L2	Lineage 2	+	
10L2	Lineage 2	+	
5L2	Lineage 2	+	
34L2	Lineage 2	+	
147L2	Lineage 2	+	
1L2	Lineage 2	+	
140L2	Lineage 2	+	
30L2	Lineage 2	+	
2L2	Lineage 2	+	
17L2	Lineage 2	+	
59L2	Lineage 2	+	
3L2	Lineage 2	+	
107L4	Lineage 4	+	+
120L4	Lineage 4	+	
142L4	Lineage 4	+	
131L4	Lineage 4	+	
148L4	Lineage 4	+	
112L4	Lineage 4	+	
101L4	Lineage 4	+	+
137L4	Lineage 4	+	
91L6	Lineage 6	+	+
88L6	Lineage 6	+	
89L6	Lineage 6	+	+
92L6	Lineage 6	+	

98L6	Lineage 6	+	+
90L6	Lineage 6	+	
60L6	Lineage 6	+	
115L6	Lineage 6	+	

4.2.3 Monocyte derived macrophages production, infection and inactivation

Monocytes were selected from frozen PBMCs using CD14 microbeads (Miltenyi Biotec, Bergisch Gladbach, Germany), following manufacturer's recommendations. Cell purity checked by flow cytometry was always greater than 95%. Macrophages were differentiated from monocytes after 6 days of culture in the presence of recombinant human GM-CSF. Cells were recovered with a cell scraper after 15 min Trypsin/EDTA (2 mM) treatment, resuspended in RPMI with 5% FCS, evenly distributed at 4.10^5 cells/well in tissue culture treated 24 well plates and transferred to the BSL3 for mycobacterial infection at a multiplicity of infection of 1:1 within 4 to 6 h. 72 h post-infection, the supernatants were discarded and the cells scrapped in 500 µL of PBS before pelleting at 300 g for 5 min and finally resuspended in 500 µL of chloroform/methanol (2:1).

4.2.4 Isolation of mycolic acids from infected macrophages and cultured *Mycobacterium tuberculosis*

MA from inactivated Mtb culture and macrophage were extracted using the protocol described in Sec.2.2.2.

4.2.5 Multiple Reaction Monitoring (MRM)-based MS for relative quantification of MA in *Mycobacterium tuberculosis* strains

An Applied Biosystems Triple Quadrupole/Ion Trap mass spectrometer (4000 QTRAP, Foster City, California, USA) was used for relative quantification of individual MA. The extracted MA was resuspended in 1mL (lineage culture samples) or 100μL (macrophage samples) of chloroform/methanol (1:1). The MA extracts were diluted using chloroform/methanol (1:1) containing 2% of 300 mM piperidine and subjected to direct infusion at a flow rate of 15 μL/min. MA of Mtb strains were measured in the negative ESI mode using a list of MRM transitions established by Shui.G *et al*., [75]. A total of 80 MRM transitions were used to quantify major Mtb mycolic acid species. The number of MRM measured for each class of MA namely alpha, methoxy and keto were 26, 24 and 30 respectively. The individual MA intensities were median fold normalized. For MA extracted from infected macrophage samples, synthetic C32 MA [74] with a MRM transition of 495/255 was used as an internal standard to quantify individual levels of various alpha-, keto- and methoxy-MA.

4.2.6 Statistical analysis

Statistical analysis was performed in R package, version 2.15.0.

ANOVA: To test for any significant variation among the lineage strains in the different culture models, ANOVA with Tukey's HSD was performed with Bonferroni correction threshold set at 0.05/80.

Decision tree: To identify the individual MA species that significantly varied among the four lineages, decision trees were plotted with party library in R. Based on the decision trees, box plots were generated for the three MA species that emerged significant.

Clustering analysis: Median fold normalized data of lineage strains from the two culture models were grouped using hierarchical clustering. Pearson correlation was chosen to be the distance measure with row scaling and with merging method of ward linking. Hierarchical clustering was performed in R using hclust function.

4.3 Results

4.3.1 Comparative profiling of MA from Mtb strains cultured *in vitro*

Lipid extracts from 7H9 cultures of 54 different strains covering four different Mtb lineages were subjected to MA extraction. (L1: 16 strains; L2: 22 strains; L4: 8 strains; L6: 8 strains). Relative quantification of MA contents was performed using Multiple Reaction Monitoring (MRM)-based mass spectrometry. The intensity values for the 80 abundant MA species were median-fold normalized and used for bi-clustering analysis. Bi-clustering analysis enables to capture those MA species that generate clusters among the different lineage strains. Furthermore, the clustering analysis was done separately for the three functional class of MA, to determine their individual contribution towards variations in different lineages. All lineage strains varied widely in alpha MA intensity but with no clear grouping of the lineage and/or the alpha MA species (Fig.4.2A). Both methoxy and keto MA species showed two clear clusters of MA with C26 alkyl side chain and C24 MA (Fig.4.2B & 4.2C). However, only in the case of methoxy MA did the clusters correlate with a lineage-based cluster. The cluster 'a' highlighted by a rectangle in Fig.4.2B corresponds to a group of Lineage 1 strains that have higher intensity of C24 methoxy MA than C26 MA. The clustering analysis, though did not yield any specific MA class that could differentiate all lineages but indicated the possibility of biochemically defined sub-clusters.

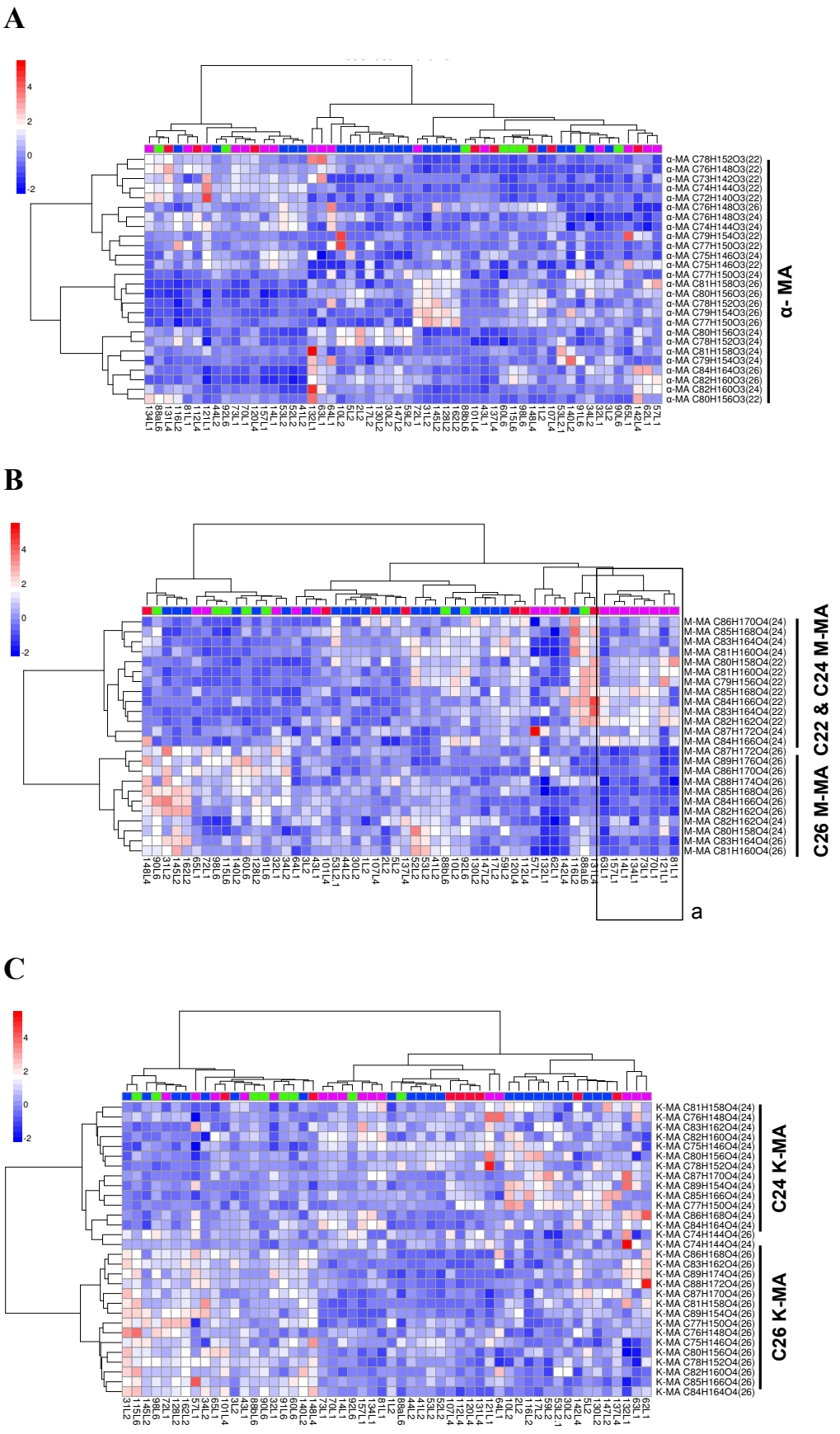

Figure 4.2: Hierarchical clustering of the four lineages based on MA profile.

Figure 4.2: Hierarchical clustering of the four lineages based on MA profile. MA extracted from 7H9 cultures of strains from the four lineages were measured in MRM mode. The resulting intensities of 80 MA were median-fold normalized, subjected to clustering analysis and depicted as a dendrogram. The colour bar indicates the range of MA variations across the different Mtb strains. The contribution of the three major class of MA towards any lineage based variation, has been explored in the three hierarchical clusters for alpha MA **(A)**, methoxy MA **(B)** and keto MA **(C)**. To quickly correlate the clusters with lineages, coloured rectangles have been incorporated on top of the three dendrogram. Pink corresponds to Lineage 1; blue to Lineage 2; red to Lineage 4 and green to Lineage 6.

4.3.2 Oxygenated MA profile distinguishes Lineage 1 from other lineages in 7H9 cultures.

MA profiles from each Mtb strain taken independently were found extremely variable, and following a bi-clustering analysis, we could not detect specific patterns that would allow the discrimination of each Mtb lineages (Fig.4.2). But the clustering pattern clearly indicated the existence of biochemically-defined sub-families based on MA profile within lineages of Mtb. We then executed detailed analysis, to verify the oxygenated MA profile variations in Lineage 1 strains (Fig.4.2B & C). A comparison of the ratio of different classes of MA exposed the significantly higher ratio of keto to methoxy in Lineage 1 strains as compared to other three lineages. In other words, the normal higher abundance of methoxy MA in 7H9 cultures was reversed in Lineage 1 strains. Additionally, the ANOVA results revealed higher intensity of C24 oxygenated MA than C26 MA with three individual MA species showing significant variation in Lineage 1 (Fig.4.3A). Though a varied distribution of MA profile was observed for Mtb lineages, it would be more interesting to examine their modulation in a host environment like the macrophages.

A

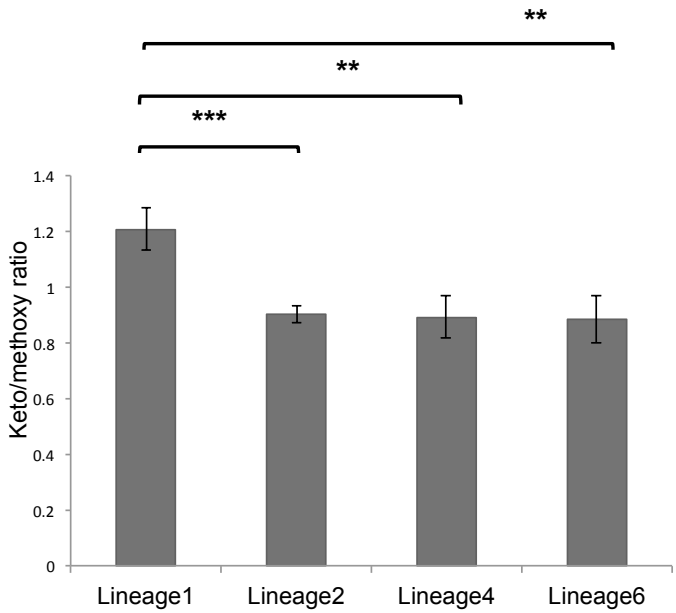

B

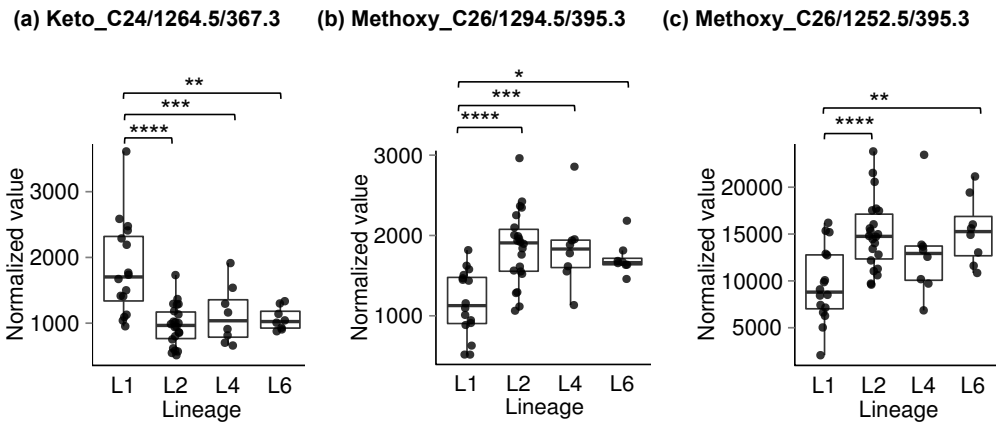

Figure 4.3: Oxygenated MA profile variations between Lineage 1 and other lineages. (A) The ratio of total keto MA to total methoxy MA was determined for all the 53 strains. The mean ratio of all strains in a lineage was plotted as a column chart for comparison. Data represents mean ± standard error of all the strains studied in each lineage. The ratio of keto MA to methoxy MA was significantly higher in Lineage 1. (Student's t test, *p<0.05, **p<0.01, ***p<0.001) **(B)** Decision tree plotted (Appendix) for MA from *in vitro* cultured lineage strains identified three MA species that had the potential to distinguish the lineage strains. Box plot, further enabled to visualize the variation of MA species among the lineages. An ANOVA followed by Tukey's HSD (Bonferroni correction threshold set at 0.05/80 MA species) gave the p value for their significance (*p<0.05, **p<0.01, ***p<0.001). Boxplots (a), (b) and (c) represent the variation of individual MA species such as keto_C24/1264.5/367.3, methoxy_C26/1294.5/395.3,and methoxy_C26/1252.5/395.

As revealed in Fig.4.2B, C24 MA species were of higher intensity in L1 compared to other lineages.

4.3.3 MA profile of Mtb lineage strains in macrophage

Human monocyte derived macrophages from three independent donors were infected with Mtb strains from all four Mtb lineages (L1: 3 strains; L2: 3 strains; L4: 2 strains; L6: 3 strains). Thus a total of 33 infected macrophage samples and three control samples for each donor were subjected to lipid extraction and analysis. The organic phase obtained in the initial stage of lipid extraction was used to analyze macrophage lipids. The delipidated cell debris was further subjected to alkaline hydrolysis to analyze mycolic acids within macrophages. MA extracted from Mtb infected macrophage was relatively quantified using the same MRM approach used for the *in vitro* (culture) study. In parallel, MA was extracted from each of the Mtb suspension used to infect the macrophage samples and compared.

4.3.4 MA profile changes following macrophage infection

It is noteworthy that despite the specific pattern observed for each Mtb lineage, the distribution of the three main MA classes was observed to be comparable across the three-macrophage preparations. Indicating a potent influence of the macrophage environment on the metabolism of MA in mycobacteria, we observed a very substantial decrease of methoxy MA following macrophage infection in comparison to the pattern of MA obtained from Mtb in 7H9 cultures. This observation was consistent for all four lineages (Figure.4.4A). In return, alpha-MA was found to be more abundant during macrophage infection than in *in vitro* cultures. (Figure.4.4A).

Consequently, we focused our analysis on looking at changes on the length of the alkyl chain (Figure.4B.). We could not detect significant changes between different lineages but we observed a clear tendency towards lower levels of C24 alkyl chain in favour of C26 following macrophage infection, therefore independently of the lineage.

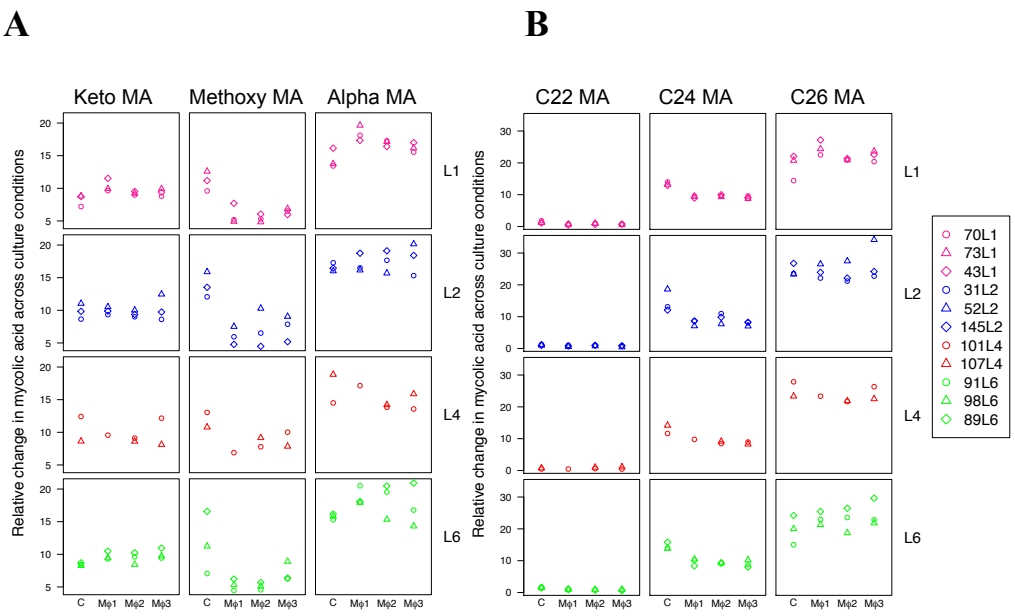

Figure 4.4. MA adaptations in Mtb infected macrophages are lineage independent. A. Parallel plots illustrate the changes in MA profile in different Mtb lineage strains extracted from infected macrophages (Mϕ1, Mϕ2, Mϕ3- different macrophage donors) against MA extracted from 7H9 culture (C). **(A)** Three strains were chosen from Lineage 1, 2 and 6 and two strains were chosen from Lineage 4 for the culture vs. macrophage experiments. Each square or circle or triangle point represent the mean total of alpha MA, methoxy MA and keto MA in culture and three macrophage experiments for individual lineage strains. Total alpha MA abundance increased in macrophages (Mϕ1, Mϕ2, Mϕ3) compared to culture Mtb. Relative composition of methoxy MA to keto MA decreased in macrophages compared to culture. **(B)** The abundance of total MA with C26 alkyl chain increased in macrophage compared to culture for all lineages.

4.4 Discussion

Using representative strains from different lineages, the analysis presented here shows that genetically diverse strains of MTBC vary extensively in their MA profile in 7H9 cultures, but exhibited a conserved core of MA changes in macrophages.

Previous reports (Table.4.1) have described lineage specific lipid profile but the present study is the first to investigate signature MA profile in different lineages. It is important to note that the diversity caused in MA profile is certainly influenced by individual strain diversity in MA biosynthetic pathway mutations. One biochemically-defined cluster of Lineage 1 is the only significant lineage specific MA profile obtained from our study (Fig.4.2). A personal communication from Dr. Mireilla Coscola (Swiss TPH, Basel) revealed a non-synonymous SNP in *virS* gene in 53 strains of Lineage 1, including the 16 strains examined in our study for lipid profile. VirS is a transcriptional factor that induces *mymA* operon, which in turn regulates cell wall modifications. A *virS* mutant has been reported to be associated with increase in C24 over C26 MA [210]. The SNP in Lineage 1 strains could be possibly associated with altered ratio of C24 to C26 MA in 7H9 cultures (Fig.4.3B). Although all the 16 strains examined in this study carry the *virS* SNP, only 7 strains exhibited this MA phenotype. This could be due to a sub-lineage branching among the Lineage 1 strains. The altered ratio of oxygenated MA in Lineage 1 still needs to be explained with a possible genetic determinant.

In macrophages, Mtb alters itself metabolically as well as the macrophage, to make the macrophage environment favourable for its persistent lifestyle. Our study has monitored the alteration in MA metabolism upon infection with additionally describing the MTBC phylogeny link to MA variations, for the first time. The macrophage model used is valid to study the macrophage induced Mtb lipid metabolism owing to the success of the model in studying lineage specific immune response [200]. Moreover, host lipid metabolism analysis (Appendix 2) results were

consistent with the work done by other groups in different experimental models to study Mtb triggered lipid metabolic modifications [211-213]. The different strains from the four lineages exhibited comparable MA changes within the macrophage. However, individual strain based variations could be observed in the MA profile (Fig.4.4). One possible reason could also be the interaction with the macrophages obtained from human donors. In order to avoid any such basal macrophage variations, human macrophage cell lines can be used for infection experiments.

The key MA variations exhibited are:

(i) Abundance of alpha MA in macrophages compared to cultivated mycobacteria;
(ii) Increase in the relative proportion of keto-MA to methoxy-MA in macrophages; and
(iii) Increase in the abundance of C26 MA following infection of macrophages (Fig.4.4).

The relative compositional changes of mycolic acid in macrophages have been observed in two other studies. Davidson *et al.,* [214] observed higher levels of keto-MA in *Mycobacterium microti* isolated from mouse lung tissue compared to *in vitro* grown mycobacteria. Yuan *et al*., [215] observed an increase in the abundance of alpha and keto-MA *in vivo* than *in vitro* and reciprocally methoxy-MA was found less abundant *in vivo* than *in vitro.* Our findings are consistent with these earlier observations and additionally illustrate that MA metabolic adaptations within the macrophage are consistent among phylogenetically distant Mtb strains.

The abundance of alpha MA and MA with C26 alkyl chain is necessary for bacterial resistance to oxidative stress and membrane integrity. Transcriptional profiles of Mtb under anaerobic conditions have indicated increased levels of ketoacyl synthase (KasB) [216]. Assuming the occurrence of similar anaerobic conditions in the

macrophage, augmented levels of KasB could signal the increase in mycolate chain length. Structure-function data and the high abundance of alpha MA in the cell wall encourages to propose a non-immune and structural role for alpha-MA in maintaining bacillary cell wall stability. Beken *et al.,* [205] have identified cis-alpha-MA as hypo-inflammatory, the cis-methoxy-MA as pro-inflammatory and the trans-keto-MA as non-inflammatory. This signifies the importance of oxygenated mycolates in regulating the host immune responses.

The decrease in methoxy MA during macrophage infection suggests one of the attempts by Mtb to suppress pro-inflammatory host responses. One of the strategies employed by Mtb to overcome elimination by the host is the selective repression of IL-12p40 production by host macrophage. A mutation in the methyl transferase *mmaA4* gene that induces distal oxygen containing modifications in MA caused higher levels of IL12p40 and TNF-alpha as compared to the wild type in stimulated macrophages [116]. Also, *mmaA4* was up regulated at transcriptional level in macrophages [217]. This finding underlines the importance of oxygenated MA composition in fine-tuning the host cytokine responses. The differences in degree of pro-inflammatory immune response suppression have been reported earlier in different lineages [200, 208]. Both these recent studies confirmed the statistically significant expression of higher pro inflammatory response in ancient lineage strains (Lineage 1 and Lineage 6) as compared to modern lineage strains (Lineage 2 and Lineage 4). All these findings strongly indicate the possible role played by MA modifications along with other Mtb virulence factors in modulating the host immune response.

The macrophage study was conducted at 72 hours post infection in order to allow enough time for the Mtb strains to adapt to the macrophage environment and accumulate lipid metabolic changes. After 24 hours post-infection most of the bacteria are phagocytosed, which has been confirmed by negligible colonies of plated

supernatants. Ideally, Mtb starts to grow between 24 to 48 h but though the rate varies between different groups [218, 219]. Selection of one time point is valid to observe MA changes due to different strains in a host environment. Since we observed a conserved core of MA changes in all the lineage strains, it is essential to monitor different time points in order to observe the progressive changes in MA for better understanding of the host-pathogen interactions. A 24hour time point could have possibly shown higher keto/methoxy MA ratio in Lineage 1 than other lineages, following its *in vitro* phenotype. At 72 hours the other lineages might have adapted to the host environment and attained similar levels of keto/ methoxy MA ratio. Also, the role of higher keto/methoxy MA could have been captured at 24-hour time point that might match the higher inflammatory phenotype in Lineage 1.

In conclusion, we have presented the first study on MA variations across the phylogeny of Mtb strains together with its impact on the host. We described variable strain specific pattern within each lineage, which is in line with the monomorphic genetic characteristic of Mtb. Also, we described important changes in the distribution of the different MA species following macrophage infection. This should be considered in the structure/function relationship between Mtb derived lipids and the pathogenesis of Mtb.

5 Conclusion and Future Perspectives

The cell envelope is a key player in a bacterium's interaction with its immediate surroundings and the major protection against anti-bacterial agents. Corynebacterineae are a special group of bacteria with a very complex cell envelope composed of specialized lipids to protect them from the dynamic and changing environments, threatening the bacteria. Biosynthesis of these complex lipids confers a huge metabolic burden on Corynebacterineae members. Nevertheless, these bacteria have utilized the highly complex lipid metabolism to favour their survival in very diverse living conditions from human alveolar macrophages to soils contaminated with organic solvents and chemicals. The study of the overall biology of a bacterium can never be completed without the knowledge of its cell envelope biology.

Mycobacterium tuberculosis (Mtb), the successful human pathogen has developed a sophisticated way to encounter the host immune attack. The lipid components of the cell envelope are the primary soldiers in Mtb's fight against the host immune defense. The structure and compositional features of Mtb's lipid repertoire has been studied in great detail over the years. But the understanding of lipid metabolic regulation governing Mtb's pathogenesis is at an early stage.

Rhodococcus, another fascinating genus of Corynebacterineae is known for its metabolic versatility and biotechnological applications. The lipid rich cell envelope hugely influences the biology and environmental significance of these members. However, the basic structural information of the cell envelope lipids is poorly studied in *Rhodococcus* when compared to the pathogenic relative, Mtb. Hence, studies aimed at deciphering the basic lipid biology in *Rhodococcus* species will greatly promote the biotechnological potential.

Therefore in this thesis, we utilized various biochemical techniques to decipher lipid variations in the pathogenic and non-pathogenic members of Corynebacterineae, with special focus on mycolic acids, the principal lipid component of the cell envelope.

5.1 Lipid metabolism of *Rhodococcus*

Members of *Rhodococcus* genus are well known for their bioremediation and biotransformation capabilities, which are attributed to their multi-faceted catabolic power. In spite of continued recognition and exploitation of *Rhodococcus* species in biotechnological applications, the lipid composition of cell wall assembly and the various lipid-metabolizing enzymes have been poorly studied.

In chapter 2 of this thesis, mycolic acid (MA), the major lipid component of the cell wall was characterized using ESI-MS analysis. MA profile of *Rhodococcus opacus* PD630 and seven other *Rhodococcus* species was characterized using ESI-MS/MS analysis. The largest library of MA comprising of 768 individual MA species was developed for *Rhodococcus*. This library acts to serve as a reference for defining the MA signature of newly identified *Rhodococcus* species. For the first time in *Rhodococcus* species, the targeted MRM method was successfully applied to monitor MA perturbations in a comprehensive and high throughput manner.

Apart from MA, fatty acid (FA) and acyl glycerol distribution of *Rhodococcus* was also examined. This analysis revealed the odd chain FA distribution across the different lipid components of *Rhodococcus*. Major odd chain fatty acids were identified. These findings are consistent with previous studies that hinted the odd-chain FA incorporation in acyl glycerols. TAG structural knowledge is very essential with regard to technological characteristics such as viscosity and melting temperature. Increasing number of studies are carried out to develop *R.opacus* PD630 as a biofuel-producing organism, overcoming the limitations of oil palms. The structural knowledge of the different TAG molecules synthesized by *R.opacus* PD630, will

provide cues to genetically engineer *R.opacus* PD630 that can synthesize specific types of TAG.

The combined knowledge of attached MA and acyl glycerols facilitated the characterization of a new lipid molecule. In this thesis, mycolyl diacyl glycerol (MDAG) species was identified in those *Rhodococcus* species that are specialized in accumulating large amounts of TAG. This observation predicts a combined storage and structural role for MDAG. Thus, all the lipid analysis results are part of the first step in achieving the complete lipidome characterization of *Rhodococcus opacus* PD630.

Apart from lipids, the proteins (enzymes) involved in lipid metabolism of Corynebacterineae species are of great interest for biotechnological applications as wells as for designing drug targets against disease causing species. ABPP approach was utilized in this thesis to identify lipid-metabolizing enzymes using Tetrahydrolipstatin (THL) analogues in *Rhodococcus opacus* PD630. As illustrated in chapter 3 of this thesis, we identified 25 proteins with THL probe in logarithmic phase *R.opacus* PD630 cells. Proteins were majorly identified from hydrolase, oxidoreductases and ligase class of enzymes. Recent studies have identified novel hydrolase enzymes in different *Rhodococcus* species [220]. The identified proteins chosen for future characterization experiments are probable carboxyl esterases OPAG_04938 and OPAG_07833; lipid droplet associated OPAG_05807; OPAG_07191 and OPAG_04877. Hence the functional validation of the protein targets will enable the identification of such novel lipid metabolizing enzymes. Thus the knowledge about lipid metabolizing enzymes of *Rhodococcus* will increase and also expand the catalytic toolbox for potential industrial applications.

5.1.1 Future perspectives

An in depth knowledge of the lipidomic and proteomic diversity of *Rhodococcus* will be further improved with the following objectives.

1. **Establishing a comprehensive *Rhodococcus* lipidome:** A comprehensive lipid analysis including phospholipids and other cell envelope lipids will enable the establishment of the lipidomic signature of *R.opacus* PD630.

2. Structure confirmation studies: Mass spectrometry (MS) as applied here allows only retrieving a preliminary level of structural characterization of the lipids. Using other recent sophisticated MS techniques such as ion mobility MS and NMR techniques the localization of fatty acyls and desaturations can be determined in MA, TAG and MDAG molecules.

3. Functional validation of ABPP protein hits: The proteins identified by the ABPP approach have to be characterized deeper with validation studies to confirm the predicted functions. This can be achieved by developing over expressed and down regulated mutants for specific proteins and followed by appropriate enzymatic assays and Lipidomics analysis.

4. Deciphering the lipid-droplet specific lipidome and proteome in *R.opacus* PD630: Lipid droplets are neutral cores surrounded by phospholipid monolayer and in addition, coated with functional proteins. Lipid droplets act as a repository of building blocks such as sterols, phospholipids for biological membrane formation. Molecular mechanisms governing the lipid droplets formation are largely unknown. In bacteria, lipid droplets are easily formed and hence serve as a better model to study biogenesis and degradation. *R.opacus* PD630 is specialized in accumulating large amounts of lipid bodies in specific growth conditions. *R.opacus* PD630 has served as a best model to study mechanism of lipid body formation in prokaryotes. A recent work on *R.jostii*, a close relative of *R.opacus* identified a number of proteins

associated with lipid droplets. However the published data did not identify any TAG specific lipases crucial for TAG breakdown and hence, for the lipid mobilization in lipid droplets. The lipidomics and proteomics methodologies used in this thesis exhibit immense potential to determine the lipid metabolism events localized in lipid droplets. Specifically ABPP approach will enable the identification of proteins involved in lipid droplet synthesis and break down. ABPP will help to capture proteins based on their activity irrespective of their minor concentration in lipid droplets.

5.2 Lineage independent modifications of MA in Mtb infected macrophage

In recent years, genetic studies have demonstrated diverse strain population of Mtb. These Mtb strains have coevolved with the host in causing differential immune responses. MA in *Mtb* and other *Mycobacterium* species has been studied in detail for their role in virulence mechanisms. However, the contribution of MA in varied immune responses among the different *Mtb* lineages is unknown.

As discussed in chapter 3 of this thesis, we have extended the targeted MS approach to study the MA variations from four different lineages. MA extracted from culture of these four lineages was highly variable. In a host environment such as the macrophage, MA variations were of similar pattern among all the lineages. In the macrophages, the alpha-and C26 alkyl chain MA increased in abundance and the relative proportion of keto-MA to methoxy MA decreased among all lineages. This signifies the highly conserved Mtb strategy to encounter the host environment despite the variable strain characteristics. The specific alteration in the ratio of oxygenated MA could specifically alter the host immune response.

Several strategies have been proposed to design drug targets against persistent Mtb. One such strategy is inhibiting the lipid modifications that promote the survival of persistent and drug resistant Mtb. In this study we have identified the conserved MA modifications in Mtb infected macrophages. Thus the methyl transferases involved in the functional modifications of mycolic acids could possibly serve as drug targets for TB. The exact role of Mtb strain specific variations in TB pathogenesis is yet not clearly understood. More importantly the natural forces behind the selection and dissemination of different lineage strains is also not known. Studies on Mtb isolates from regions covered by mass BCG vaccination have hypothesized the selection of Mtb isolates that resist BCG-induced immunity as a result of mass BCG vaccination.

Thus changes in the population structure of Mtb strains is important to understand the adaptation of Mtb lineage strains to control measures such as vaccination and drug treatments.

5.2.1 Future perspectives

A better knowledge of the lipid-based variations in the different lineages and the corresponding effect on pathogenesis can be achieved with the following objectives.

1. **Biochemical characterization of all forms of MA**: In this thesis we focused mainly on the determination of attached MA variations in the four lineages. Given the significant role of trehalose mycolates in host immune responses, a more detailed MA analysis including all forms of MA (free, attached to sugar molecules and acyl glycerols) should be considered.

2. **Genetic variations of MA pathway genes in Mtb lineages:** Nucleotide sequence comparisons of the different lineage strains will allow the identification of possible insertions/deletions and polymorphisms in MA biosynthetic pathway. Such information could be correlated to the MA profile of different lineage strains. In addition transcriptomics level expression of different MA biosynthetic genes can be monitored in an infected macrophage for different lineages to complement the SNP data.

3. Lineage directed host immune responses

Several studies have attempted to correlate phylogenetic relationship and inflammatory pattern of various Mtb clinical isolates representative of the global diversity. All the studies have proposed a varied immune response pattern by the different lineage strains. However it is equally important to identify the Mtb virulence factors that lead to such a varied response. MA is one of the prime modulators of host immune response. Based on the MA profile, it is essential to determine the cytokine expression level in the supernatants of different Mtb strains infected macrophage cells. Also the MA changes monitored in this study are from resting macrophages. It sis equally important to assess the changes in an activated macrophage such as an IFN-γ activated macrophage. In resting macrophages, Mtb can block the maturation

of phagosomes to enhance its persistence and survival. In contrast, IFN-γ activated macrophages are capable to overcome the inhibition of phagosome maturation. Mtb is subjected to a more stressful environment caused by nutrient limitation and reactive oxygen and nitrogen species. Mtb might be subjected to more crucial metabolic changes in a stressed environment. Also the cytokine profile from resting and activated macrophage can be compared, to better understand the host-pathogen interactions.

In conclusion, an integrated systems biology approach involving the different omics platforms will enable to decipher mechanism of lipid metabolism in Corynebacterineae. Such an approach will definitely accelerate research efforts in deciphering the role of lipids in the interaction of Corynebacterineae members with its adverse environment, be it a chemically harsh gas plant or an acidic human macrophage.

Bibliography

1. Fu, L.M. and C.S. Fu-Liu, *Is Mycobacterium tuberculosis a closer relative to Gram-positive or Gram-negative bacterial pathogens?* Tuberculosis, 2002. **82**(2-3): p. 85-90.
2. Goren, M.B., and P.J.Brennan, *Mycobacterial lipids: chemistry and biological activities*. Tuberculosis. 1979, W.B.Saunders Company, Philadelphia,PA: G.P.Youmans. 63-193.
3. Banerjee, A., R. Sharma, and U.C. Banerjee, *The nitrile-degrading enzymes: current status and future prospects.* Appl Microbiol Biotechnol, 2002. **60**(1-2): p. 33-44.
4. Kim, L.B.a.K.S., *Mycobacterium.* Microbiology and Molecular Biology Reviews, 1977. **41**(1).
5. Hartmans, S., J.A.M. Bont, and E. Stackebrandt, *The Genus Mycobacterium--Nonmedical.* 2006: p. 889-918.
6. Larkin, M.J., L.A. Kulakov, and C.C.R. Allen, *Biodegradation by Members of the Genus Rhodococcus: Biochemistry, Physiology, and Genetic Adaptation.* 2006. **59**: p. 1-29.
7. Finnerty, W.R., *The biology and genetics of the genus Rhodococcus.* Annu Rev Microbiol, 1992. **46**: p. 193-218.
8. Larkin MJ, D.M.R., Kulakov LA, Nagy I, *Applied aspects of Rhodococcus genetics.* Antonie Van Leeuwenhoek, 1998. **74**: p. 133-153.
9. Warhurst, A.M. and C.A. Fewson, *Biotransformations catalyzed by the genus Rhodococcus.* Crit Rev Biotechnol, 1994. **14**(1): p. 29-73.
10. K.S.Bell, J.C.P., D.W.J.Aw adn N.Christofi, *The genus Rhodococcus.* Journal of Applied Microbiology, 1998. **85**: p. 195-210.
11. Gürtler V, M.B., Seviour R, *Can whole genome analysis refine the taxonomy of the genus Rhodococcus?* FEMS Microbiol Rev, 2004. **28**(3): p. 377-403.
12. F. Zakham, L.B., D. Ussery, M. Akrim, A. Benjouad, R. Elaouad AND M. M. Ennaji, *Mycobacterial species as case- study of Comparative Genome Analysis.* Cell. Mol. Biol., 2011: p. OL1462-OL1469.
13. M Seto, K.K., M Shimura, T Hatta, M Fukuda and K Yano, *A Novel Transformation of Polychlorinated Biphenyls by Rhodococcus sp. Strain RHA1.* Appl. Environ.Microbiol., 1995. **61**(9).

14. McLeod, M.P., et al., *The complete genome of Rhodococcus sp. RHA1 provides insights into a catabolic powerhouse.* Proc Natl Acad Sci U S A, 2006. **103**(42): p. 15582-7.
15. Alvarez, H.M., et al., *Formation of intracytoplasmic lipid inclusions by Rhodococcus opacus strain PD630.* Archives of Microbiology, 1996. **165**(6): p. 377-386.
16. Holder, J.W., et al., *Comparative and functional genomics of Rhodococcus opacus PD630 for biofuels development.* PLoS Genet, 2011. **7**(9): p. e1002219.
17. Muscatello, G., et al., *Rhodococcus equi infection in foals: the science of 'rattles'.* Equine Veterinary Journal, 2007. **39**(5): p. 470-478.
18. Letek, M., et al., *The genome of a pathogenic rhodococcus: cooptive virulence underpinned by key gene acquisitions.* PLoS Genet, 2010. **6**(9).
19. NA, B., *1927.* Phytopathology, 1927. **17**: p. 29-30.
20. Koen Goethals, D.V., Mondher Jaziri, Marc Van Montagu, and Marcelle Holsters, *Leafy gall formation by Rhodococcus fascians.* Annu.Rev.Phytopathol, 2001. **39**: p. 27-52.
21. Chartrain, M., et al., *Bioconversion of indene to cis (1S,2R) indandiol and trans (1R,2R) indandiol by Rhodococcus species.* Journal of Fermentation and Bioengineering, 1998. **86**(6): p. 550-558.
22. M. Goodfellow, C.R.W.A.D.E.M., *Numerical Classification of Some Rhodococci, Corynebacteria and Related Organisms.* Journal of General Microbiology, 1982. **128**: p. 731-745.
23. Michael R. Barnes, W.A.D., and Peter A. Williams, *A 3-(3-Hydroxyphenyl)propionic Acid Catabolic Pathway in Rhodococcus globerulus PWD1: Cloning and Characterization of the hpp Operon.* Journal of Bacteriology, 1997. **179**(19): p. 6145-6153.
24. M, T., *A further numerical taxonomic study of the rhodochrous group.* Jpn J Microbiol, 1974. **18**: p. 37-44.
25. Gopaul D, E.C., Maki A Jr, Joseph MG., *Isolation of Rhodococcus rhodochrous from a chronic corneal ulcer.* Diagn Microbiol Infect Dis., 1988. **10**(3).
26. Fagard, M., et al., *AGO1, QDE-2, and RDE-1 are related proteins required for post-transcriptional gene silencing in plants, quelling in fungi, and RNA interference in animals.* Proc Natl Acad Sci U S A, 2000. **97**(21): p. 11650-4.

27. T.Cross, T.J.R.a., *Rhodococcus coprophilus sp. nov. : An Aerobic Nocardioform Actinomycete Belonging to the uhuduchrous' Complex.* Journal of General Microbiology, 1976. **100**: p. 123-138.
28. Oragui, D.D.M.a.J.I., *Occurrence of Rhodococcus coprophilus and associated actinomycetes in feces, sewage, and freshwater.* Appl Environ Microbiol, 1981. **42**(6): p. 1037-1042.
29. Stoecker, M.A., R.P. Herwig, and J.T. Staley, *Rhodococcus zopfii sp. nov., a toxicant-degrading bacterium.* Int J Syst Bacteriol, 1994. **44**(1): p. 106-10.
30. Brennan, P.J. and H. Nikaido, *The envelope of mycobacteria.* Annu Rev Biochem, 1995. **64**: p. 29-63.
31. Hoffmann, C., et al., *Disclosure of the mycobacterial outer membrane: cryo-electron tomography and vitreous sections reveal the lipid bilayer structure.* Proc Natl Acad Sci U S A, 2008. **105**(10): p. 3963-7.
32. Zuber, B., et al., *Direct visualization of the outer membrane of mycobacteria and corynebacteria in their native state.* J Bacteriol, 2008. **190**(16): p. 5672-80.
33. Daffe, M.a.D., P., *The Envelope Layers of Mycobacteria with Reference to their Pathogenicity.* Adv.Microb.Physiol.,, 1998. **39**: p. 131-203.
34. Sutcliffe, I.C., *Cell envelope composition and organisation in the genus Rhodococcus.* Antonie Van Leeuwenhoek, 1998. **74**(1-3): p. 49-58.
35. Sutcliffe, I.C., *Cell envelope composition and organisation in the genus Rhodococcus.* Antonie Van Leeuwenhoek International Journal of General and Molecular Microbiology, 1998. **74**(1-3): p. 49-58.
36. Dover, L.G., et al., *Comparative cell wall core biosynthesis in the mycolated pathogens, Mycobacterium tuberculosis and Corynebacterium diphtheriae.* FEMS Microbiol Rev, 2004. **28**(2): p. 225-50.
37. Minnikin, D.E., *The bilogy of the Mycobacteria*, ed. S.J. Ratledge C. 1982, Sandiego CA: Academic Press. 95-184.
38. Kaur, D., et al., *Chapter 2 Biogenesis of the Cell Wall and Other Glycoconjugates of Mycobacterium tuberculosis.* 2009. **69**: p. 23-78.
39. Chatterjee, D., *The mycobacterial cell wall: structure, biosynthesis and sites of drug action.* Current Opinion in cell biology, 1997. **1**(4): p. 579-588.
40. Jr, M.H.S., *Cell Membrane, Prokrayotic*, in *Encyclopedia of Microbiology*, M. Schaechter, Editor. 2009, Academic Press: Oxford, UK.
41. Ouellet, H., J.B. Johnston, and P.R. Ortiz de Montellano, *The Mycobacterium tuberculosis cytochrome P450 system.* Arch Biochem Biophys, 2010. **493**(1): p. 82-95.

42. Michael Goodfellow, G.A.J.C., *Rhodococcal systematics: problems and developments.* Antonie van leewenhoek, 1998. **74**: p. 3-20.

43. Butler, W.R. and L.S. Guthertz, *Mycolic acid analysis by high-performance liquid chromatography for identification of Mycobacterium species.* Clin Microbiol Rev, 2001. **14**(4): p. 704-26, table of contents.

44. Song, S.H., et al., *Electrospray ionization-tandem mass spectrometry analysis of the mycolic acid profiles for the identification of common clinical isolates of mycobacterial species.* J Microbiol Methods, 2009. **77**(2): p. 165-77.

45. El Khe´chine A, C.C., Flaudrops C, Raoult D, Drancourt M, *Matrix-Assisted Laser Desorption/Ionization Time-of-Flight Mass Spectrometry Identification of Mycobacteria in Routine Clinical Practice.* PLoS ONE, 2011.

46. Magee, M.G.a.j.G., *Taxonomy of Mycobacteria*, in *Mycobacteria*, P.R.J.gangadharan et al., Editor. 1998, Chapman & amp; Hall.

47. Seviour, V.G.r.a.R.J., *Systematics of Members of the Genus Rhodococcus (Zopf 1891) Emend Goodfellow et al. 1998. The Past, Present and Future.*, in *Biology of Rhodococcus*, H.M. Alvarez, Editor 2010, Springer: Verlag Berlin Heidelberg.

48. Dean C. Crick, S.M.a.P.J.B., *Biosynthesis of the arabinogalactan-peptidoglycan complex of Mycobacterium tuber.* Glycobiology, 2001. **11**(9): p. 107R-118R.

49. Hunter, R.L., et al., *Trehalose 6,6'-dimycolate and lipid in the pathogenesis of caseating granulomas of tuberculosis in mice.* Am J Pathol, 2006. **168**(4): p. 1249-61.

50. Ryll R, K.Y., Yano I, *Immunological properties of trehalose dimycolate (cord factor) and other mycolic acid-containing glycolipids—a review.* Microbiol Immunol., 2001. **45**(12): p. 801-811.

51. Hsu, F.F., et al., *Structural definition of trehalose 6-monomycolates and trehalose 6,6'-dimycolates from the pathogen Rhodococcus equi by multiple-stage linear ion-trap mass spectrometry with electrospray ionization.* J Am Soc Mass Spectrom, 2011. **22**(12): p. 2160-70.

52. Takayama, K., C. Wang, and G.S. Besra, *Pathway to synthesis and processing of mycolic acids in Mycobacterium tuberculosis.* Clin Microbiol Rev, 2005. **18**(1): p. 81-101.

53. Kremer, L., et al., *Identification and structural characterization of an unusual mycobacterial monomeromycolyl-diacylglycerol.* Mol Microbiol, 2005. **57**(4): p. 1113-26.

54. Alvarez, H.M. and A. Steinbuchel, *Triacylglycerols in prokaryotic microorganisms.* Appl Microbiol Biotechnol, 2002. **60**(4): p. 367-76.

55. Alvarez, H.M., R. Kalscheuer, and A. Steinbuchel, *Accumulation and mobilization of storage lipids by Rhodococcus opacus PD630 and Rhodococcus ruber NCIMB 40126.* Appl Microbiol Biotechnol, 2000. **54**(2): p. 218-23.

56. Natalie J. Garton, H.C., David E. Minnikin,Richard A. Adegbola and Michael R. Barer, *Intracellular lipophilic inclusions of mycobacteria in vitro and in sputum.* Microbiology, 2002. **148**: p. 2951-2958.

57. Ioneda, T. and S.S. Ono, *Chromatographic and mass spectrometric analyses of 1-monomycoloyl glycerol fraction from Rhodococcus lentifragmentus as per-O-benzoyl derivatives.* Chemistry and Physics of Lipids, 1996. **81**(1): p. 11-19.

58. Layre, E., et al., *Mycolic acids constitute a scaffold for mycobacterial lipid antigens stimulating CD1-restricted T cells.* Chem Biol, 2009. **16**(1): p. 82-92.

59. Claire S. Andersen, E.M.A., Ida Rosenkrands, Jessica M. Gomes, Veemal Bhowruth, Kevin J. C. Gibson, Rune V. Petersen, David E. Minnikin, Gurdyal S. Besra and Peter Andersen, *A Simple Mycobacterial Monomycolated Glycerol Lipid Has Potent Immunostimulatory Activity.* Journal of Immunology, 2009. **182**: p. 424-432.

60. Chen, J.M., et al., *Roles of Lsr2 in colony morphology and biofilm formation of Mycobacterium smegmatis.* J Bacteriol, 2006. **188**(2): p. 633-41.

61. Layre, E., et al., *A comparative lipidomics platform for chemotaxonomic analysis of Mycobacterium tuberculosis.* Chem Biol, 2011. **18**(12): p. 1537-49.

62. Barry, C.E., 3rd, et al., *Mycolic acids: structure, biosynthesis and physiological functions.* Prog Lipid Res, 1998. **37**(2-3): p. 143-79.

63. Nishiuchi, Y., et al., *Mycolic acid analysis in Nocardia species. The mycolic acid compositions of Nocardia asteroides, N. farcinica, and N. nova.* J Microbiol Methods, 1999. **37**(2): p. 111-22.

64. Hsu, F.F., et al., *Characterization of mycolic acids from the pathogen Rhodococcus equi by tandem mass spectrometry with electrospray ionization.* Anal Biochem, 2011. **409**(1): p. 112-22.

65. Nishiuchi, Y., T. Baba, and I. Yano, *Mycolic acids from Rhodococcus, Gordonia, and Dietzia.* Journal of Microbiological Methods, 2000. **40**(1): p. 1-9.

66. Yang, Y., et al., *Purification and structure analysis of mycolic acids in Corynebacterium glutamicum.* J Microbiol, 2012. **50**(2): p. 235-40.
67. Gebhardt, H., et al., *The key role of the mycolic acid content in the functionality of the cell wall permeability barrier in Corynebacterineae.* Microbiology, 2007. **153**(Pt 5): p. 1424-34.
68. Watanabe, M., et al., *Separation and characterization of individual mycolic acids in representative mycobacteria.* Microbiology, 2001. **147**(Pt 7): p. 1825-37.
69. RJ, A., *The separation of lipoid fractions from tubercle bacilli.* Journal of Biological Chemistry, 1927. **74**: p. 525-535.
70. I. Yano, K.K., Y. Ohno, M. Masui, E. Kusunose, M. Kusunose, and N. Akimori, *Separation and analysis of molecular species of mycolic acids in Nocardia and related taxa by gas chromatography mass spectrometry.* Biomed Mass Spectrom., 1986. **5**: p. 14-74.
71. Chantal Gailly, P.S., Maurice Verzele, and Carlo Cocito, *Analysis of Mycolic Acids from a Group of Corynebacteria by Capillary Gas Chromatography and Mass Spectrometry.* European Journal of Biochemistry, 1982. **125**: p. 83-94.
72. Suzanne E. Glickman, J.O.K., W. Ray Butler, and L. Scott Ramos, *Rapid Identification of Mycolic Acid Patterns of Mycobacteria byHigh-PerformanceLiquidChromatographyUsingPattern Recognition Software and a Mycobacterium Library.* Journal of Clinical Microbiology, 1994: p. 740-745.
73. Shui, G., et al., *Sensitive profiling of chemically diverse bioactive lipids.* J Lipid Res, 2007. **48**(9): p. 1976-84.
74. Laval, F., et al., *Accurate molecular mass determination of mycolic acids by MALDI-TOF mass spectrometry.* Anal Chem, 2001. **73**(18): p. 4537-44.
75. Shui, G.H., et al., *Mycolic acids as diagnostic markers for tuberculosis case detection in humans and drug efficacy in mice.* Embo Molecular Medicine, 2012. **4**(1): p. 27-37.
76. Verschoor JA, B.M., Grooten J, *Towards understanding the functional diversity of cell wall mycolic acids of Mycobacterium tuberculosis.* Prog Lipid Res, 2012. **51**(4): p. 325-329.
77. Bhatt, A., et al., *The Mycobacterium tuberculosis FAS-II condensing enzymes: their role in mycolic acid biosynthesis, acid-fastness, pathogenesis and in future drug development.* Molecular Microbiology, 2007. **64**(6): p. 1442-1454.

78. Barkan, D., et al., *Mycolic Acid Cyclopropanation is Essential for Viability, Drug Resistance, and Cell Wall Integrity of Mycobacterium tuberculosis.* Chemistry & Biology, 2009. **16**(5): p. 499-509.
79. Sutcliffe, I.C.e.a., *The rhodococcal cell envelope: composition, organisation and biosynthesis.*, in *Biology of Rhodococcus*, H.M. Alvarez, Editor 2010, Springer.
80. Ojha, A.K., et al., *Growth of Mycobacterium tuberculosis biofilms containing free mycolic acids and harbouring drug-tolerant bacteria.* Mol Microbiol, 2008. **69**(1): p. 164-74.
81. *<A Point Mutation in the mma3 Gene Is Responsible for Impaired Methoxymycolic Acid Production in Mycobacterium bovis BCG Strains Obtained after 1927.pdf>*.
82. Dubnau, E., et al., *Oxygenated mycolic acids are necessary for virulence of Mycobacterium tuberculosis in mice.* Mol Microbiol, 2000. **36**(3): p. 630-7.
83. Glickman, M.S., *The mmaA2 gene of Mycobacterium tuberculosis encodes the distal cyclopropane synthase of the alpha-mycolic acid.* J Biol Chem, 2003. **278**(10): p. 7844-9.
84. Glickman, M.S., S.M. Cahill, and W.R. Jacobs, Jr., *The Mycobacterium tuberculosis cmaA2 gene encodes a mycolic acid trans-cyclopropane synthetase.* J Biol Chem, 2001. **276**(3): p. 2228-33.
85. Behr MA, S.B., Brinkman JN, Slayden RA, Barry CE 3rd, *A Point Mutation in the mma3 Gene Is Responsible for Impaired Methoxymycolic Acid Production in Mycobacterium bovis BCG Strains Obtained after 1927.* Journal of Bacteriology, 2000. **182**(12): p. 3394-3399.
86. George, K.M., et al., *The biosynthesis of cyclopropanated mycolic acids in Mycobacterium tuberculosis. Identification and functional analysis of CMAS-2.* J Biol Chem, 1995. **270**(45): p. 27292-8.
87. Barkan, D., et al., *Mycobacterium tuberculosis Lacking All Mycolic Acid Cyclopropanation Is Viable but Highly Attenuated and Hyperinflammatory in Mice.* Infection and Immunity, 2012. **80**(6): p. 1958-1968.
88. Philips, J.A. and J.D. Ernst, *Tuberculosis pathogenesis and immunity.* Annu Rev Pathol, 2012. **7**: p. 353-84.
89. Dixit, A.J.a.P., *Multidrug resistant to extensively drug resistant tuberculosis: What is next?* J.Biosci., 2008. **33**(4): p. 605-616.
90. Sharma, S.K. and A. Mohan, *Multidrug-resistant tuberculosis: a menace that threatens to destabilize tuberculosis control.* Chest, 2006. **130**(1): p. 261-72.

91. Carpenter, J.L., et al., *Antituberculosis drug resistance in south Texas.* Am Rev Respir Dis, 1983. **128**(6): p. 1055-8.

92. Neel R Gandhi, A.M., A Willem Sturm, Robert Pawinski, Thiloshini Govender, Umesh Lalloo, Kimberly Zeller, Jason Andrews, and G. Friedland, *Extensively drug-resistant tuberculosis as a cause of death in patients co-infected with tuberculosis and HIV in a rural area of South Africa.* Lancet, 2006. **368**: p. 1575-1580.

93. Velayati, A.A., et al., *Emergence of new forms of totally drug-resistant tuberculosis bacilli: super extensively drug-resistant tuberculosis or totally drug-resistant strains in iran.* Chest, 2009. **136**(2): p. 420-5.

94. Udwadia, Z.F.A., R. A.; Ajbani, K. K.; Rodrigues, C., *Totally Drug-Resistant Tuberculosis in India.* Clinical Infectious Diseases, 2010. **54**(4): p. 579-581.

95. Kelly E. Dooley, C.M., Mary Ann DeGroote,Ekwaro Obuku,Vera Belitsky,Carol D. Hamilton,Mamodikoe Makhene,Sarita Shah,James C.M. Brust, Nadza Durakovic,and Eric Nuermberger on behalf of the Efficacy Subgroup, RESIST-TB* *Old drugs, new purpose: Retooling existing drugs for optimized treatment of resistant tuberculosis.* Infectious Diseases Society of

America, 2012.

96. Sacchettini, J.C., E.J. Rubin, and J.S. Freundlich, *Drugs versus bugs: in pursuit of the persistent predator Mycobacterium tuberculosis.* Nat Rev Microbiol, 2008. **6**(1): p. 41-52.

97. North, R.J. and Y.J. Jung, *Immunity to tuberculosis.* Annu Rev Immunol, 2004. **22**: p. 599-623.

98. Korbel, D.S., B.E. Schneider, and U.E. Schaible, *Innate immunity in tuberculosis: myths and truth.* Microbes Infect, 2008. **10**(9): p. 995-1004.

99. de Chastellier, C., *The many niches and strategies used by pathogenic mycobacteria for survival within host macrophages.* Immunobiology, 2009. **214**(7): p. 526-42.

100. Young, D.B., H.P. Gideon, and R.J. Wilkinson, *Eliminating latent tuberculosis.* Trends Microbiol, 2009. **17**(5): p. 183-8.

101. Kim MJ, W.H., Locketz M, Bekker LG, Walther GB, Dittrich C, Visser A, Wang W, Hsu FF, Wiehart U, Tsenova L, Kaplan G, Russell DG, *Caseation of human tuberculosis granulomas correlates with elevated host lipid metabolism.* EMBO Mol Med, 2010. **2**(7): p. 258-274.

102. Davis, J.M. and L. Ramakrishnan, *The role of the granuloma in expansion and dissemination of early tuberculous infection.* Cell, 2009. **136**(1): p. 37-49.

103. Guenin-Mace L, S.R., Demangel C, *Lipids of pathogenic Mycobacteria: contributions to virulence and host immune suppression.* . Transbound Emerg Dis., 2009. **56**: p. 255-268.

104. Lanbo Shi, C.D.S., Carmen Pfeiffer,Pratik Datta,Michael Parks,Johnjoe McFadden, Robert J. North and Maria L. Gennaro, *Carbon flux rerouting during Mycobacterium tuberculosis growth arrest.* Molecular Microbiology, 2010. **78**(5): p. 1199-1215.

105. Vergne, I., et al., *Cell biology of mycobacterium tuberculosis phagosome.* Annu Rev Cell Dev Biol, 2004. **20**: p. 367-94.

106. Basu, D.M.A.B.a.J., *Lipoarabinomannan from Mycobacterium tuberculosis promotes macrophage survival by phosphorylating Bad through a phosphatidylinositol 3-kinase/Akt pathway.* Journal of Biological Chemistry, 2000.

107. Axelrod, S., et al., *Delay of phagosome maturation by a mycobacterial lipid is reversed by nitric oxide.* Cell Microbiol, 2008. **10**(7): p. 1530-45.

108. Robinson, N., et al., *Mycobacterial phenolic glycolipid inhibits phagosome maturation and subverts the pro-inflammatory cytokine response.* Traffic, 2008. **9**(11): p. 1936-47.

109. Shirron, N. and S. Yaron, *Active Suppression of Early Immune Response in Tobacco by the Human Pathogen Salmonella Typhimurium.* Plos One, 2011. **6**(4).

110. Tan, K.S., et al., *Suppression of Host Innate Immune Response by Burkholderia pseudomallei through the Virulence Factor TssM.* Journal of Immunology, 2010. **184**(9): p. 5160-5171.

111. Pitarque, S., et al., *The immunomodulatory lipoglycans, lipoarabinomannan and lipomannan, are exposed at the mycobacterial cell surface.* Tuberculosis (Edinb), 2008. **88**(6): p. 560-5.

112. Mishra, A.K., et al., *Lipoarabinomannan biosynthesis in Corynebacterineae: the interplay of two alpha(1-->2)-mannopyranosyltransferases MptC and MptD in mannan branching.* Mol Microbiol, 2011. **80**(5): p. 1241-59.

113. Russell, D.G., C.E. Barry, 3rd, and J.L. Flynn, *Tuberculosis: what we don't know can, and does, hurt us.* Science, 2010. **328**(5980): p. 852-6.

114. *<Disparate responses to oxidative stress in saprophytic and pathogenic mycobacteria.pdf>*.

115. Beckman, E.M., et al., *Recognition of a lipid antigen by CD1-restricted alpha beta+ T cells.* Nature, 1994. **372**(6507): p. 691-4.

116. Dao, D.N., et al., *Mycolic acid modification by the mmaA4 gene of M. tuberculosis modulates IL-12 production.* Plos Pathogens, 2008. **4**(6).

117. Singh, P.P., et al., *Exosomes isolated from mycobacteria-infected mice or cultured macrophages can recruit and activate immune cells in vitro and in vivo.* J Immunol, 2012. **189**(2): p. 777-85.

118. Winder, F.G. and P.B. Collins, *Inhibition by isoniazid of synthesis of mycolic acids in Mycobacterium tuberculosis.* J Gen Microbiol, 1970. **63**(1): p. 41-8.

119. Hayes, L.G.W.a.L.G., *An In Vitro Model for Sequential Study of Shiftdown of Mycobacterium tuberculosis through Two Stages of Nonreplicating Persistence.* Infection adn Immunity, 1996: p. 2062-2069.

120. Paramasivan, C.N., et al., *Bactericidal action of gatifloxacin, rifampin, and isoniazid on logarithmic- and stationary-phase cultures of Mycobacterium tuberculosis.* Antimicrob Agents Chemother, 2005. **49**(2): p. 627-31.

121. Barry, C.E., et al., *The spectrum of latent tuberculosis: rethinking the biology and intervention strategies.* Nature Reviews Microbiology, 2009. **7**(12): p. 845-855.

122. Dijkhuizen, R.v.d.G.a.L., *Harnessing the catabolic diversity of rhodococci for environmental and biotechnological applications.* Current Opinion in Microbiology, 2004. **7**: p. 255-261.

123. Erable, B., Goubet, I., Lamare, S., Seltana, A., Legoy, M. D., and Maugard, T., *Nonconventional hydrolytic dehalogenation of 1−chlorobutane by dehydrated bacte- ria in a continuous solid−gas biofilter.* Erable, B., Goubet, I., Lamare, S., Seltana, A., Legoy, M. D., and Maugard, T., 2005. **91**: p. 304-313.

124. Larkin, M.J., L.A. Kulakov, and C.C. Allen, *Biodegradation and Rhodococcus--masters of catabolic versatility.* Curr Opin Biotechnol, 2005. **16**(3): p. 282-90.

125. Bouchez-Naitali, M., et al., *Relation between bacterial strain resistance to solvents and biodesulfurization activity in organic medium.* Applied Microbiology and Biotechnology, 2004. **65**(4): p. 440-445.

126. de Carvalho, C.C.C.R., A. Poretti, and M.M.R. da Fonseca, *Cell adaptation to solvent, substrate and product: a successful strategy to overcome product inhibition in a bioconversion system.* Applied Microbiology and Biotechnology, 2005. **69**(3): p. 268-275.

127. L. G. Whyte, S.J.S., F. PietrantonioL. Bourbonnière,S. F. Koval,J. R. Lawrence,W. E. Inniss,and C. W. Greer, *Physiological Adaptations Involved in Alkane Assimilation at a Low Temperature by Rhodococcus sp. Strain Q15.* Applied and Environmental Microbiology, 1999. **65**(7): p. 2961-2968.

128. Whyte, L.G., Slagman, S. J., Pietrantonio, F., Bourbonniere, L., Koval, S. F., Lawrence, J. R., Inniss, W. E., and Greer, C. W. , *Physiological adaptations involved in alkane assimilation at a low temperature by Rhodococcus sp. strain Q15.* Appl Environ Microbiol, 1999. **65**: p. 2961-2968.

129. T.R.Neu, T.D., B,.Jan and K. Poralla, *Structural studies of an emulsion-stabilizing exopolysaccharide produced by an adhesive, hydrophobic Rhodococcus strain.* Journal of General Microbiology, 1992. **138**: p. 2531-2537.

130. Kunihiro, N., Haruki, M., Takano, K., Morikawa, M., and Kanaya, S., *Isolation and characterization of Rhodococcus sp. strains TMP2 and T12 that degrade 2,6,10,14− tetramethylpentadecane (pristane) at moderately low temperatures.* J.Biotechnol., 2005. **115**: p. 129-136.

131. Bej, A.K., Saul, D., and Aislabie, J. , *Cold−tolerant alkane−degrading Rhodococcus species from Antarctica.* . Polar Biol., 2000. **23**(100-105).

132. Mustacchi, R., Knowles, C. J., Li, H., Dalrymple, I., Sunderland, G., Skibar, W., and Jackman, S. A., *Enhanced biotransformations and product recovery in a membrane bioreactor through application of a direct electric current.* Biotecnol. Bioeng., 2005. **89**: p. 18-23.

133. Sokolovska, I., et al., *Carbon source-induced modifications in the mycolic acid content and cell wall permeability of Rhodococcus erythropolis E1.* Applied and Environmental Microbiology, 2003. **69**(12): p. 7019-7027.

134. Cole, S.T., et al., *Deciphering the biology of Mycobacterium tuberculosis from the complete genome sequence.* Nature, 1998. **393**(6685): p. 537-44.

135. Krishna, S.H. and N.G. Karanth, *Lipases and lipase-catalyzed esterification reactions in nonaqueous media.* Catalysis Reviews-Science and Engineering, 2002. **44**(4): p. 499-591.

136. Levisson, M., J. van der Oost, and S.W. Kengen, *Carboxylic ester hydrolases from hyperthermophiles.* Extremophiles, 2009. **13**(4): p. 567-81.

137. Bornscheuer, U.T., *Microbial carboxyl esterases: classification, properties and application in biocatalysis.* Fems Microbiology Reviews, 2002. **26**(1): p. 73-81.

138. Arpigny, J.L. and K.E. Jaeger, *Bacterial lipolytic enzymes: classification and properties.* Biochemical Journal, 1999. **343**: p. 177-183.

139. Leticia Casas-Godoy, S.D., Florence Bordes, Georgina Sandoval, and Alain Marty, *Lipases: An Overview*, in *Lipases and Phospholipases: Methods and Protocols*, G. Sandoval, Editor 2012, pringer Science+Business Media New York: New York.

140. Ollis, D.L., et al., *The Alpha/Beta-Hydrolase Fold.* Protein Engineering, 1992. **5**(3): p. 197-211.

141. M, H., *Alpha/Beta-hydrolase fold enzymes: structures, functions and mechanisms.* Current Protein Pept. Sci., 2000. **1**(2): p. 209-235.

142. Nardini, M. and B.W. Dijkstra, *alpha/beta hydrolase fold enzymes: the family keeps growing.* Current Opinion in Structural Biology, 1999. **9**(6): p. 732-737.

143. Qian, Z., et al., *Recent progress in engineering alpha/beta hydrolase-fold family members.* Biotechnol J, 2007. **2**(2): p. 192-200.

144. Kim, D., et al., *Monocyclic Aromatic Hydrocarbon Degradation by Rhodococcus sp. Strain DK17.* Applied and Environmental Microbiology, 2002. **68**(7): p. 3270-3278.

145. Priefert, H., et al., *Indene bioconversion by a toluene inducible dioxygenase of Rhodococcus sp. I24.* Appl Microbiol Biotechnol, 2004. **65**(2): p. 168-76.

146. Taguchi K, M.M., Kudo T, *PCB/biphenyl degradation gene cluster in Rhodococcus rhodochrous K37, is different from the well-known bph gene cluster in Rhodococcus sp. P6, RHA1, and TA421.* Riken Rev, 2001. **42**: p. 23-26.

147. Konig, C., et al., *A linear megaplasmid, p1CP, carrying the genes for chlorocatechol catabolism of Rhodococcus opacus 1CP.* Microbiology, 2004. **150**(Pt 9): p. 3075-87.

148. Irina V. Tsitko, G.M.Z., Anatoli G. Lobanok, and Mirja S. Salkinoja-Salonen, *Effect of Aromatic Compounds on Cellular Fatty Acid Composition of Rhodococcus opacus.* Applied and Environmental Microbiology, 1999: p. 853-855.

149. Steinbu!chel, H.c.M.A.a.A., *Physiology, Biochemistry, and Molecular Biology of Triacylglycerol Accumulation by Rhodococcus*, in *Biology of Rhodococcus*, H.M. Alvarez, Editor 2010, Springer: Verlag Berlin Heidelberg.

150. Alvarez, A.F., et al., *Cloning and characterization of a gene involved in triacylglycerol biosynthesis and identification of additional homologous genes in the oleaginous bacterium Rhodococcus opacus PD630.* Microbiology, 2008. **154**(Pt 8): p. 2327-35.

151. Yen, C.L.E., et al., *DGAT enzymes and triacylglycerol biosynthesis.* Journal of Lipid Research, 2008. **49**(11): p. 2283-2301.

152. Marc Waltermann, H.L., Dirk Baumeister, Rainer Kalscheuerand Alexander Steinbuchel, *Rhodococcus opacus strain PD630 as a new source of high-value single-cell oil? Isolation and characterization of triacylglycerols and other storage lipids.* Microbiology, 2000. **146**: p. 1143-1149.

153. Gouda, M.K., S.H. Omar, and L.M. Aouad, *Single cell oil production by Gordonia sp. DG using agro-industrial wastes.* World Journal of Microbiology and Biotechnology, 2008. **24**(9): p. 1703-1711.

154. Christopher J. Brigham, K.K., ChoKyun Rha and Anthony J. Sinskey, *Bacterial Carbon Storage to Value Added Products.* Journal of Microbial and Biochemical Technoogy, 2011. **S3**(002).

155. Ali, Y. and M.A. Hanna, *Alternative Diesel Fuels from Vegetable-Oils.* Bioresource Technology, 1994. **50**(2): p. 153-163.

156. Rezanka, T., et al., *RP-HPLC/MS-APCI analysis of odd-chain TAGs from Rhodococcus erythropolis including some regioisomers.* Chemistry and Physics of Lipids, 2010. **163**(4-5): p. 373-380.

157. Layre, E., et al., *A Comparative Lipidomics Platform for Chemotaxonomic Analysis of Mycobacterium tuberculosis.* Chemistry & Biology, 2011. **18**(12): p. 1537-1549.

158. Sartain, M.J., et al., *Lipidomic analyses of Mycobacterium tuberculosis based on accurate mass measurements and the novel "Mtb LipidDB".* J Lipid Res, 2011. **52**(5): p. 861-72.

159. Stratton, H.M., P.R. Brooks, and R.J. Serviour, *Analysis of the structural diversity of mycolic acids of Rhodococcus and Gordonia isolates from activated sludge foams by selective ion monitoring gas chromatography mass spectrometry (SIM GC-MS) (vol 35, pg 53, 1999).* Journal of Microbiological Methods, 1999. **35**(3): p. 261-261.

160. Kolouchova, I., et al., *Structural analysis of mycolic acids from phenol-degrading strain of Rhodococcus erythropolis by liquid chromatography-tandem mass spectrometry.* Folia Microbiol (Praha), 2012. **57**(6): p. 473-83.

161. Baba, T., Y. Nishiuchi, and I. Yano, *Composition of mycolic acid molecular species as a criterion in nocardial classification.* International Journal of Systematic Bacteriology, 1997. **47**(3): p. 795-801.

162. Kurosawa, K., et al., *High-cell-density batch fermentation of Rhodococcus opacus PD630 using a high glucose concentration for triacylglycerol production.* J Biotechnol, 2010. **147**(3-4): p. 212-8.

163. Kurane, R., et al., *Chemical-Structure of Lipid Bioflocculant Produced by Rhodococcus-Erythropolis.* Bioscience Biotechnology and Biochemistry, 1995. **59**(9): p. 1652-1656.

164. Stratton, H.M., et al., *Effects of culture conditions on the mycolic acid composition of isolates of Rhodococcus spp. from activated sludgefoams.* Syst Appl Microbiol, 2003. **26**(2): p. 165-71.

165. Simon, G.M. and B.F. Cravatt, *Activity-based proteomics of enzyme superfamilies: serine hydrolases as a case study.* J Biol Chem, 2010. **285**(15): p. 11051-5.

166. Cravatt, B.F., A.T. Wright, and J.W. Kozarich, *Activity-based protein profiling: from enzyme chemistry to proteomic chemistry.* Annu Rev Biochem, 2008. **77**: p. 383-414.

167. Yongsheng Liu, M.P.P., and Benjamin F. Cravatt, *Activity-based protein profiling: The serine hydrolases.* PNAS, 1999. **96**(26).

168. Dana Kidd, Y.L., and Benjamin F. Cravatt, *Profiling Serine Hydrolase Activities in Complex Proteomes.* Biochemistry, 2001. **40**: p. 4005-4015.

169. Saghatelian, A., et al., *Activity-based probes for the proteomic profiling of metalloproteases.* Proc Natl Acad Sci U S A, 2004. **101**(27): p. 10000-5.

170. *<Epoxide electrophiles as activity-dependent cysteine protease pro¢ling and discovery tools.pdf>*.

171. Adam, G.C., E.J. Sorensen, and B.F. Cravatt, *Proteomic profiling of mechanistically distinct enzyme classes using a common chemotype.* Nat Biotechnol, 2002. **20**(8): p. 805-9.

172. Barglow, K.T. and B.F. Cravatt, *Activity-based protein profiling for the functional annotation of enzymes.* Nat Methods, 2007. **4**(10): p. 822-7.

173. Bottcher, T. and S.A. Sieber, *Beta-lactones as privileged structures for the active-site labeling of versatile bacterial enzyme classes.* Angew Chem Int Ed Engl, 2008. **47**(24): p. 4600-3.

174. Sieber, S.A., et al., *Proteomic profiling of metalloprotease activities with cocktails of active-site probes.* Nat Chem Biol, 2006. **2**(5): p. 274-81.

175. E.K.Weibel, P.H., E.Hochuli, E.Kupper and H.Lengsfeld, *Lipstatin an inhibitor of pancreatic lipase produced by Streptomyces toxytricini I. Producing organism, fermentation, isolation and biological activity.* The Journal of Antibiotics, 1987. **8**.

176. E.Hochuli, E.K., R.Maurer, W.Mester, Y.Mercadal and K.Schimidt, *Lipstatin, an inhibitor of pancreatic lipase, produced by Streptomyces*

toxytricini II.Chemistry and strucuture elucidation. The journal of Antibiotics, 1987.

177. Paul Hadvary, H.L.a.H.W., *Inhibitionofpancreaticlipase invitrobythecovalentinhibitor tetrahydrolipstatin.* Journal of Biochemistry, 1988. **256**: p. 357-361.

178. Yang, P.Y., et al., *Chemical modification and organelle-specific localization of orlistat-like natural-product-based probes.* Chem Asian J, 2011. **6**(10): p. 2762-75.

179. Peng-Yu Yang, K.L., Mun Hong Ngai,Martin J. Lear,Markus R. Wenk,and Shao Q. Yao, *Activity-Based Proteome Profiling of Potential Cellular Targets of Orlistat - An FDA-Approved Drug with Anti-Tumor Activities.* J. AM.CHEM. SOC., 2009. **132**: p. 656-666.

180. Low, K.L., et al., *Lipid droplet-associated proteins are involved in the biosynthesis and hydrolysis of triacylglycerol in Mycobacterium bovis bacillus Calmette-Guerin.* J Biol Chem, 2010. **285**(28): p. 21662-70.

181. Alvarez, M.n.A.H.n.A.A.E.R.g.H.G.H.c.M., *The atf2 gene is involved in triacylglycerol biosynthesis and accumulation in the oleaginous Rhodococcus opacus PD630.* Appl Microbiol Biotechnol, 2012.

182. *The Rhodococcus opacus PD630 Heparin-Binding Hemagglutinin Homolog TadA Mediates Lipid Body Formation* Appl Environ Microbiol, 2010. **76**(21): p. 7217-7225.

183. Pemble, C.W.t., et al., *Crystal structure of the thioesterase domain of human fatty acid synthase inhibited by Orlistat.* Nat Struct Mol Biol, 2007. **14**(8): p. 704-9.

184. Weerapana, E., G.M. Simon, and B.F. Cravatt, *Disparate proteome reactivity profiles of carbon electrophiles.* Nat Chem Biol, 2008. **4**(7): p. 405-7.

185. Böttcher, T. and S.A. Sieber, *β-Lactams and β-lactones as activity-based probes in chemical biology.* MedChemComm, 2012. **3**(4): p. 408.

186. Rawlings, N.D., A.J. Barrett, and A. Bateman, *MEROPS: the peptidase database.* Nucleic Acids Res, 2010. **38**(Database issue): p. D227-33.

187. Zhang, Y., et al., *Characterization of Thermobifida fusca cutinase-carbohydrate-binding module fusion proteins and their potential application in bioscouring.* Appl Environ Microbiol, 2010. **76**(20): p. 6870-6.

188. Wältermann M, H.A., Robenek H, Troyer D, Reichelt R, Malkus U, Galla HJ, Kalscheuer R, Stöveken T, von Landenberg P, Steinbüchel A., *Mechanism of lipid-body formation in prokaryotes: how bacteria fatten up.* Mol Microbiol, 2005. **55**(3): p. 750-763.

189. Gagneux, S., *Host-pathogen coevolution in human tuberculosis.* Philos Trans R Soc Lond B Biol Sci, 2012. **367**(1590): p. 850-9.

190. Gagneux, S., et al., *The competitive cost of antibiotic resistance in Mycobacterium tuberculosis.* Science, 2006. **312**(5782): p. 1944-6.

191. Wan, K., et al., *Investigation on Mycobacterium tuberculosis diversity in China and the origin of the Beijing clade.* PLoS One, 2011. **6**(12): p. e29190.

192. Jagielski, T., et al., *Spoligotype-based comparative population structure analysis of multidrug-resistant and isoniazid-monoresistant Mycobacterium tuberculosis complex clinical isolates in Poland.* J Clin Microbiol, 2010. **48**(11): p. 3899-909.

193. Stavrum, R., et al., *Genomic diversity among Beijing and non-Beijing Mycobacterium tuberculosis isolates from Myanmar.* PLoS One, 2008. **3**(4): p. e1973.

194. Comas, I., et al., *Human T cell epitopes of Mycobacterium tuberculosis are evolutionarily hyperconserved.* Nat Genet, 2010. **42**(6): p. 498-503.

195. Brosch, R., et al., *A new evolutionary scenario for the Mycobacterium tuberculosis complex.* Proc Natl Acad Sci U S A, 2002. **99**(6): p. 3684-9.

196. Hershberg, R., et al., *High functional diversity in Mycobacterium tuberculosis driven by genetic drift and human demography.* PLoS Biol, 2008. **6**(12): p. e311.

197. North, P.L.D.a.R.J., *Virulence ranking of some Mycobacterium tuberculosis and Mycobacterium bovis strains according to their ability to multiply in the lungs, induce lung pathology, and cause mortality in mice.* Infection and Immunity. **63**(9).

198. William R. Bishai, A.M.D., JR.,Nikki Parrish,Rafael Ruiz,Ping Chen,Bernard C. Zook,Walter Johnson,James W. Boles, and M. Loise M. Pitt, *Virulence of Mycobacterium tuberculosis CDC1551 and H37Rv in Rabbits Evaluated by Lurie's Pulmonary Tubercle Count Method.* Infection and Immunity, 1999: p. 4931-4934.

199. J. Dormans, M.B., D. Agiular, R. Hernandez-Pando, K. Kremer, P. Roholl, S. M. Arend & D. Van Soolingen, *Correlation of virulence, lung pathology, bacterial load and delayed type hypersensitivity responses after infection with different Mycobacterium tuberculosis genotypes in a BALB/c mouse model.* Clin Exp Immunol, 2004. **137**: p. 460-468.

200. Portevin, D., et al., *Human Macrophage Responses to Clinical Isolates from the Mycobacterium tuberculosis Complex Discriminate between Ancient and Modern Lineages.* Plos Pathogens, 2011. **7**(3).

201. Wang, C., et al., *Innate immune response to Mycobacterium tuberculosis Beijing and other genotypes.* PLoS One, 2010. **5**(10): p. e13594.

202. Aguilar, D., et al., *Mycobacterium tuberculosis strains with the Beijing genotype demonstrate variability in virulence associated with transmission.* Tuberculosis (Edinb), 2010. **90**(5): p. 319-25.

203. Reed, M.B., et al., *A glycolipid of hypervirulent tuberculosis strains that inhibits the innate immune response.* Nature, 2004. **431**(7004): p. 84-87.

204. Rao, V., et al., *Trans-cyclopropanation of mycolic acids on trehalose dimycolate suppresses Mycobacterium tuberculosis -induced inflammation and virulence.* J Clin Invest, 2006. **116**(6): p. 1660-7.

205. Vander Beken, S., et al., *Molecular structure of the Mycobacterium tuberculosis virulence factor, mycolic acid, determines the elicited inflammatory pattern.* European Journal of Immunology, 2011. **41**(2): p. 450-460.

206. Huet, G., et al., *A lipid profile typifies the Beijing strains of Mycobacterium tuberculosis: identification of a mutation responsible for a modification of the structures of phthiocerol dimycocerosates and phenolic glycolipids.* J Biol Chem, 2009. **284**(40): p. 27101-13.

207. Michael B. Reed, S.G., Kathryn DeRiemer, Peter M. Small and Clifton E. Barry, III, *The W/Beijing lineage of Mycobacterium tuberculosis overproduces triglycerides and is constitutively upregulated for the DosR dormancy regulon.* Journal of Bacteriology, 2007.

208. Krishnan, N., et al., *Mycobacterium tuberculosis Lineage Influences Innate Immune Response and Virulence and Is Associated with Distinct Cell Envelope Lipid Profiles.* PLoS One, 2011. **6**(9).

209. Yuan, Y., et al., *Identification of a gene involved in the biosynthesis of cyclopropanated mycolic acids in Mycobacterium tuberculosis.* Proc Natl Acad Sci U S A, 1995. **92**(14): p. 6630-4.

210. Singh, A., et al., *Requirement of the mymA operon for appropriate cell wall ultrastructure and persistence of Mycobacterium tuberculosis in the spleens of guinea pigs.* J Bacteriol, 2005. **187**(12): p. 4173-86.

211. Peyron, P., et al., *Foamy macrophages from tuberculous patients' granulomas constitute a nutrient-rich reservoir for M. tuberculosis persistence.* PLoS Pathog, 2008. **4**(11): p. e1000204.

212. Kim, M.J., et al., *Caseation of human tuberculosis granulomas correlates with elevated host lipid metabolism.* EMBO Mol Med, 2010. **2**(7): p. 258-74.

213. Ordway D, H.-T.M., Orme IM, Gonzalez-Juarrero M., *Foamy macrophages within lung granulomas of mice infected with Mycobacterium tuberculosis express molecules characteristic of dendritic cells and antiapoptotic markers of the TNF receptor-associated factor family.* Journal of Immunology, 2005. **175**(6): p. 3873-3881.

214. Davidson, L.A., P. Draper, and D.E. Minnikin, *Studies on the Mycolic Acids from the Walls of Mycobacterium-Microti.* Journal of General Microbiology, 1982. **128**(Apr): p. 823-828.

215. Yuan, Y., et al., *The effect of oxygenated mycolic acid composition on cell wall function and macrophage growth in Mycobacterium tuberculosis.* Mol Microbiol, 1998. **29**(6): p. 1449-58.

216. Starck, J., et al., *Comparative proteome analysis of Mycobacterium tuberculosis grown under aerobic and anaerobic conditions.* Microbiology, 2004. **150**(Pt 11): p. 3821-9.

217. Rachman, H., et al., *Unique transcriptome signature of Mycobacterium tuberculosis in pulmonary tuberculosis.* Infect Immun, 2006. **74**(2): p. 1233-42.

218. Mehta, P.K., et al., *Comparison of in vitro models for the study of Mycobacterium tuberculosis invasion and intracellular replication.* Infection and Immunity, 1996. **64**(7): p. 2673-2679.

219. Paul, S., P. Laochumroonvorapong, and G. Kaplan, *Comparable growth of virulent and avirulent Mycobacterium tuberculosis in human macrophages in vitro.* Journal of Infectious Diseases, 1996. **174**(1): p. 105-112.

220. Bassegoda, A., et al., *Special Rhodococcus sp. CR-53 esterase Est4 contains a GGG(A)X-oxyanion hole conferring activity for the kinetic resolution of tertiary alcohols.* Appl Microbiol Biotechnol, 2013.

Appendix 1

Decision tree:

To identify the individual MA species that significantly varied among the four lineages, decision trees were plotted with party library in R. Based on the decision trees box plots were generated for the three MA species that emerged significant.

A

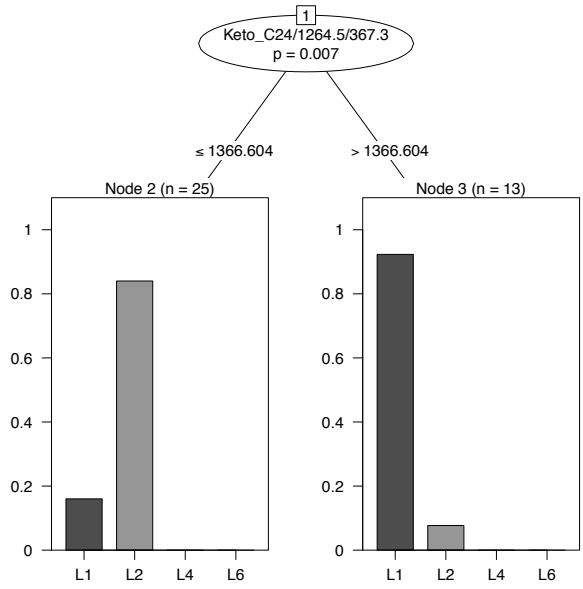

B

C

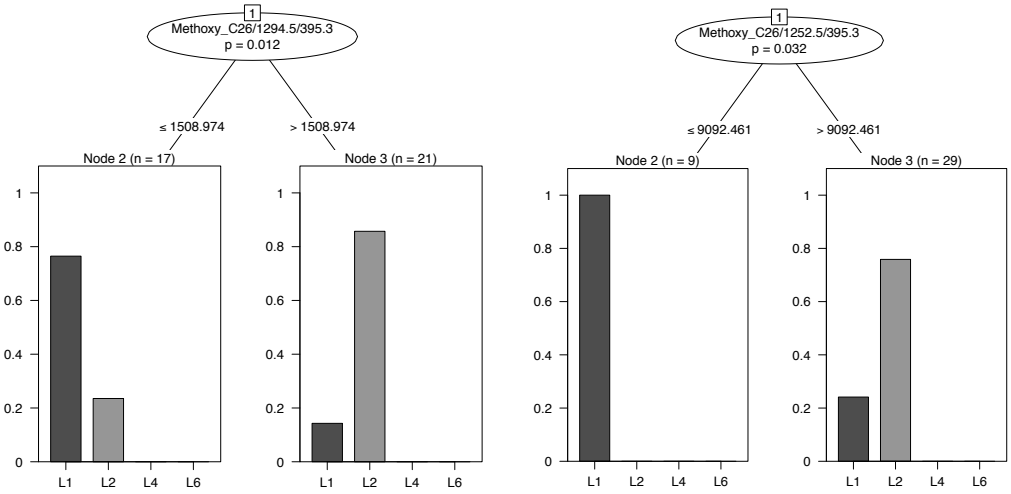

Appendix 2

Lipid analysis of Mtb infected macrophage

Neutral lipids (A-Triacylglycerol (TAG), B-Cholesterol (CHO) and C-Cholesterol esters (CE)) profiles of the different Mtb lineages used for infecting human macrophages from three independent donors. All lineage-infected macrophages exhibited a conserved core of changes in neutral lipids. All neutral lipids increased in abundance in infected macrophages compared to non-infected control macrophages. Statistical significance is expressed in comparison to non-infected macrophage samples (control) ***p≤0.001; ** p≤0.01; *p≤0.05

A **B** **C**

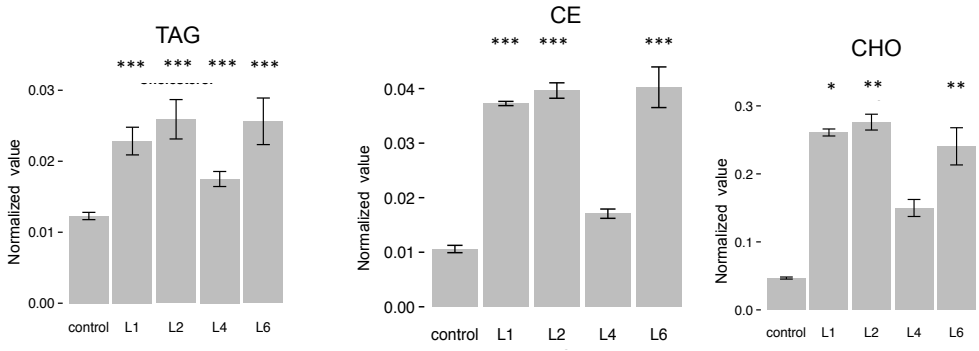

Appendix 3

Multiple reaction monitoring (MRM) transitions of rhodococcal mycolic acids developed in this thesis.

MRM	No. of Carbon	No. of Hydrogen	No. of Oxygen	α-branch	Exact mass	Deprotonated mass
839.7/297.3	57	108	3	19:0	840.85572	839.84778
837.7/297.3	57	106	3	19:0	838.83984	837.8319
825.7/297.3	56	106	3	19:0	826.83984	825.8319
823.7/297.3	56	104	3	19:0	824.82396	823.81602
811.7/297.3	55	104	3	19:0	812.82396	811.81602
809.7/297.3	55	102	3	19:0	810.80808	809.80014
797.7/297.3	54	102	3	19:0	798.80808	797.80014
795.7/297.3	54	100	3	19:0	796.7922	795.78426
783.7/297.3	53	100	3	19:0	784.7922	783.78426
781.7/297.3	53	98	3	19:0	782.77632	781.76838
769.7/297.3	52	98	3	19:0	770.77632	769.76838
767.7/297.3	52	96	3	19:0	768.76044	767.7525
755.7/297.3	51	96	3	19:0	756.76044	755.7525
753.7/297.3	51	94	3	19:0	754.74456	753.73662
743.7/297.3	50	96	3	19:0	744.76044	743.7525
741.7/297.3	50	94	3	19:0	742.74456	741.73662
739.7/297.3	50	92	3	19:0	740.72868	739.72074
729.7/297.3	49	94	3	19:0	730.74456	729.73662
727.7/297.3	49	92	3	19:0	728.72868	727.72074
725.7/297.3	49	90	3	19:0	726.7128	725.70486
713.7/297.3	48	90	3	19:0	714.7128	713.70486
711.7/297.3	48	88	3	19:0	712.69692	711.68898
699.7/297.3	47	88	3	19:0	700.69692	699.68898
697.7/297.3	47	86	3	19:0	698.68104	697.6731
685.7/297.3	47	84	3	19:0	696.66516	695.65722
671.7/297.3	45	84	3	19:0	672.66516	671.65722
669.7/297.3	45	82	3	19:0	670.64928	669.64134
657.7/297.3	44	82	3	19:0	658.64928	657.64134
643.7/297.3	43	80	3	19:0	644.6334	643.62546
627.7/297.3	42	76	3	19:0	628.60164	627.5937
613.7/297.3	41	74	3	19:0	614.58576	613.57782
595.6/297.3	39	80	3	19:0	596.6334	595.62546
593.6/297.3	39	78	3	19:0	594.61752	593.60958
585.6/297.3	38	82	3	19:0	586.64928	585.64134
581.6/297.3	38	78	3	19:0	582.61752	581.60958
575.6/297.3	38	72	3	19:0	576.56988	575.56194
565.6/297.3	37	74	3	19:0	566.58576	565.57782
563.6/297.3	37	72	3	19:0	564.56988	563.56194
553.6/297.3	36	74	3	19:0	554.58576	553.57782
551.6/297.3	36	72	3	19:0	552.56988	551.56194
549.6/297.3	36	70	3	19:0	550.554	549.54606
539.6/297.3	35	72	3	19:0	540.56988	539.56194
537.6/297.3	35	70	3	19:0	538.554	537.54606
525.6/297.3	34	70	3	19:0	526.554	525.54606

523.6/297.3	34	68	3	19:0	524.53812	523.53018
511.6/297.3	33	68	3	19:0	512.53812	511.53018
509.6/297.3	33	66	3	19:0	510.52224	509.5143
839.7/283.3	57	108	3	18:0	840.85572	839.84778
837.7/283.3	57	106	3	18:0	838.83984	837.8319
825.7/283.3	56	106	3	18:0	826.83984	825.8319
823.7/283.3	56	104	3	18:0	824.82396	823.81602
811.7/283.3	55	104	3	18:0	812.82396	811.81602
809.7/283.3	55	102	3	18:0	810.80808	809.80014
797.7/283.3	54	102	3	18:0	798.80808	797.80014
795.7/283.3	54	100	3	18:0	796.7922	795.78426
783.7/283.3	53	100	3	18:0	784.7922	783.78426
781.7/283.3	53	98	3	18:0	782.77632	781.76838
769.7/283.3	52	98	3	18:0	770.77632	769.76838
767.7/283.3	52	96	3	18:0	768.76044	767.7525
755.7/283.3	51	96	3	18:0	756.76044	755.7525
753.7/283.3	51	94	3	18:0	754.74456	753.73662
743.7/283.3	50	96	3	18:0	744.76044	743.7525
741.7/283.3	50	94	3	18:0	742.74456	741.73662
739.7/283.3	50	92	3	18:0	740.72868	739.72074
729.7/283.3	49	94	3	18:0	730.74456	729.73662
727.7/283.3	49	92	3	18:0	728.72868	727.72074
725.7/283.3	49	90	3	18:0	726.7128	725.70486
713.7/283.3	48	90	3	18:0	714.7128	713.70486
711.7/283.3	48	88	3	18:0	712.69692	711.68898
699.7/283.3	47	88	3	18:0	700.69692	699.68898
697.7/283.3	47	86	3	18:0	698.68104	697.6731
685.7/283.3	47	84	3	18:0	696.66516	695.65722
671.7/283.3	45	84	3	18:0	672.66516	671.65722
669.7/283.3	45	82	3	18:0	670.64928	669.64134
657.7/283.3	44	82	3	18:0	658.64928	657.64134
643.7/283.3	43	80	3	18:0	644.6334	643.62546
627.7/283.3	42	76	3	18:0	628.60164	627.5937
613.7/283.3	41	74	3	18:0	614.58576	613.57782
595.6/283.3	39	80	3	18:0	596.6334	595.62546
593.6/283.3	39	78	3	18:0	594.61752	593.60958
585.6/283.3	38	82	3	18:0	586.64928	585.64134
581.6/283.3	38	78	3	18:0	582.61752	581.60958
575.6/283.3	38	72	3	18:0	576.56988	575.56194
565.6/283.3	37	74	3	18:0	566.58576	565.57782
563.6/283.3	37	72	3	18:0	564.56988	563.56194
553.6/283.3	36	74	3	18:0	554.58576	553.57782
551.6/283.3	36	72	3	18:0	552.56988	551.56194
549.6/283.3	36	70	3	18:0	550.554	549.54606
539.6/283.3	35	72	3	18:0	540.56988	539.56194
537.6/283.3	35	70	3	18:0	538.554	537.54606
525.6/283.3	34	70	3	18:0	526.554	525.54606
523.6/283.3	34	68	3	18:0	524.53812	523.53018
511.6/283.3	33	68	3	18:0	512.53812	511.53018
509.6/283.3	33	66	3	18:0	510.52224	509.5143
839.7/281.3	57	108	3	18:1	840.85572	839.84778
837.7/281.3	57	106	3	18:1	838.83984	837.8319
825.7/281.3	56	106	3	18:1	826.83984	825.8319

823.7/281.3	56	104	3	18:1	824.82396	823.81602
811.7/281.3	55	104	3	18:1	812.82396	811.81602
809.7/281.3	55	102	3	18:1	810.80808	809.80014
797.7/281.3	54	102	3	18:1	798.80808	797.80014
795.7/281.3	54	100	3	18:1	796.7922	795.78426
783.7/281.3	53	100	3	18:1	784.7922	783.78426
781.7/281.3	53	98	3	18:1	782.77632	781.76838
769.7/281.3	52	98	3	18:1	770.77632	769.76838
767.7/281.3	52	96	3	18:1	768.76044	767.7525
755.7/281.3	51	96	3	18:1	756.76044	755.7525
753.7/281.3	51	94	3	18:1	754.74456	753.73662
743.7/281.3	50	96	3	18:1	744.76044	743.7525
741.7/281.3	50	94	3	18:1	742.74456	741.73662
739.7/281.3	50	92	3	18:1	740.72868	739.72074
729.7/281.3	49	94	3	18:1	730.74456	729.73662
727.7/281.3	49	92	3	18:1	728.72868	727.72074
725.7/281.3	49	90	3	18:1	726.7128	725.70486
713.7/281.3	48	90	3	18:1	714.7128	713.70486
711.7/281.3	48	88	3	18:1	712.69692	711.68898
699.7/281.3	47	88	3	18:1	700.69692	699.68898
697.7/281.3	47	86	3	18:1	698.68104	697.6731
685.7/281.3	47	84	3	18:1	696.66516	695.65722
671.7/281.3	45	84	3	18:1	672.66516	671.65722
669.7/281.3	45	82	3	18:1	670.64928	669.64134
657.7/281.3	44	82	3	18:1	658.64928	657.64134
643.7/281.3	43	80	3	18:1	644.6334	643.62546
627.7/281.3	42	76	3	18:1	628.60164	627.5937
613.7/281.3	41	74	3	18:1	614.58576	613.57782
595.6/281.3	39	80	3	18:1	596.6334	595.62546
593.6/281.3	39	78	3	18:1	594.61752	593.60958
585.6/281.3	38	82	3	18:1	586.64928	585.64134
581.6/281.3	38	78	3	18:1	582.61752	581.60958
575.6/281.3	38	72	3	18:1	576.56988	575.56194
565.6/281.3	37	74	3	18:1	566.58576	565.57782
563.6/281.3	37	72	3	18:1	564.56988	563.56194
553.6/281.3	36	74	3	18:1	554.58576	553.57782
551.6/281.3	36	72	3	18:1	552.56988	551.56194
549.6/281.3	36	70	3	18:1	550.554	549.54606
539.6/281.3	35	72	3	18:1	540.56988	539.56194
537.6/281.3	35	70	3	18:1	538.554	537.54606
525.6/281.3	34	70	3	18:1	526.554	525.54606
523.6/281.3	34	68	3	18:1	524.53812	523.53018
511.6/281.3	33	68	3	18:1	512.53812	511.53018
509.6/281.3	33	66	3	18:1	510.52224	509.5143
839.7/269.3	57	108	3	17:0	840.85572	839.84778
837.7/269.3	57	106	3	17:0	838.83984	837.8319
825.7/269.3	56	106	3	17:0	826.83984	825.8319
823.7/269.3	56	104	3	17:0	824.82396	823.81602
811.7/269.3	55	104	3	17:0	812.82396	811.81602
809.7/269.3	55	102	3	17:0	810.80808	809.80014
797.7/269.3	54	102	3	17:0	798.80808	797.80014
795.7/269.3	54	100	3	17:0	796.7922	795.78426
783.7/269.3	53	100	3	17:0	784.7922	783.78426

781.7/269.3	53	98	3	17:0	782.77632	781.76838
769.7/269.3	52	98	3	17:0	770.77632	769.76838
767.7/269.3	52	96	3	17:0	768.76044	767.7525
755.7/269.3	51	96	3	17:0	756.76044	755.7525
753.7/269.3	51	94	3	17:0	754.74456	753.73662
743.7/269.3	50	96	3	17:0	744.76044	743.7525
741.7/269.3	50	94	3	17:0	742.74456	741.73662
739.7/269.3	50	92	3	17:0	740.72868	739.72074
729.7/269.3	49	94	3	17:0	730.74456	729.73662
727.7/269.3	49	92	3	17:0	728.72868	727.72074
725.7/269.3	49	90	3	17:0	726.7128	725.70486
713.7/269.3	48	90	3	17:0	714.7128	713.70486
711.7/269.3	48	88	3	17:0	712.69692	711.68898
699.7/269.3	47	88	3	17:0	700.69692	699.68898
697.7/269.3	47	86	3	17:0	698.68104	697.6731
685.7/269.3	47	84	3	17:0	696.66516	695.65722
671.7/269.3	45	84	3	17:0	672.66516	671.65722
669.7/269.3	45	82	3	17:0	670.64928	669.64134
657.7/269.3	44	82	3	17:0	658.64928	657.64134
643.7/269.3	43	80	3	17:0	644.6334	643.62546
627.7/269.3	42	76	3	17:0	628.60164	627.5937
613.7/269.3	41	74	3	17:0	614.58576	613.57782
595.6/269.3	39	80	3	17:0	596.6334	595.62546
593.6/269.3	39	78	3	17:0	594.61752	593.60958
585.6/269.3	38	82	3	17:0	586.64928	585.64134
581.6/269.3	38	78	3	17:0	582.61752	581.60958
575.6/269.3	38	72	3	17:0	576.56988	575.56194
565.6/269.3	37	74	3	17:0	566.58576	565.57782
563.6/269.3	37	72	3	17:0	564.56988	563.56194
553.6/269.3	36	74	3	17:0	554.58576	553.57782
551.6/269.3	36	72	3	17:0	552.56988	551.56194
549.6/269.3	36	70	3	17:0	550.554	549.54606
539.6/269.3	35	72	3	17:0	540.56988	539.56194
537.6/269.3	35	70	3	17:0	538.554	537.54606
525.6/269.3	34	70	3	17:0	526.554	525.54606
523.6/269.3	34	68	3	17:0	524.53812	523.53018
511.6/269.3	33	68	3	17:0	512.53812	511.53018
509.6/269.3	33	66	3	17:0	510.52224	509.5143
839.7/267.3	57	108	3	17:0	840.85572	839.84778
837.7/267.3	57	106	3	17:0	838.83984	837.8319
825.7/267.3	56	106	3	17:0	826.83984	825.8319
823.7/267.3	56	104	3	17:0	824.82396	823.81602
811.7/267.3	55	104	3	17:0	812.82396	811.81602
809.7/267.3	55	102	3	17:0	810.80808	809.80014
797.7/267.3	54	102	3	17:0	798.80808	797.80014
795.7/267.3	54	100	3	17:0	796.7922	795.78426
783.7/267.3	53	100	3	17:0	784.7922	783.78426
781.7/267.3	53	98	3	17:0	782.77632	781.76838
769.7/267.3	52	98	3	17:0	770.77632	769.76838
767.7/267.3	52	96	3	17:0	768.76044	767.7525
755.7/267.3	51	96	3	17:0	756.76044	755.7525
753.7/267.3	51	94	3	17:0	754.74456	753.73662
743.7/267.3	50	96	3	17:0	744.76044	743.7525

741.7/267.3	50	94	3	17:0	742.74456	741.73662
739.7/267.3	50	92	3	17:0	740.72868	739.72074
729.7/267.3	49	94	3	17:0	730.74456	729.73662
727.7/267.3	49	92	3	17:0	728.72868	727.72074
725.7/267.3	49	90	3	17:0	726.7128	725.70486
713.7/267.3	48	90	3	17:0	714.7128	713.70486
711.7/267.3	48	88	3	17:0	712.69692	711.68898
699.7/267.3	47	88	3	17:0	700.69692	699.68898
697.7/267.3	47	86	3	17:0	698.68104	697.6731
685.7/267.3	47	84	3	17:0	696.66516	695.65722
671.7/267.3	45	84	3	17:0	672.66516	671.65722
669.7/267.3	45	82	3	17:0	670.64928	669.64134
657.7/267.3	44	82	3	17:0	658.64928	657.64134
643.7/267.3	43	80	3	17:0	644.6334	643.62546
627.7/267.3	42	76	3	17:0	628.60164	627.5937
613.7/267.3	41	74	3	17:0	614.58576	613.57782
595.6/267.3	39	80	3	17:0	596.6334	595.62546
593.6/267.3	39	78	3	17:0	594.61752	593.60958
585.6/267.3	38	82	3	17:0	586.64928	585.64134
581.6/267.3	38	78	3	17:0	582.61752	581.60958
575.6/267.3	38	72	3	17:0	576.56988	575.56194
565.6/267.3	37	74	3	17:0	566.58576	565.57782
563.6/267.3	37	72	3	17:0	564.56988	563.56194
553.6/267.3	36	74	3	17:0	554.58576	553.57782
551.6/267.3	36	72	3	17:0	552.56988	551.56194
549.6/267.3	36	70	3	17:0	550.554	549.54606
539.6/267.3	35	72	3	17:0	540.56988	539.56194
537.6/267.3	35	70	3	17:0	538.554	537.54606
525.6/267.3	34	70	3	17:0	526.554	525.54606
523.6/267.3	34	68	3	17:0	524.53812	523.53018
511.6/267.3	33	68	3	17:0	512.53812	511.53018
509.6/267.3	33	66	3	17:0	510.52224	509.5143
497.5/267.3	32	66	3	17:0	498.52224	497.5143
495.5/267.3	32	64	3	17:0	496.50636	495.49842
483.5/267.3	31	64	3	17:0	484.50636	483.49842
481.5/267.3	31	62	3	17:0	482.49048	481.48254
473.5/267.3	30	66	3	17:0	474.52224	473.5143
469.5/267.3	30	62	3	17:0	470.49048	469.48254
455.5/267.3	29	60	3	17:0	456.4746	455.46666
453.5/267.3	29	58	3	17:0	454.45872	453.45078
441.5/267.3	28	58	3	17:0	442.45872	441.45078
439.5/267.3	28	56	3	17:0	440.44284	439.4349
839.7/255.3	57	108	3	16:0	840.85572	839.84778
837.7/255.3	57	106	3	16:0	838.83984	837.8319
825.7/255.3	56	106	3	16:0	826.83984	825.8319
823.7/255.3	56	104	3	16:0	824.82396	823.81602
811.7/255.3	55	104	3	16:0	812.82396	811.81602
809.7/255.3	55	102	3	16:0	810.80808	809.80014
797.7/255.3	54	102	3	16:0	798.80808	797.80014
795.7/255.3	54	100	3	16:0	796.7922	795.78426
783.7/255.3	53	100	3	16:0	784.7922	783.78426
781.7/255.3	53	98	3	16:0	782.77632	781.76838
769.7/255.3	52	98	3	16:0	770.77632	769.76838

767.7/255.3	52	96	3	16:0	768.76044	767.7525
755.7/255.3	51	96	3	16:0	756.76044	755.7525
753.7/255.3	51	94	3	16:0	754.74456	753.73662
743.7/255.3	50	96	3	16:0	744.76044	743.7525
741.7/255.3	50	94	3	16:0	742.74456	741.73662
739.7/255.3	50	92	3	16:0	740.72868	739.72074
729.7/255.3	49	94	3	16:0	730.74456	729.73662
727.7/255.3	49	92	3	16:0	728.72868	727.72074
725.7/255.3	49	90	3	16:0	726.7128	725.70486
713.7/255.3	48	90	3	16:0	714.7128	713.70486
711.7/255.3	48	88	3	16:0	712.69692	711.68898
699.7/255.3	47	88	3	16:0	700.69692	699.68898
697.7/255.3	47	86	3	16:0	698.68104	697.6731
685.7/255.3	47	84	3	16:0	696.66516	695.65722
671.7/255.3	45	84	3	16:0	672.66516	671.65722
669.7/255.3	45	82	3	16:0	670.64928	669.64134
657.7/255.3	44	82	3	16:0	658.64928	657.64134
643.7/255.3	43	80	3	16:0	644.6334	643.62546
627.7/255.3	42	76	3	16:0	628.60164	627.5937
613.7/255.3	41	74	3	16:0	614.58576	613.57782
595.6/255.3	39	80	3	16:0	596.6334	595.62546
593.6/255.3	39	78	3	16:0	594.61752	593.60958
585.6/255.3	38	82	3	16:0	586.64928	585.64134
581.6/255.3	38	78	3	16:0	582.61752	581.60958
575.6/255.3	38	72	3	16:0	576.56988	575.56194
565.6/255.3	37	74	3	16:0	566.58576	565.57782
563.6/255.3	37	72	3	16:0	564.56988	563.56194
553.6/255.3	36	74	3	16:0	554.58576	553.57782
551.6/255.3	36	72	3	16:0	552.56988	551.56194
549.6/255.3	36	70	3	16:0	550.554	549.54606
539.6/255.3	35	72	3	16:0	540.56988	539.56194
537.6/255.3	35	70	3	16:0	538.554	537.54606
525.6/255.3	34	70	3	16:0	526.554	525.54606
523.6/255.3	34	68	3	16:0	524.53812	523.53018
511.6/255.3	33	68	3	16:0	512.53812	511.53018
509.6/255.3	33	66	3	16:0	510.52224	509.5143
497.5/255.3	32	66	3	16:0	498.52224	497.5143
495.5/255.3	32	64	3	16:0	496.50636	495.49842
483.5/255.3	31	64	3	16:0	484.50636	483.49842
481.5/255.3	31	62	3	16:0	482.49048	481.48254
473.5/255.3	30	66	3	16:0	474.52224	473.5143
469.5/255.3	30	62	3	16:0	470.49048	469.48254
455.5/255.3	29	60	3	16:0	456.4746	455.46666
453.5/255.3	29	58	3	16:0	454.45872	453.45078
441.5/255.3	28	58	3	16:0	442.45872	441.45078
439.5/255.3	28	56	3	16:0	440.44284	439.4349
839.7/253.3	57	108	3	16:1	840.85572	839.84778
837.7/253.3	57	106	3	16:1	838.83984	837.8319
825.7/253.3	56	106	3	16:1	826.83984	825.8319
823.7/253.3	56	104	3	16:1	824.82396	823.81602
811.7/253.3	55	104	3	16:1	812.82396	811.81602
809.7/253.3	55	102	3	16:1	810.80808	809.80014
797.7/253.3	54	102	3	16:1	798.80808	797.80014

795.7/253.3	54	100	3	16:1	796.7922	795.78426
783.7/253.3	53	100	3	16:1	784.7922	783.78426
781.7/253.3	53	98	3	16:1	782.77632	781.76838
769.7/253.3	52	98	3	16:1	770.77632	769.76838
767.7/253.3	52	96	3	16:1	768.76044	767.7525
755.7/253.3	51	96	3	16:1	756.76044	755.7525
753.7/253.3	51	94	3	16:1	754.74456	753.73662
743.7/253.3	50	96	3	16:1	744.76044	743.7525
741.7/253.3	50	94	3	16:1	742.74456	741.73662
739.7/253.3	50	92	3	16:1	740.72868	739.72074
729.7/253.3	49	94	3	16:1	730.74456	729.73662
727.7/253.3	49	92	3	16:1	728.72868	727.72074
725.7/253.3	49	90	3	16:1	726.7128	725.70486
713.7/253.3	48	90	3	16:1	714.7128	713.70486
711.7/253.3	48	88	3	16:1	712.69692	711.68898
699.7/253.3	47	88	3	16:1	700.69692	699.68898
697.7/253.3	47	86	3	16:1	698.68104	697.6731
685.7/253.3	47	84	3	16:1	696.66516	695.65722
671.7/253.3	45	84	3	16:1	672.66516	671.65722
669.7/253.3	45	82	3	16:1	670.64928	669.64134
657.7/253.3	44	82	3	16:1	658.64928	657.64134
643.7/253.3	43	80	3	16:1	644.6334	643.62546
627.7/253.3	42	76	3	16:1	628.60164	627.5937
613.7/253.3	41	74	3	16:1	614.58576	613.57782
595.6/253.3	39	80	3	16:1	596.6334	595.62546
593.6/253.3	39	78	3	16:1	594.61752	593.60958
585.6/253.3	38	82	3	16:1	586.64928	585.64134
581.6/253.3	38	78	3	16:1	582.61752	581.60958
575.6/253.3	38	72	3	16:1	576.56988	575.56194
565.6/253.3	37	74	3	16:1	566.58576	565.57782
563.6/253.3	37	72	3	16:1	564.56988	563.56194
553.6/253.3	36	74	3	16:1	554.58576	553.57782
551.6/253.3	36	72	3	16:1	552.56988	551.56194
549.6/253.3	36	70	3	16:1	550.554	549.54606
539.6/253.3	35	72	3	16:1	540.56988	539.56194
537.6/253.3	35	70	3	16:1	538.554	537.54606
525.6/253.3	34	70	3	16:1	526.554	525.54606
523.6/253.3	34	68	3	16:1	524.53812	523.53018
511.6/253.3	33	68	3	16:1	512.53812	511.53018
509.6/253.3	33	66	3	16:1	510.52224	509.5143
497.5/253.3	32	66	3	16:1	498.52224	497.5143
495.5/253.3	32	64	3	16:1	496.50636	495.49842
483.5/253.3	31	64	3	16:1	484.50636	483.49842
481.5/253.3	31	62	3	16:1	482.49048	481.48254
473.5/253.3	30	66	3	16:1	474.52224	473.5143
469.5/253.3	30	62	3	16:1	470.49048	469.48254
455.5/253.3	29	60	3	16:1	456.4746	455.46666
453.5/253.3	29	58	3	16:1	454.45872	453.45078
441.5/253.3	28	58	3	16:1	442.45872	441.45078
439.5/253.3	28	56	3	16:1	440.44284	439.4349
797.7/241.2	54	102	3	15:0	798.80808	797.80014
795.7/241.2	54	100	3	15:0	796.7922	795.78426
783.7/241.2	53	100	3	15:0	784.7922	783.78426

781.7/241.2	53	98	3	15:0	782.77632	781.76838
769.7/241.2	52	98	3	15:0	770.77632	769.76838
767.7/241.2	52	96	3	15:0	768.76044	767.7525
755.7/241.2	51	96	3	15:0	756.76044	755.7525
753.7/241.2	51	94	3	15:0	754.74456	753.73662
743.7/241.2	50	96	3	15:0	744.76044	743.7525
741.7/241.2	50	94	3	15:0	742.74456	741.73662
739.7/241.2	50	92	3	15:0	740.72868	739.72074
729.7/241.2	49	94	3	15:0	730.74456	729.73662
727.7/241.2	49	92	3	15:0	728.72868	727.72074
725.7/241.2	49	90	3	15:0	726.7128	725.70486
713.7/241.2	48	90	3	15:0	714.7128	713.70486
711.7/241.2	48	88	3	15:0	712.69692	711.68898
699.7/241.2	47	88	3	15:0	700.69692	699.68898
697.7/241.2	47	86	3	15:0	698.68104	697.6731
685.7/241.2	47	84	3	15:0	696.66516	695.65722
671.7/241.2	45	84	3	15:0	672.66516	671.65722
669.7/241.2	45	82	3	15:0	670.64928	669.64134
657.7/241.2	44	82	3	15:0	658.64928	657.64134
643.7/241.2	43	80	3	15:0	644.6334	643.62546
627.7/241.2	42	76	3	15:0	628.60164	627.5937
613.7/241.2	41	74	3	15:0	614.58576	613.57782
595.6/241.2	39	80	3	15:0	596.6334	595.62546
593.6/241.2	39	78	3	15:0	594.61752	593.60958
585.6/241.2	38	82	3	15:0	586.64928	585.64134
581.6/241.2	38	78	3	15:0	582.61752	581.60958
575.6/241.2	38	72	3	15:0	576.56988	575.56194
565.6/241.2	37	74	3	15:0	566.58576	565.57782
563.6/241.2	37	72	3	15:0	564.56988	563.56194
553.6/241.2	36	74	3	15:0	554.58576	553.57782
551.6/241.2	36	72	3	15:0	552.56988	551.56194
549.6/241.2	36	70	3	15:0	550.554	549.54606
539.6/241.2	35	72	3	15:0	540.56988	539.56194
537.6/241.2	35	70	3	15:0	538.554	537.54606
525.6/241.2	34	70	3	15:0	526.554	525.54606
523.6/241.2	34	68	3	15:0	524.53812	523.53018
511.6/241.2	33	68	3	15:0	512.53812	511.53018
509.6/241.2	33	66	3	15:0	510.52224	509.5143
497.5/241.2	32	66	3	15:0	498.52224	497.5143
495.5/241.2	32	64	3	15:0	496.50636	495.49842
483.5/241.2	31	64	3	15:0	484.50636	483.49842
481.5/241.2	31	62	3	15:0	482.49048	481.48254
473.5/241.2	30	66	3	15:0	474.52224	473.5143
469.5/241.2	30	62	3	15:0	470.49048	469.48254
455.5/241.2	29	60	3	15:0	456.4746	455.46666
453.5/241.2	29	58	3	15:0	454.45872	453.45078
441.5/241.2	28	58	3	15:0	442.45872	441.45078
439.5/241.2	28	56	3	15:0	440.44284	439.4349
797.7/239.2	54	102	3	15:1	798.80808	797.80014
795.7/239.2	54	100	3	15:1	796.7922	795.78426
783.7/239.2	53	100	3	15:1	784.7922	783.78426
781.7/239.2	53	98	3	15:1	782.77632	781.76838
769.7/239.2	52	98	3	15:1	770.77632	769.76838

767.7/239.2	52	96	3	15:1	768.76044	767.7525
755.7/239.2	51	96	3	15:1	756.76044	755.7525
753.7/239.2	51	94	3	15:1	754.74456	753.73662
743.7/239.2	50	96	3	15:1	744.76044	743.7525
741.7/239.2	50	94	3	15:1	742.74456	741.73662
739.7/239.2	50	92	3	15:1	740.72868	739.72074
729.7/239.2	49	94	3	15:1	730.74456	729.73662
727.7/239.2	49	92	3	15:1	728.72868	727.72074
725.7/239.2	49	90	3	15:1	726.7128	725.70486
713.7/239.2	48	90	3	15:1	714.7128	713.70486
711.7/239.2	48	88	3	15:1	712.69692	711.68898
699.7/239.2	47	88	3	15:1	700.69692	699.68898
697.7/239.2	47	86	3	15:1	698.68104	697.6731
685.7/239.2	47	84	3	15:1	696.66516	695.65722
671.7/239.2	45	84	3	15:1	672.66516	671.65722
669.7/239.2	45	82	3	15:1	670.64928	669.64134
657.7/239.2	44	82	3	15:1	658.64928	657.64134
643.7/239.2	43	80	3	15:1	644.6334	643.62546
627.7/239.2	42	76	3	15:1	628.60164	627.5937
613.7/239.2	41	74	3	15:1	614.58576	613.57782
595.6/239.2	39	80	3	15:1	596.6334	595.62546
593.6/239.2	39	78	3	15:1	594.61752	593.60958
585.6/239.2	38	82	3	15:1	586.64928	585.64134
581.6/239.2	38	78	3	15:1	582.61752	581.60958
575.6/239.2	38	72	3	15:1	576.56988	575.56194
565.6/239.2	37	74	3	15:1	566.58576	565.57782
563.6/239.2	37	72	3	15:1	564.56988	563.56194
553.6/239.2	36	74	3	15:1	554.58576	553.57782
551.6/239.2	36	72	3	15:1	552.56988	551.56194
549.6/239.2	36	70	3	15:1	550.554	549.54606
539.6/239.2	35	72	3	15:1	540.56988	539.56194
537.6/239.2	35	70	3	15:1	538.554	537.54606
525.6/239.2	34	70	3	15:1	526.554	525.54606
523.6/239.2	34	68	3	15:1	524.53812	523.53018
511.6/239.2	33	68	3	15:1	512.53812	511.53018
509.6/239.2	33	66	3	15:1	510.52224	509.5143
497.5/239.2	32	66	3	15:1	498.52224	497.5143
495.5/239.2	32	64	3	15:1	496.50636	495.49842
483.5/239.2	31	64	3	15:1	484.50636	483.49842
481.5/239.2	31	62	3	15:1	482.49048	481.48254
473.5/239.2	30	66	3	15:1	474.52224	473.5143
469.5/239.2	30	62	3	15:1	470.49048	469.48254
455.5/239.2	29	60	3	15:1	456.4746	455.46666
453.5/239.2	29	58	3	15:1	454.45872	453.45078
441.5/239.2	28	58	3	15:1	442.45872	441.45078
439.5/239.2	28	56	3	15:1	440.44284	439.4349
797.7/227.2	54	102	3	14:0	798.80808	797.80014
795.7/227.2	54	100	3	14:0	796.7922	795.78426
783.7/227.2	53	100	3	14:0	784.7922	783.78426
781.7/227.2	53	98	3	14:0	782.77632	781.76838
769.7/227.2	52	98	3	14:0	770.77632	769.76838
767.7/227.2	52	96	3	14:0	768.76044	767.7525
755.7/227.2	51	96	3	14:0	756.76044	755.7525

753.7/227.2	51	94	3	14:0	754.74456	753.73662
743.7/227.2	50	96	3	14:0	744.76044	743.7525
741.7/227.2	50	94	3	14:0	742.74456	741.73662
739.7/227.2	50	92	3	14:0	740.72868	739.72074
729.7/227.2	49	94	3	14:0	730.74456	729.73662
727.7/227.2	49	92	3	14:0	728.72868	727.72074
725.7/227.2	49	90	3	14:0	726.7128	725.70486
713.7/227.2	48	90	3	14:0	714.7128	713.70486
711.7/227.2	48	88	3	14:0	712.69692	711.68898
699.7/227.2	47	88	3	14:0	700.69692	699.68898
697.7/227.2	47	86	3	14:0	698.68104	697.6731
685.7/227.2	47	84	3	14:0	696.66516	695.65722
671.7/227.2	45	84	3	14:0	672.66516	671.65722
669.7/227.2	45	82	3	14:0	670.64928	669.64134
657.7/227.2	44	82	3	14:0	658.64928	657.64134
643.7/227.2	43	80	3	14:0	644.6334	643.62546
627.7/227.2	42	76	3	14:0	628.60164	627.5937
613.7/227.2	41	74	3	14:0	614.58576	613.57782
595.6/227.2	39	80	3	14:0	596.6334	595.62546
593.6/227.2	39	78	3	14:0	594.61752	593.60958
585.6/227.2	38	82	3	14:0	586.64928	585.64134
581.6/227.2	38	78	3	14:0	582.61752	581.60958
575.6/227.2	38	72	3	14:0	576.56988	575.56194
565.6/227.2	37	74	3	14:0	566.58576	565.57782
563.6/227.2	37	72	3	14:0	564.56988	563.56194
553.6/227.2	36	74	3	14:0	554.58576	553.57782
551.6/227.2	36	72	3	14:0	552.56988	551.56194
549.6/227.2	36	70	3	14:0	550.554	549.54606
539.6/227.2	35	72	3	14:0	540.56988	539.56194
537.6/227.2	35	70	3	14:0	538.554	537.54606
525.6/227.2	34	70	3	14:0	526.554	525.54606
523.6/227.2	34	68	3	14:0	524.53812	523.53018
511.6/227.2	33	68	3	14:0	512.53812	511.53018
509.6/227.2	33	66	3	14:0	510.52224	509.5143
497.5/227.2	32	66	3	14:0	498.52224	497.5143
495.5/227.2	32	64	3	14:0	496.50636	495.49842
483.5/227.2	31	64	3	14:0	484.50636	483.49842
481.5/227.2	31	62	3	14:0	482.49048	481.48254
473.5/227.2	30	66	3	14:0	474.52224	473.5143
469.5/227.2	30	62	3	14:0	470.49048	469.48254
455.5/227.2	29	60	3	14:0	456.4746	455.46666
453.5/227.2	29	58	3	14:0	454.45872	453.45078
441.5/227.2	28	58	3	14:0	442.45872	441.45078
439.5/227.2	28	56	3	14:0	440.44284	439.4349
797.7/225.2	54	102	3	14:1	798.80808	797.80014
795.7/225.2	54	100	3	14:1	796.7922	795.78426
783.7/225.2	53	100	3	14:1	784.7922	783.78426
781.7/225.2	53	98	3	14:1	782.77632	781.76838
769.7/225.2	52	98	3	14:1	770.77632	769.76838
767.7/225.2	52	96	3	14:1	768.76044	767.7525
755.7/225.2	51	96	3	14:1	756.76044	755.7525
753.7/225.2	51	94	3	14:1	754.74456	753.73662
743.7/225.2	50	96	3	14:1	744.76044	743.7525

741.7/225.2	50	94	3	14:1	742.74456	741.73662
739.7/225.2	50	92	3	14:1	740.72868	739.72074
729.7/225.2	49	94	3	14:1	730.74456	729.73662
727.7/225.2	49	92	3	14:1	728.72868	727.72074
725.7/225.2	49	90	3	14:1	726.7128	725.70486
713.7/225.2	48	90	3	14:1	714.7128	713.70486
711.7/225.2	48	88	3	14:1	712.69692	711.68898
699.7/225.2	47	88	3	14:1	700.69692	699.68898
697.7/225.2	47	86	3	14:1	698.68104	697.6731
685.7/225.2	47	84	3	14:1	696.66516	695.65722
671.7/225.2	45	84	3	14:1	672.66516	671.65722
669.7/225.2	45	82	3	14:1	670.64928	669.64134
657.7/225.2	44	82	3	14:1	658.64928	657.64134
643.7/225.2	43	80	3	14:1	644.6334	643.62546
627.7/225.2	42	76	3	14:1	628.60164	627.5937
613.7/225.2	41	74	3	14:1	614.58576	613.57782
595.6/225.2	39	80	3	14:1	596.6334	595.62546
593.6/225.2	39	78	3	14:1	594.61752	593.60958
585.6/225.2	38	82	3	14:1	586.64928	585.64134
581.6/225.2	38	78	3	14:1	582.61752	581.60958
575.6/225.2	38	72	3	14:1	576.56988	575.56194
565.6/225.2	37	74	3	14:1	566.58576	565.57782
563.6/225.2	37	72	3	14:1	564.56988	563.56194
553.6/225.2	36	74	3	14:1	554.58576	553.57782
551.6/225.2	36	72	3	14:1	552.56988	551.56194
549.6/225.2	36	70	3	14:1	550.554	549.54606
539.6/225.2	35	72	3	14:1	540.56988	539.56194
537.6/225.2	35	70	3	14:1	538.554	537.54606
525.6/225.2	34	70	3	14:1	526.554	525.54606
523.6/225.2	34	68	3	14:1	524.53812	523.53018
511.6/225.2	33	68	3	14:1	512.53812	511.53018
509.6/225.2	33	66	3	14:1	510.52224	509.5143
497.5/225.2	32	66	3	14:1	498.52224	497.5143
495.5/225.2	32	64	3	14:1	496.50636	495.49842
483.5/225.2	31	64	3	14:1	484.50636	483.49842
481.5/225.2	31	62	3	14:1	482.49048	481.48254
473.5/225.2	30	66	3	14:1	474.52224	473.5143
469.5/225.2	30	62	3	14:1	470.49048	469.48254
455.5/225.2	29	60	3	14:1	456.4746	455.46666
453.5/225.2	29	58	3	14:1	454.45872	453.45078
441.5/225.2	28	58	3	14:1	442.45872	441.45078
439.5/225.2	28	56	3	14:1	440.44284	439.4349
797.7/213.2	54	102	3	13:0	798.80808	797.80014
795.7/213.2	54	100	3	13:0	796.7922	795.78426
783.7/213.2	53	100	3	13:0	784.7922	783.78426
781.7/213.2	53	98	3	13:0	782.77632	781.76838
769.7/213.2	52	98	3	13:0	770.77632	769.76838
767.7/213.2	52	96	3	13:0	768.76044	767.7525
755.7/213.2	51	96	3	13:0	756.76044	755.7525
753.7/213.2	51	94	3	13:0	754.74456	753.73662
743.7/213.2	50	96	3	13:0	744.76044	743.7525
741.7/213.2	50	94	3	13:0	742.74456	741.73662
739.7/213.2	50	92	3	13:0	740.72868	739.72074

729.7/213.2	49	94	3	13:0	730.74456	729.73662
727.7/213.2	49	92	3	13:0	728.72868	727.72074
725.7/213.2	49	90	3	13:0	726.7128	725.70486
713.7/213.2	48	90	3	13:0	714.7128	713.70486
711.7/213.2	48	88	3	13:0	712.69692	711.68898
699.7/213.2	47	88	3	13:0	700.69692	699.68898
697.7/213.2	47	86	3	13:0	698.68104	697.6731
685.7/213.2	47	84	3	13:0	696.66516	695.65722
671.7/213.2	45	84	3	13:0	672.66516	671.65722
669.7/213.2	45	82	3	13:0	670.64928	669.64134
657.7/213.2	44	82	3	13:0	658.64928	657.64134
643.7/213.2	43	80	3	13:0	644.6334	643.62546
627.7/213.2	42	76	3	13:0	628.60164	627.5937
613.7/213.2	41	74	3	13:0	614.58576	613.57782
595.6/213.2	39	80	3	13:0	596.6334	595.62546
593.6/213.2	39	78	3	13:0	594.61752	593.60958
585.6/213.2	38	82	3	13:0	586.64928	585.64134
581.6/213.2	38	78	3	13:0	582.61752	581.60958
575.6/213.2	38	72	3	13:0	576.56988	575.56194
565.6/213.2	37	74	3	13:0	566.58576	565.57782
563.6/213.2	37	72	3	13:0	564.56988	563.56194
553.6/213.2	36	74	3	13:0	554.58576	553.57782
551.6/213.2	36	72	3	13:0	552.56988	551.56194
549.6/213.2	36	70	3	13:0	550.554	549.54606
539.6/213.2	35	72	3	13:0	540.56988	539.56194
537.6/213.2	35	70	3	13:0	538.554	537.54606
525.6/213.2	34	70	3	13:0	526.554	525.54606
523.6/213.2	34	68	3	13:0	524.53812	523.53018
511.6/213.2	33	68	3	13:0	512.53812	511.53018
509.6/213.2	33	66	3	13:0	510.52224	509.5143
497.5/213.2	32	66	3	13:0	498.52224	497.5143
495.5/213.2	32	64	3	13:0	496.50636	495.49842
483.5/213.2	31	64	3	13:0	484.50636	483.49842
481.5/213.2	31	62	3	13:0	482.49048	481.48254
473.5/213.2	30	66	3	13:0	474.52224	473.5143
469.5/213.2	30	62	3	13:0	470.49048	469.48254
455.5/213.2	29	60	3	13:0	456.4746	455.46666
453.5/213.2	29	58	3	13:0	454.45872	453.45078
441.5/213.2	28	58	3	13:0	442.45872	441.45078
439.5/213.2	28	56	3	13:0	440.44284	439.4349
797.7/199.2	54	102	3	12:0	798.80808	797.80014
795.7/199.2	54	100	3	12:0	796.7922	795.78426
783.7/199.2	53	100	3	12:0	784.7922	783.78426
781.7/199.2	53	98	3	12:0	782.77632	781.76838
769.7/199.2	52	98	3	12:0	770.77632	769.76838
767.7/199.2	52	96	3	12:0	768.76044	767.7525
755.7/199.2	51	96	3	12:0	756.76044	755.7525
753.7/199.2	51	94	3	12:0	754.74456	753.73662
743.7/199.2	50	96	3	12:0	744.76044	743.7525
741.7/199.2	50	94	3	12:0	742.74456	741.73662
739.7/199.2	50	92	3	12:0	740.72868	739.72074
729.7/199.2	49	94	3	12:0	730.74456	729.73662
727.7/199.2	49	92	3	12:0	728.72868	727.72074

725.7/199.2	49	90	3	12:0	726.7128	725.70486
713.7/199.2	48	90	3	12:0	714.7128	713.70486
711.7/199.2	48	88	3	12:0	712.69692	711.68898
699.7/199.2	47	88	3	12:0	700.69692	699.68898
697.7/199.2	47	86	3	12:0	698.68104	697.6731
685.7/199.2	47	84	3	12:0	696.66516	695.65722
671.7/199.2	45	84	3	12:0	672.66516	671.65722
669.7/199.2	45	82	3	12:0	670.64928	669.64134
657.7/199.2	44	82	3	12:0	658.64928	657.64134
643.7/199.2	43	80	3	12:0	644.6334	643.62546
627.7/199.2	42	76	3	12:0	628.60164	627.5937
613.7/199.2	41	74	3	12:0	614.58576	613.57782
595.6/199.2	39	80	3	12:0	596.6334	595.62546
593.6/199.2	39	78	3	12:0	594.61752	593.60958
585.6/199.2	38	82	3	12:0	586.64928	585.64134
581.6/199.2	38	78	3	12:0	582.61752	581.60958
575.6/199.2	38	72	3	12:0	576.56988	575.56194
565.6/199.2	37	74	3	12:0	566.58576	565.57782
563.6/199.2	37	72	3	12:0	564.56988	563.56194
553.6/199.2	36	74	3	12:0	554.58576	553.57782
551.6/199.2	36	72	3	12:0	552.56988	551.56194
549.6/199.2	36	70	3	12:0	550.554	549.54606
539.6/199.2	35	72	3	12:0	540.56988	539.56194
537.6/199.2	35	70	3	12:0	538.554	537.54606
525.6/199.2	34	70	3	12:0	526.554	525.54606
523.6/199.2	34	68	3	12:0	524.53812	523.53018
511.6/199.2	33	68	3	12:0	512.53812	511.53018
509.6/199.2	33	66	3	12:0	510.52224	509.5143
497.5/199.2	32	66	3	12:0	498.52224	497.5143
495.5/199.2	32	64	3	12:0	496.50636	495.49842
483.5/199.2	31	64	3	12:0	484.50636	483.49842
481.5/199.2	31	62	3	12:0	482.49048	481.48254
473.5/199.2	30	66	3	12:0	474.52224	473.5143
469.5/199.2	30	62	3	12:0	470.49048	469.48254
455.5/199.2	29	60	3	12:0	456.4746	455.46666
453.5/199.2	29	58	3	12:0	454.45872	453.45078
441.5/199.2	28	58	3	12:0	442.45872	441.45078
439.5/199.2	28	56	3	12:0	440.44284	439.4349
797.7/185.2	54	102	3	11:0	798.80808	797.80014
795.7/185.2	54	100	3	11:0	796.7922	795.78426
783.7/185.2	53	100	3	11:0	784.7922	783.78426
781.7/185.2	53	98	3	11:0	782.77632	781.76838
769.7/185.2	52	98	3	11:0	770.77632	769.76838
767.7/185.2	52	96	3	11:0	768.76044	767.7525
755.7/185.2	51	96	3	11:0	756.76044	755.7525
753.7/185.2	51	94	3	11:0	754.74456	753.73662
743.7/185.2	50	96	3	11:0	744.76044	743.7525
741.7/185.2	50	94	3	11:0	742.74456	741.73662
739.7/185.2	50	92	3	11:0	740.72868	739.72074
729.7/185.2	49	94	3	11:0	730.74456	729.73662
727.7/185.2	49	92	3	11:0	728.72868	727.72074
725.7/185.2	49	90	3	11:0	726.7128	725.70486
713.7/185.2	48	90	3	11:0	714.7128	713.70486

711.7/185.2	48	88	3	11:0	712.69692	711.68898
699.7/185.2	47	88	3	11:0	700.69692	699.68898
697.7/185.2	47	86	3	11:0	698.68104	697.6731
685.7/185.2	47	84	3	11:0	696.66516	695.65722
671.7/185.2	45	84	3	11:0	672.66516	671.65722
669.7/185.2	45	82	3	11:0	670.64928	669.64134
657.7/185.2	44	82	3	11:0	658.64928	657.64134
643.7/185.2	43	80	3	11:0	644.6334	643.62546
627.7/185.2	42	76	3	11:0	628.60164	627.5937
613.7/185.2	41	74	3	11:0	614.58576	613.57782
595.6/185.2	39	80	3	11:0	596.6334	595.62546
593.6/185.2	39	78	3	11:0	594.61752	593.60958
585.6/185.2	38	82	3	11:0	586.64928	585.64134
581.6/185.2	38	78	3	11:0	582.61752	581.60958
575.6/185.2	38	72	3	11:0	576.56988	575.56194
565.6/185.2	37	74	3	11:0	566.58576	565.57782
563.6/185.2	37	72	3	11:0	564.56988	563.56194
553.6/185.2	36	74	3	11:0	554.58576	553.57782
551.6/185.2	36	72	3	11:0	552.56988	551.56194
549.6/185.2	36	70	3	11:0	550.554	549.54606
539.6/185.2	35	72	3	11:0	540.56988	539.56194
537.6/185.2	35	70	3	11:0	538.554	537.54606
525.6/185.2	34	70	3	11:0	526.554	525.54606
523.6/185.2	34	68	3	11:0	524.53812	523.53018
511.6/185.2	33	68	3	11:0	512.53812	511.53018
509.6/185.2	33	66	3	11:0	510.52224	509.5143
497.5/185.2	32	66	3	11:0	498.52224	497.5143
495.5/185.2	32	64	3	11:0	496.50636	495.49842
483.5/185.2	31	64	3	11:0	484.50636	483.49842
481.5/185.2	31	62	3	11:0	482.49048	481.48254
473.5/185.2	30	66	3	11:0	474.52224	473.5143
469.5/185.2	30	62	3	11:0	470.49048	469.48254
455.5/185.2	29	60	3	11:0	456.4746	455.46666
453.5/185.2	29	58	3	11:0	454.45872	453.45078
441.5/185.2	28	58	3	11:0	442.45872	441.45078
439.5/185.2	28	56	3	11:0	440.44284	439.4349
797.7/157.2	54	102	3	9:0	798.80808	797.80014
795.7/157.2	54	100	3	9:0	796.7922	795.78426
783.7/157.2	53	100	3	9:0	784.7922	783.78426
781.7/157.2	53	98	3	9:0	782.77632	781.76838
769.7/157.2	52	98	3	9:0	770.77632	769.76838
767.7/157.2	52	96	3	9:0	768.76044	767.7525
755.7/157.2	51	96	3	9:0	756.76044	755.7525
753.7/157.2	51	94	3	9:0	754.74456	753.73662
743.7/157.2	50	96	3	9:0	744.76044	743.7525
741.7/157.2	50	94	3	9:0	742.74456	741.73662
739.7/157.2	50	92	3	9:0	740.72868	739.72074
729.7/157.2	49	94	3	9:0	730.74456	729.73662
727.7/157.2	49	92	3	9:0	728.72868	727.72074
725.7/157.2	49	90	3	9:0	726.7128	725.70486
713.7/157.2	48	90	3	9:0	714.7128	713.70486
711.7/157.2	48	88	3	9:0	712.69692	711.68898
699.7/157.2	47	88	3	9:0	700.69692	699.68898

697.7/157.2	47	86	3	9:0	698.68104	697.6731
685.7/157.2	47	84	3	9:0	696.66516	695.65722
671.7/157.2	45	84	3	9:0	672.66516	671.65722
669.7/157.2	45	82	3	9:0	670.64928	669.64134
657.7/157.2	44	82	3	9:0	658.64928	657.64134
643.7/157.2	43	80	3	9:0	644.6334	643.62546
627.7/157.2	42	76	3	9:0	628.60164	627.5937
613.7/157.2	41	74	3	9:0	614.58576	613.57782
595.6/157.2	39	80	3	9:0	596.6334	595.62546
593.6/157.2	39	78	3	9:0	594.61752	593.60958
585.6/157.2	38	82	3	9:0	586.64928	585.64134
581.6/157.2	38	78	3	9:0	582.61752	581.60958
575.6/157.2	38	72	3	9:0	576.56988	575.56194
565.6/157.2	37	74	3	9:0	566.58576	565.57782
563.6/157.2	37	72	3	9:0	564.56988	563.56194
553.6/157.2	36	74	3	9:0	554.58576	553.57782
551.6/157.2	36	72	3	9:0	552.56988	551.56194
549.6/157.2	36	70	3	9:0	550.554	549.54606
539.6/157.2	35	72	3	9:0	540.56988	539.56194
537.6/157.2	35	70	3	9:0	538.554	537.54606
525.6/157.2	34	70	3	9:0	526.554	525.54606
523.6/157.2	34	68	3	9:0	524.53812	523.53018
511.6/157.2	33	68	3	9:0	512.53812	511.53018
509.6/157.2	33	66	3	9:0	510.52224	509.5143
497.5/157.2	32	66	3	9:0	498.52224	497.5143
495.5/157.2	32	64	3	9:0	496.50636	495.49842
483.5/157.2	31	64	3	9:0	484.50636	483.49842
481.5/157.2	31	62	3	9:0	482.49048	481.48254
473.5/157.2	30	66	3	9:0	474.52224	473.5143
469.5/157.2	30	62	3	9:0	470.49048	469.48254
455.5/157.2	29	60	3	9:0	456.4746	455.46666
453.5/157.2	29	58	3	9:0	454.45872	453.45078
441.5/157.2	28	58	3	9:0	442.45872	441.45078
439.5/157.2	28	56	3	9:0	440.44284	439.4349

Appendix 4

List of proteins identified in *R.opacus* PD630 using ABPP approach (Sample 1).

***R.opacus* PD630**	**Protein description**	**Amino acid**	**Mw (kDa)**	**Ion Score**	**Peptide match**
OPAG_05674	dipeptidyl aminopeptidase	682	74234	1402	24
OPAG_00516	DNA-directed RNA polymerase, beta~ subunit	1318	146935	781	34
OPAG_04218	transketolase	704	75611	777	19
OPAG_06066	acyl-CoA synthetase	992	106876	464	13
OPAG_03159	ATP-dependent chaperone ClpB	845	93557	382	12
OPAG_03804	fatty oxidation complex, alpha subunit FadB	702	74083	239	4
OPAG_07773	ATP-dependent chaperone ClpB	850	92558	231	8
OPAG_02426	neprilysin	666	74068	231	7
OPAG_07498	leucyl-tRNA synthetase	950	106314	219	12
OPAG_08351	helicase	1146	128473	205	13
OPAG_05606	NAD-specific glutamate dehydrogenase	1633	179606	153	3
OPAG_09184	malate synthase G	731	79428	144	9
OPAG_00217	hypothetical protein OPAG_00217	1083	118859	117	4
OPAG_06045	excinuclease ABC, A subunit	992	109331	106	4
OPAG_00165	indolepyruvate ferredoxin oxidoreductase	1170	125740	100	6
OPAG_04792	aminodeoxychorismate synthase	691	75917	94	3
OPAG_04767	betaine aldehyde dehydrogenase	507	55258	561	16

OPAG_07869	4-aminobutyrate transaminase	446	47099	541	17
OPAG_02754	adenylosuccinate lyase	473	51625	419	14
OPAG_04877	hydrolase	354	37835	337	11
OPAG_00604	uroporphyrinogen-III synthase	521	55264	330	2
OPAG_07191	hypothetical protein OPAG_07191	575	59145	320	7
OPAG_05885	anthranilate phosphoribosyltransferase	362	37206	306	7
OPAG_03495	glutamyl-tRNA synthetase	491	54248	274	11
OPAG_03759	UDP-glucose 4-epimerase	427	35016	259	6
OPAG_01816	glutamate dehydrogenase	408	44395	256	10
OPAG_05109	mycothiol-dependent formaldehyde dehydrogenase	341	36129	256	3
OPAG_07840	betaine aldehyde dehydrogenase	484	50915	234	9
OPAG_09096	betaine aldehyde dehydrogenase	484	51096	234	8
OPAG_01370	hypothetical protein OPAG_01370	473	49667	223	7
OPAG_09135	methylmalonate-semialdehyde dehydrogenase (acylating)	502	52900	222	8
OPAG_00323	betaine aldehyde dehydrogenase	474	49841	218	5
OPAG_02610	mycothiol-dependent formaldehyde dehydrogenase	347	36958	217	8
OPAG_04575	fumarate hydratase, class I	565	61452	190	3
OPAG_02340	3-oxoacyl-[acyl-carrier-protein] reductase	448	46133	188	7
OPAG_00857	cyclohexanecarboxyl-CoA dehydrogenase	385	41664	178	3
OPAG_07851	phosphoribosylaminoimidazolecarboxamide formyltransferase/IMP cyclohydrolase	518	54612	177	5
OPAG_06327	beta-lactamase	437	45821	175	2
OPAG_06017	branched-chain amino acid ABC transporter	440	44717	171	2
OPAG_03574	4-hydroxy-3-methylbut-2-en-1-yl diphosphate synthase	385	40829	171	3
OPAG_03338	fatty acid desaturase	412	46955	159	5

OPAG_02598	luciferase	329	36152	154	3
OPAG_03810	uroporphyrinogen decarboxylase	362	38215	151	3
OPAG_06350	cysteine desulfurase	445	47081	150	3
OPAG_01355	metal-dependent amidohydrolase	569	60710	149	3
OPAG_04938	carboxylesterase	500	53112	148	9
OPAG_04321	methionyl-tRNA synthetase	519	58371	147	6
OPAG_05485	peptidase M20	450	48560	147	2
OPAG_05435	proteasome component	447	50888	146	8
OPAG_03248	thymidine phosphorylase	431	45001	144	4
OPAG_01899	pyruvate dehydrogenase complex dihydrolipoamide acetyltransferase	410	43824	142	5
OPAG_04741	lactaldehyde reductase	423	46486	130	2
OPAG_03319	phosphoglucosamine mutase	463	49262	129	4
OPAG_03239	tryptophanyl-tRNA synthetase	344	37473	127	6
OPAG_06406	trehalose corynomycolyl transferase C	634	67686	122	4
OPAG_03492	tartrate dehydrogenase	336	35364	121	5
OPAG_01900	pyruvate dehydrogenase E1 component beta subunit	334	36215	117	4
OPAG_07833	carboxylesterase	509	54634	111	2
OPAG_04201	3,4-dihydroxy-2-butanone 4-phosphate synthase/GTP cyclohydrolase II	417	45384	110	4
OPAG_06519	beta-ketoadipyl CoA thiolase	397	41183	108	2
OPAG_07740	isoniazid inducible protein iniC	498	53924	106	3
OPAG_00864	cyclohexanecarboxyl-CoA dehydrogenase	390	42346	106	3
OPAG_00606	glutamyl-tRNA reductase	479	50075	102	3
OPAG_00904	mycothiol-dependent formaldehyde dehydrogenase	329	34842	102	2
OPAG_00543	heptaprenyl diphosphate synthase component II	346	36563	101	3

OPAG_07978	beta-lactamase	397	43464	99	3
OPAG_00043	NADH:quinone reductase	327	33522	98	3
OPAG_05840	proline iminopeptidase	321	35881	98	5
OPAG_04216	glucose-6-phosphate dehydrogenase	514	57466	97	2
OPAG_07409	tryptophan 2-monooxygenase	562	62756	96	2
OPAG_04228	FeS assembly protein SufB	486	53764	93	3
OPAG_02259	pyruvate dehydrogenase complex dihydrolipoamide acetyltransferase	511	54111	92	3
OPAG_03138	aspartate ammonia-lyase	473	51052	92	7
OPAG_03597	hypothetical protein OPAG_03597	336	37287	91	2
OPAG_03972	cyclohexanecarboxyl-CoA dehydrogenase	387	41551	91	2
OPAG_04171	xaa-Pro dipeptidase	367	38766	90	2
OPAG_00962	glycerol-3-phosphate dehydrogenase (NAD)	335	35121	87	6
OPAG_05807	propionyl-CoA carboxylase beta subunit	477	50065	85	4
OPAG_05629	ATP-dependent Clp protease ATP-binding subunit ClpX	426	46921	85	2
OPAG_00869	fumarylacetoacetase	393	42502	84	4
OPAG_05427	5~3~ exonuclease	318	33360	84	5

Appendix 5

List of proteins identified in *R.opacus* PD630 using ABPP approach (Sample 2).

***R.opacus* PD630**	**Protein description**	**Amino acid**	**Mw (kDa)**	**Ion score**	**Peptide match**
OPAG_06066	acyl-CoA synthetase	992	106876	142	7
OPAG_05674	dipeptidyl aminopeptidase	682	74234	113	9
OPAG_05540	beta-ketoadipyl CoA thiolase	397	40816	699	18
OPAG_04877	hydrolase	354	37835	534	9
OPAG_00820	oxidoreductase	346	37470	532	19
OPAG_07191	hypothetical protein	575	59145	403	7
OPAG_04783	cyclohexanecarboxyl-CoA dehydrogenase	386	41501	337	10
OPAG_05885	anthranilate phosphoribosyltransferase	362	37206	292	6
OPAG_04447	phosphopyruvate hydratase	428	44849	280	9
OPAG_04186	methionine adenosyltransferase	404	43266	274	11
OPAG_04849	DNA-directed RNA polymerase, alpha subunit	353	37948	247	9
OPAG_03340	3-phosphoshikimate 1-carboxyvinyltransferase	433	44666	246	2
OPAG_02020	cyclohexanecarboxyl-CoA dehydrogenase	380	40721	241	9
OPAG_06327	beta-lactamase	437	45821	237	3
OPAG_00021	homoserine dehydrogenase	437	45713	232	10
OPAG_09106	propionyl-CoA carboxylase beta subunit	546	58467	213	3
OPAG_00169	L-threonine 3-dehydrogenase	351	37498	191	3
OPAG_05109	mycothiol-dependent formaldehyde dehydrogenase	341	36129	185	2
OPAG_01370	hypothetical protein	473	49667	184	6
OPAG_08032	beta-ketoadipyl CoA thiolase	399	40936	182	4
OPAG_02258	acetoin:DCPIP oxidoreductase beta subunit	343	36402	163	2
OPAG_09096	betaine aldehyde dehydrogenase	484	51096	160	6

OPAG_03492	tartrate dehydrogenase	336	35364	158	4
OPAG_02340	3-oxoacyl-[acyl-carrier-protein] reductase	448	46133	157	3
OPAG_05435	proteasome component	447	50888	154	5
OPAG_03759	UDP-glucose 4-epimerase	427	35016	153	5
OPAG_04179	carbamoyl-phosphate synthase, small subunit	386	40825	152	4
OPAG_07298	NADH dehydrogenase	463	50331	151	4
OPAG_03810	uroporphyrinogen decarboxylase	362	38215	145	3
OPAG_01900	pyruvate dehydrogenase E1 component beta subunit	334	36215	144	2
OPAG_04557	translation-associated GTPase	359	38980	140	2
OPAG_06519	beta-ketoadipyl CoA thiolase	397	41183	130	3
OPAG_02598	luciferase	329	36152	119	3
OPAG_04938	carboxylesterase	500	53112	116	7
OPAG_00626	chloride peroxidase	275	28486	110	3
OPAG_02754	adenylosuccinate lyase	473	51625	109	5
OPAG_00077	cyclohexanecarboxyl-CoA dehydrogenase	387	41553	108	2
OPAG_05292	betaine aldehyde dehydrogenase	449	48474	107	2
OPAG_05840	proline iminopeptidase	321	35881	106	4
OPAG_01532	aspartate ammonia-lyase	482	51034	103	2
OPAG_00543	heptaprenyl diphosphate synthase component II	346	36563	98	3
OPAG_01373	phenylacetic acid degradation ring hydroxlyating complex protein 5	367	40277	96	4
OPAG_07543	DNA polymerase III, subunit beta	394	41610	95	3
OPAG_09314	NAD(P) transhydrogenase alpha subunit, partial	146	15047	93	5
OPAG_02545	citrate (Si)-synthase	431	48082	90	5
OPAG_05427	5~-3~ exonuclease	318	33360	90	3
OPAG_03044	4-aminobutyrate transaminase	413	43817	89	2
OPAG_04662	ATPase	378	39703	88	4
OPAG_02259	pyruvate dehydrogenase complex dihydrolipoamide acetyltransferase	511	54111	86	4

OPAG_01520	formyl-CoA transferase	398	42962	86	3
OPAG_07833	carboxylesterase	509	54634	85	2
OPAG_04243	MoxR family protein	391	42046	85	2
OPAG_07311	inosine-5~-monophosphate dehydrogenase	478	50108	83	5
OPAG_07263	hypothetical protein OPAG_07263	333	36725	83	2
OPAG_05807	propionyl-CoA carboxylase beta subunit	477	50065	83	3
OPAG_04896	inositol-5-monophosphate dehydrogenase	379	39556	81	4